

ICES REPORT 12-03

January 2012

Isogeometric Divergence-conforming B-splines for the Darcy-Stokes-Brinkman Equations

by

John A. Evans and Thomas J.R. Hughes



The Institute for Computational Engineering and Sciences
The University of Texas at Austin
Austin, Texas 78712

Reference: John A. Evans and Thomas J.R. Hughes, Isogeometric Divergence-conforming B-splines for the Darcy-Stokes-Brinkman Equations, ICES REPORT 12-03, The Institute for Computational Engineering and Sciences, The University of Texas at Austin, January 2012.

Report Documentation Page		Form Approved OMB No. 0704-0188
Public reporting burden for the collection of information is estimated to average 1 hour per response, including the time for reviewing instructions, searching existing data sources, gathering and maintaining the data needed, and completing and reviewing the collection of information. Send comments regarding this burden estimate or any other aspect of this collection of information, including suggestions for reducing this burden, to Washington Headquarters Services, Directorate for Information Operations and Reports, 1215 Jefferson Davis Highway, Suite 1204, Arlington VA 22202-4302. Respondents should be aware that notwithstanding any other provision of law, no person shall be subject to a penalty for failing to comply with a collection of information if it does not display a currently valid OMB control number.		
1. REPORT DATE JAN 2012	2. REPORT TYPE	3. DATES COVERED 00-00-2012 to 00-00-2012
4. TITLE AND SUBTITLE Isogeometric Divergence-conforming B-splines for the Darcy-Stokes-Brinkman Equations		5a. CONTRACT NUMBER
		5b. GRANT NUMBER
		5c. PROGRAM ELEMENT NUMBER
6. AUTHOR(S)	5d. PROJECT NUMBER	
	5e. TASK NUMBER	
	5f. WORK UNIT NUMBER	
7. PERFORMING ORGANIZATION NAME(S) AND ADDRESS(ES) University of Texas at Austin, Institute for Computational Engineering and Sciences, Austin, TX, 78712		8. PERFORMING ORGANIZATION REPORT NUMBER
9. SPONSORING/MONITORING AGENCY NAME(S) AND ADDRESS(ES)		10. SPONSOR/MONITOR'S ACRONYM(S)
		11. SPONSOR/MONITOR'S REPORT NUMBER(S)
12. DISTRIBUTION/AVAILABILITY STATEMENT Approved for public release; distribution unlimited		
13. SUPPLEMENTARY NOTES		
14. ABSTRACT <p>We develop divergence-conforming B-spline discretizations for the numerical solution of the Darcy-Stokes-Brinkman equations. These discretizations are motivated by the recent theory of isogeometric discrete differential forms and may be interpreted as smooth generalizations of Raviart-Thomas elements. The new discretizations are (at least) patch-wise C_0 and can be directly utilized in the Galerkin solution of Darcy-Stokes-Brinkman flow for single-patch configurations. When applied to incompressible flows, these discretizations produce pointwise divergence-free velocity fields and hence exactly satisfy mass conservation. In the presence of no-slip boundary conditions and multi-patch geometries, the discontinuous Galerkin framework is invoked to enforce tangential continuity without upsetting the conservation or stability properties of the method across patch boundaries. Furthermore, as no-slip boundary conditions are enforced weakly, the method automatically defaults to a compatible discretization of Darcy flow in the limit of vanishing viscosity. The proposed discretizations are extended to general mapped geometries using divergence-preserving transformations. For sufficiently regular single-patch solutions, we prove a priori error estimates which are optimal for the discrete velocity field and suboptimal, by one order, for the discrete pressure field. Our estimates are additionally robust with respect to the parameters of the Darcy-Stokes-Brinkman problem. We present a comprehensive suite of numerical experiments which indicate optimal convergence rates for both the discrete velocity and pressure fields for general configurations, suggesting that our a priori estimates may be conservative. The focus of the current paper is strictly on incompressible flows, but our theoretical results naturally extend to flows characterized by mass sources and sinks.</p>		
15. SUBJECT TERMS		

16. SECURITY CLASSIFICATION OF:			17. LIMITATION OF ABSTRACT Same as Report (SAR)	18. NUMBER OF PAGES 86	19a. NAME OF RESPONSIBLE PERSON
a. REPORT unclassified	b. ABSTRACT unclassified	c. THIS PAGE unclassified			

Isogeometric Divergence-conforming B-splines for the Darcy-Stokes-Brinkman Equations

John A. Evans ^{a,*} and Thomas J.R. Hughes ^a

^a *Institute for Computational Engineering and Sciences, The University of Texas at Austin,*

^{*} Corresponding author. *E-mail address:* evans@ices.utexas.edu

Abstract

We develop divergence-conforming B-spline discretizations for the numerical solution of the Darcy-Stokes-Brinkman equations. These discretizations are motivated by the recent theory of isogeometric discrete differential forms and may be interpreted as smooth generalizations of Raviart-Thomas elements. The new discretizations are (at least) patch-wise C^0 and can be directly utilized in the Galerkin solution of Darcy-Stokes-Brinkman flow for single-patch configurations. When applied to incompressible flows, these discretizations produce pointwise divergence-free velocity fields and hence exactly satisfy mass conservation. In the presence of no-slip boundary conditions and multi-patch geometries, the discontinuous Galerkin framework is invoked to enforce tangential continuity without upsetting the conservation or stability properties of the method across patch boundaries. Furthermore, as no-slip boundary conditions are enforced weakly, the method automatically defaults to a compatible discretization of Darcy flow in the limit of vanishing viscosity. The proposed discretizations are extended to general mapped geometries using divergence-preserving transformations. For sufficiently regular single-patch solutions, we prove *a priori* error estimates which are optimal for the discrete velocity field and suboptimal, by one order, for the discrete pressure field. Our estimates are additionally robust with respect to the parameters of the Darcy-Stokes-Brinkman problem. We present a comprehensive suite of numerical experiments which indicate optimal convergence rates for both the discrete velocity and pressure fields for general configurations, suggesting that our *a priori* estimates may be conservative. The focus of the current paper is strictly on incompressible flows, but our theoretical results naturally extend to flows characterized by mass sources and sinks.

Keywords: Darcy-Stokes-Brinkman equations, Generalized Stokes equations, B-splines, Isogeometric analysis, Divergence-conforming discretizations

1 Introduction

The Stokes equations describe a wide variety of fluid flows where advective inertial forces are so small when compared with viscous forces that they can be neglected altogether. Such flows arise in a large number of applications in nature and technology, from the flow of lava in the Earth’s mantle [54] to microfluidic flow in micro-electromechanical devices [41]. The Darcy-Stokes-Brinkman equations are a simple extension of the Stokes equations which account for Darcy drag forces in highly porous media [13]. These equations, also referred to as the generalized Stokes equations, have been used to model groundwater flow [22], heat and mass transfer in pipes [39], and flow in biological tissues [40]. One also obtains a generalized Stokes problem when nonlinear terms are treated explicitly during semi-implicit time-integration of the unsteady Navier-Stokes equations.

Despite their simple appearance, the Stokes and generalized Stokes equations have presented considerable difficulty in their numerical approximation. At the heart of the matter is the celebrated Babuška-Brezzi inf-sup condition [3, 12]. Simply put, the condition states that one must properly select discrete velocity and pressure spaces in order to arrive at a stable and convergent discrete mixed formulation. Since the inception of the Marker-and-Cell scheme in 1965 [34], a large number of finite difference, finite volume, and finite element methods have been devised to address the discrete inf-sup condition in the context of the Stokes equations. For reference, see the review by Boffi, Brezzi, and Fortin [9]. Most methods for Stokes flow only satisfy the incompressibility constraint in an approximate sense. Some bypass the inf-sup condition entirely through the use of a stabilized Petrov-Galerkin method [27]. However, methods which return discretely divergence-free velocity fields are generally not robust in the limit of vanishing viscosity when applied to generalized Stokes flows [45]. Moreover, mass conservation is considered to be of prime importance for coupled flow-transport [46], and it has been demonstrated that methods which fail to exactly satisfy the incompressibility constraint suffer from spurious velocity oscillations when applied to “high pressure, low flow” problems [28, 44]. These issues have motivated the development of discretization procedures which satisfy the incompressibility constraint exactly.

One of the simplest methods returning a divergence-free velocity field is the $\mathbf{P}^k - P^{k-1}$ triangular element which approximates velocity fields using continuous piecewise polynomials of degree k and pressure fields using discontinuous polynomials of degree $k - 1$. This method satisfies the Babuška-Brezzi condition for meshes containing no nearly-singular vertices provided $k \geq 4$ [53] and for certain macro-element configurations [2, 63]. Unfortunately, the method is not stable for general meshes and polynomial degrees. Recently, the use of $\mathbf{H}(\text{div}; \Omega)$ elements has arisen as a new paradigm for the simulation of generalized Stokes flows [38, 42, 61]. As these approximations are typically not members of $\mathbf{H}^1(\Omega)$, techniques such as the interior penalty method [1, 24, 62] must be employed to enforce tangential continu-

ity across elements. Alternatively, one can modify divergence-conforming elements to ensure they have some limited tangential continuity [56], and some authors have elected to release continuity entirely in favor of hybridization [18, 17]. In the same vein, divergence-free wavelets have been proposed for the solution of Stokes flows [43, 58, 59, 55], though these discretizations have a complicated construction and are entirely limited to periodic and cuboidal domains.

In this paper, we present new divergence-conforming B-spline discretizations for the generalized Stokes problem. These discretizations are motivated by the theory of isogeometric discrete differential forms [15, 16] and may be interpreted as smooth generalizations of Raviart-Thomas elements [49]. The new discretizations are (at least) patch-wise C^0 and hence can be directly used in the Galerkin solution of generalized Stokes flow for single-patch configurations. We enforce no-slip boundary conditions weakly by means of Nitsche’s method [48], allowing our method to default to a compatible discretization of Darcy flow in the limit of vanishing viscosity. Alternative inf-sup stable treatments of no-slip boundary conditions have been investigated in the context of Stokes flow in [14]. In the presence of multi-patch geometries, we invoke the discontinuous Galerkin framework in order to enforce tangential continuity across patch interfaces while maintaining the stability and conservation properties of the method. The proposed discretizations are extended to general mapped geometries using divergence- and integral-preserving transformations. For single-patch solutions, we are able to prove robust *a priori* error estimates which are optimal for the discrete velocity field and suboptimal, by one order, for the discrete pressure field. This is reminiscent of error estimates for stabilized equal-order interpolations of the Stokes equations [27, 37]. Our derived estimates are also robust with respect to the parameters of generalized Stokes flow. We utilize the methods of exact and manufactured solutions to validate our estimates, and we find that pressure actually converges at optimal order. We further test the effectiveness of our method using a collection of benchmark problems: two-dimensional creeping lid-driven cavity flow, three-dimensional creeping lid-driven cavity flow, and Darcy-dominated generalized Stokes flow subject to boundary layers.

An outline of this paper is as follows. In the following section, we present some basic notation. In Section 3, we recall the generalized Stokes problem subject to homogeneous boundary conditions. In Section 4, we briefly review B-splines, the basic building blocks of our new discretization technique, and in Section 5, we define the B-spline spaces which we will utilize to discretize velocity and pressure fields. In Section 6, we present our discrete variational formulation for the generalized Stokes problem and prove continuity, stability, and *a priori* error estimates for the single-patch setting. In Section 7, we discuss how to extend our methodology to the multi-patch setting. In Sections 8 and 9, we present numerical results, and in Section 10, we draw conclusions. Throughout this paper, we make explicit all of our estimates’ dependencies on the problem parameters as well as the penalty parameter of Nitsche’s method. This will require a lengthy and tedious analysis, but we believe that knowledge of

such dependencies is of great practical importance. Additionally, the focus of this paper is strictly on incompressible flows. Our theoretical results naturally extend to flows characterized by mass sources and sinks.

2 Notation

We begin this paper with some basic notation. For d a positive integer representing dimension, let $D \subset \mathbb{R}^d$ denote an arbitrary bounded Lipschitz domain with boundary ∂D . As usual, let $L^2(D)$ denote the space of square integrable functions on D and define $\mathbf{L}^2(D) = (L^2(D))^d$. We will also utilize the more general Lebesgue spaces $L^p(D)$ where $1 \leq p \leq \infty$ and their vectorial counterpart $\mathbf{L}^p(D)$. Let $H^k(D)$ denote the space of functions in $L^2(D)$ whose k^{th} -order derivatives belong to $L^2(D)$ and define $\mathbf{H}^k(D) = (H^k(D))^d$. We identify with $H^k(D)$ the standard Sobolev norm

$$\|v\|_{H^k(D)} = \left(\sum_{|\alpha| \leq k} \|D^\alpha v\|_{L^2(D)}^2 \right)^{1/2}$$

where $\alpha = (\alpha_1, \alpha_2, \dots, \alpha_d)$ is a multi-index of non-negative integers, $|\alpha| = \alpha_1 + \alpha_2 + \dots + \alpha_d$, and

$$D^\alpha = \frac{\partial^{|\alpha|}}{\partial x_1^{\alpha_1} \partial x_2^{\alpha_2} \dots \partial x_d^{\alpha_d}}.$$

We denote the Sobolev semi-norms as $|\cdot|_{H^k(D)}$, and we use the convention $H^0(D) = L^2(D)$. Throughout, Sobolev spaces of fractional order are defined using function space interpolation (see, e.g., Chapter 1 of [57]). We define $H_0^1(D) \subset H^1(D)$ to be the subspace of functions with homogeneous boundary conditions and define $\mathbf{H}_0^1(D)$ to be the vectorial counterpart of $H_0^1(D)$. We define $\mathbf{H}^s(\text{div}; D)$ to be the Sobolev space of all functions in $\mathbf{H}^s(\Omega)$ whose divergence also belongs to $H^s(D)$. This space is equipped with the norm

$$\|\mathbf{v}\|_{\mathbf{H}^s(\text{div}; D)} = \left(\|\mathbf{v}\|_{\mathbf{H}^s(D)}^2 + \|\text{div } \mathbf{v}\|_{H^s(D)}^2 \right)^{1/2}.$$

When $s = 0$, we drop the index. We also define

$$\mathbf{H}_0(\text{div}; D) = \{\mathbf{v} \in \mathbf{H}(\text{div}; D) : \mathbf{v} \cdot \mathbf{n} = 0 \text{ on } \partial D\}$$

where \mathbf{n} denotes the outward pointing unit normal. Finally, we denote $L_0^2(D) \subset L^2(D)$ as the space of square-integrable functions with zero average on D .

3 The Generalized Stokes Problem

In this section, we recall the generalized Stokes problem subject to homogeneous Dirichlet boundary conditions. For d a positive integer, let Ω denote a Lipschitz

bounded open set of \mathbb{R}^d . Throughout this paper, d will be either 2 or 3. The problem of interest is as follows.

$$(S) \left\{ \begin{array}{l} \text{Given } \sigma : \Omega \rightarrow \mathbb{R}, \nu : \Omega \rightarrow \mathbb{R}, \text{ and } \mathbf{f} : \Omega \rightarrow \mathbb{R}^d, \text{ find } \mathbf{u} : \bar{\Omega} \rightarrow \mathbb{R}^d \text{ and } p : \Omega \rightarrow \mathbb{R} \\ \text{such that} \\ \sigma \mathbf{u} - \nabla \cdot (2\nu \nabla^s \mathbf{u}) + \mathbf{grad} p = \mathbf{f} \text{ in } \Omega \quad (1) \\ \operatorname{div} \mathbf{u} = 0 \text{ in } \Omega \quad (2) \\ \mathbf{u} = \mathbf{0} \text{ on } \partial\Omega. \quad (3) \end{array} \right.$$

Above, \mathbf{u} denotes the flow velocity of a fluid moving through the domain Ω , p denotes the pressure acting on the fluid divided by the fluid density, ν denotes the kinematic viscosity of the fluid, σ denotes the reaction coefficient which gives the ratio of the viscosity to the permeability of the fluid, and \mathbf{f} denotes a body force acting on the fluid divided by the density. We assume that the viscosity is taken to be uniformly positive (i.e., $\exists \nu_0 > 0$ such that $\nu \geq \nu_0$) and that the reaction coefficient is taken to be non-negative (i.e., $\sigma \geq 0$). Note that the pressure is only determined up to an arbitrary constant.

Let us now make an assumption regarding the data of our problem. Notably, let us assume that $\sigma, \nu \in L^\infty(\Omega)$ and $\mathbf{f} \in \mathbf{L}^2(\Omega)$. The weak form for the generalized Stokes problem is then written as follows:

$$(W) \left\{ \begin{array}{l} \text{Find } \mathbf{u} \in \mathbf{H}_0^1(\Omega) \text{ and } p \in L_0^2(\Omega) \text{ such that} \\ a(\mathbf{u}, \mathbf{v}) - b(p, \mathbf{v}) + b(q, \mathbf{u}) = (\mathbf{f}, \mathbf{v})_{\mathbf{L}^2(\Omega)} \quad (4) \\ \text{for all } \mathbf{v} \in \mathbf{H}_0^1(\Omega) \text{ and } q \in L_0^2(\Omega) \text{ where} \\ a(\mathbf{w}, \mathbf{v}) = (2\nu \nabla^s \mathbf{w}, \nabla^s \mathbf{v})_{(L^2(\Omega))^{d \times d}} + (\sigma \mathbf{w}, \mathbf{v})_{\mathbf{L}^2(\Omega)}, \quad \forall \mathbf{w}, \mathbf{v} \in \mathbf{H}_0^1(\Omega), \quad (5) \\ b(q, \mathbf{v}) = (q, \operatorname{div} \mathbf{v})_{L^2(\Omega)}, \quad \forall q \in L_0^2(\Omega), \mathbf{v} \in \mathbf{H}_0^1(\Omega). \quad (6) \end{array} \right.$$

We have the following theorem which is a simple consequence of coercivity, continuity, and a continuous inf-sup condition.

Theorem 3.1. *Problem (W) has a unique weak solution $(\mathbf{u}, p) \in \mathbf{H}_0^1(\Omega) \times L_0^2(\Omega)$.*

4 B-splines and Geometrical Mappings

In this section, we briefly introduce B-splines, the primary ingredient in our discretization technique for the generalized Stokes equations. We also introduce mappings which will allow us to extend our discretization technique to general geometries

of engineering interest. For an overview of B-splines, their properties, and robust algorithms for evaluating their values and derivatives, see de Boor [23] and Schumaker [52]. For the application of B-splines to finite element analysis, see Höllig [35] and Cottrell, Hughes, and Bazilevs [20].

4.1 Univariate B-splines

For two positive integers k and n , representing degree and dimensionality respectively, let us introduce the ordered knot vector

$$\Xi := \{0 = \xi_1, \xi_2, \dots, \xi_{n+k+1} = 1\} \quad (7)$$

where

$$\xi_1 \leq \xi_2 \leq \dots \leq \xi_{n+k+1}.$$

Given Ξ and k , univariate B-spline basis functions are constructed recursively starting with piecewise constants ($k = 0$):

$$B_i^0(\xi) = \begin{cases} 1 & \text{if } \xi_i \leq \xi < \xi_{i+1} \\ 0 & \text{otherwise.} \end{cases} \quad (8)$$

For $k = 1, 2, 3, \dots$, they are defined by

$$B_i^k(\xi) = \frac{\xi - \xi_i}{\xi_{i+k} - \xi_i} B_i^{k-1}(\xi) + \frac{\xi_{i+k+1} - \xi}{\xi_{i+k+1} - \xi_{i+1}} B_{i+1}^{k-1}(\xi). \quad (9)$$

When $\xi_{i+k} - \xi_i = 0$, $\frac{\xi - \xi_i}{\xi_{i+k} - \xi_i}$ is taken to be zero, and similarly, when $\xi_{i+k+1} - \xi_{i+1} = 0$, $\frac{\xi_{i+k+1} - \xi}{\xi_{i+k+1} - \xi_{i+1}}$ is taken to be zero. B-spline basis functions are piecewise polynomials of degree k , form a partition of unity, have local support, and are non-negative. An example of a cubic B-spline basis is shown in Fig. 1. Note the basis is C^2 everywhere in the interval $(0, 1)$. Enhanced smoothness is one of the defining features of B-splines. We refer to linear combinations of B-spline basis functions as B-splines or simply splines.

Let us now introduce the vector $\zeta = \{\zeta_1, \dots, \zeta_m\}$ of knots without repetitions and a corresponding vector $\{r_1, \dots, r_m\}$ of knot multiplicities. That is, r_i is defined to be the multiplicity of the knot ζ_i in Ξ . By construction, $\sum_{i=1}^m r_i = n + k + 1$. We assume that $r_i \leq k + 1$. Let us further assume throughout that $r_1 = r_m = k + 1$, *i.e.*, that Ξ is an open knot vector. This allows us to easily prescribe Dirichlet boundary conditions. At the point ζ_i , B-spline basis functions have $\alpha_j := k - r_j$ continuous derivatives. Therefore, $-1 \leq \alpha_j \leq p - 1$, and the maximum multiplicity allowed, $r_j = k + 1$, gives a discontinuity at ζ_j . We define the regularity vector α by $\alpha := \{\alpha_1, \dots, \alpha_m\}$. By construction, $\alpha_1 = \alpha_m = -1$. In what follows, we utilize the notation

$$|\alpha| = \min\{\alpha_i : 2 \leq i \leq m - 1\} \quad (10)$$

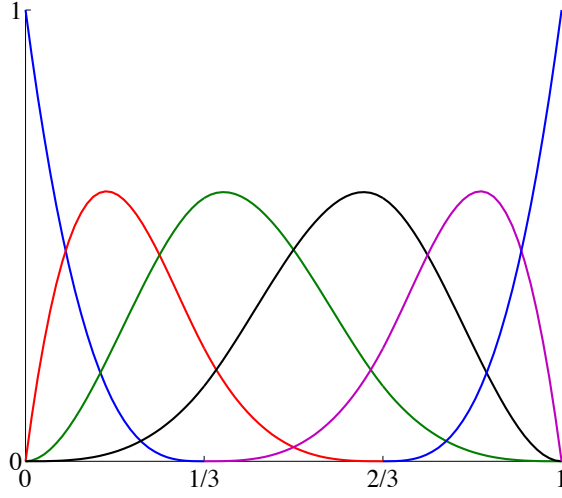


Figure 1: Cubic B-spline basis functions for open, non-uniform knot vector $\Xi = \{0, 0, 0, 0, 1/3, 2/3, 1, 1, 1, 1\}$. Note the basis is C^2 everywhere in the interval $(0, 1)$.

and $\alpha - 1 := \{-1, \alpha_2 - 1, \dots, \alpha_{m-1} - 1, -1\}$ when $\alpha_i \geq 0$ for $2 \leq i \leq m - 1$.

We denote the space of B-splines spanned by the basis functions B_i^k as

$$S_{\alpha}^k := \text{span} \{B_i^k\}_{i=1}^n. \quad (11)$$

When $k \geq 1$ and $\alpha_i \geq 0$ for $2 \leq i \leq m - 1$, the derivatives of functions in S_{α}^k are splines as well. In fact, we have the stronger relationship

$$\left\{ \frac{d}{dx} v : v \in S_{\alpha}^k \right\} \equiv S_{\alpha-1}^{k-1}. \quad (12)$$

That is, the derivative operator $\partial_x : S_{\alpha}^k \rightarrow S_{\alpha-1}^{k-1}$ is surjective. One of the most important properties of univariate B-splines is refinement and, perhaps more importantly, nestedness of refinement. Notably, knot insertion and degree elevation allow one to define a sequence of nested, refined B-spline spaces. Knot insertion and degree elevation algorithms are described in detail in Chapter 2 of [20].

4.2 Multivariate B-splines

The definition of multivariate B-splines follows easily through a tensor-product construction. For d again a positive integer, let us consider the unit cube $\bar{\Omega} = (0, 1)^d \subset \mathbb{R}^d$, which we will henceforth refer to as the parametric domain. Mimicking the one-dimensional case, given integers k_l and n_l for $l = 1, \dots, d$, let us introduce open knot vectors $\Xi_l = \{\xi_{1,l}, \dots, \xi_{n_l+k_l+1,l}\}$ and the associated vectors $\zeta_l = \{\zeta_{1,l}, \dots, \zeta_{m_l,l}\}$, $\{r_{1,l}, \dots, r_{m_l,l}\}$, and $\alpha_l = \{\alpha_{1,l}, \dots, \alpha_{m_l,l}\}$. There is a parametric Cartesian mesh \mathcal{M}_h

associated with these knot vectors partitioning the parametric domain into rectangular parallelepipeds. Visually,

$$\mathcal{M}_h = \{Q = \otimes_{l=1,\dots,d} (\zeta_{i_l,l}, \zeta_{i_l+1,l}), 1 \leq i_l \leq m_l - 1\}. \quad (13)$$

For each element $Q \in \mathcal{M}_h$ we associate a parametric mesh size $h_Q = \text{diam}(Q)$. We also define a shape regularity constant λ which satisfies the inequality

$$\lambda^{-1} \leq \frac{h_{Q,\min}}{h_Q} \leq \lambda, \quad \forall Q \in \mathcal{M}_h, \quad (14)$$

where $h_{Q,\min}$ denotes the length of the smallest edge of Q . A sequence of parametric meshes that satisfy the above inequality for an identical shape regularity constant is said to be locally quasi-uniform.

We associate with each knot vector Ξ_l ($l = 1, \dots, d$) univariate B-spline basis functions $B_{i_l,l}^{k_l}$ of degree k_l for $i_l = 1, \dots, n_l$. On the mesh \mathcal{M}_h , we define the tensor-product B-spline basis functions as

$$B_{i_1,\dots,i_d}^{k_1,\dots,k_d} := B_{i_1,1}^{k_1} \otimes \dots \otimes B_{i_d,d}^{k_d}, \quad i_1 = 1, \dots, n_1, \dots, i_d = 1, \dots, n_d. \quad (15)$$

We then accordingly define the tensor-product B-spline space as

$$S_{\alpha_1,\dots,\alpha_d}^{k_1,\dots,k_d} \equiv S_{\alpha_1,\dots,\alpha_d}^{k_1,\dots,k_d}(\mathcal{M}_h) := \text{span} \left\{ B_{i_1,\dots,i_d}^{k_1,\dots,k_d} \right\}_{i_1=1,\dots,i_d=1}^{n_1,\dots,n_d}. \quad (16)$$

The space is fully characterized by the mesh \mathcal{M}_h , the degrees k_l , and the regularity vectors α_l , as the notation reflects. Like their univariate counterparts, multivariate B-spline basis functions are piecewise polynomial, form a partition of unity, have local support, and are non-negative. Defining the regularity constant

$$\alpha := \min_{l=1,\dots,d} \min_{2 \leq i_l \leq m_l-1} \{\alpha_{i_l,l}\} \quad (17)$$

we see that our B-splines are C^α -continuous throughout the domain $\widehat{\Omega}$. Refinement of multivariate B-spline bases is obtained by applying knot insertion and degree elevation in tensor-product fashion. In the remainder of the text, we consider a family of nested meshes $\{\mathcal{M}_h\}_{h \leq h_0}$ and associated B-spline spaces $\{S_{\alpha_1,\dots,\alpha_d}^{k_1,\dots,k_d}(\mathcal{M}_h)\}_{h \leq h_0}$ that have been obtained by successive applications of knot refinement. Furthermore, we assume throughout that the mesh family $\{\mathcal{M}_h\}_{h \leq h_0}$ is locally quasi-uniform.

Note that each element $Q = \otimes_{l=1,\dots,d} (\zeta_{i_l,l}, \zeta_{i_l+1,l})$ has the equivalent representation $Q = \otimes_{l=1,\dots,d} (\xi_{j_l,l}, \xi_{j_l+1,l})$ for some index j_l . With this in mind, we associate with each element a support extension \tilde{Q} , defined as

$$\tilde{Q} := \otimes_{l=1,\dots,d} (\xi_{j_l-p_l,l}, \xi_{j_l+p_l+1,l}). \quad (18)$$

The support extension is the interior of the set formed by the union of the supports of all B-spline basis functions whose support intersects Q . Note that each element belongs to the support extension of at most $\prod_{l=1,\dots,d} (2p_l + 1)$ elements. The support extension is a natural object to consider when examining the local approximation properties of a B-spline space.

4.3 Piecewise Smooth Functions, Geometrical Mappings, and Physical Mesh Entities

On the parametric mesh \mathcal{M}_h , we define the space of piecewise smooth functions with interelement regularity given by the vectors $\alpha_1, \dots, \alpha_d$ as

$$C_{\alpha_1, \dots, \alpha_d}^\infty = C_{\alpha_1, \dots, \alpha_d}^\infty(\mathcal{M}_h). \quad (19)$$

Precisely, a function in $C_{\alpha_1, \dots, \alpha_d}^\infty$ is a function whose restriction to an element $Q \in \mathcal{M}_h$ admits a C^∞ extension in the closure of that element and which has $\alpha_{i_l, l}$ continuous derivatives with respect to the l th coordinate along the internal mesh faces $\{(x_1, \dots, x_d) : x_l = \zeta_{i_l, l}, \zeta_{j_{l'}, l'} < x_{l'} < \zeta_{j_{l'+1}, l'}, l' \neq l\}$ for all $i_l = 2, \dots, m_l - 1$ and $j_{l'} = 1, \dots, m_{l'} - 1$. Note immediately that any function lying in the B-spline space $S_{\alpha_1, \dots, \alpha_d}^{k_1, \dots, k_d}$ also lies in $C_{\alpha_1, \dots, \alpha_d}^\infty$.

Unless specified otherwise, we assume throughout the rest of the paper that the physical domain $\Omega \subset \mathbb{R}^d$ can be exactly parametrized by a geometrical mapping $\mathbf{F} : \widehat{\Omega} \rightarrow \Omega$ belonging to $(C_{\alpha_1, \dots, \alpha_d}^\infty)^d$ with piecewise smooth inverse. We further assume that the physical domain Ω is simply connected with connected boundary $\partial\Omega$ and the geometrical mapping is independent of the mesh family index h . See, for example, the sequence of mapped meshes depicted in Figure 2. A geometrical mapping meeting our criteria could be defined utilizing B-splines or Non-Uniform Rational B-Splines (NURBS) on the coarsest mesh \mathcal{M}_{h_0} . For examples of such mappings, see Chapter 2 of [20]. NURBS mappings are especially useful as they can represent many geometries of scientific and engineering interest and are the main tools employed in Computer Aided Design (CAD) software. Later in this paper, we will utilize polar mappings to solve flow problems on cylindrical geometries in order to preserve symmetries.

The geometrical mapping \mathbf{F} naturally induces a mesh

$$\mathcal{K}_h = \{K : K = \mathbf{F}(Q), Q \in \mathcal{M}_h\} \quad (20)$$

on the physical domain Ω . We define for each element $K \in \mathcal{K}_h$ a physical mesh size

$$h_K = \|D\mathbf{F}\|_{L^\infty(Q)} h_Q \quad (21)$$

where Q is the pre-image of K , and we also define the support extension $\tilde{K} = \mathbf{F}(\tilde{Q})$. We define for a given mesh the global mesh size

$$h = \max\{h_K, K \in \mathcal{K}_h\}.$$

Note that as the parametric mesh family $\{\mathcal{M}_h\}_{h \leq h_0}$ is locally quasi-uniform and the geometrical mapping \mathbf{F} is independent of the mesh family index h , the physical mesh family $\{\mathcal{K}_h\}_{h \leq h_0}$ is also locally quasi-uniform. We refer to the physical domain Ω and its pre-image $\widehat{\Omega}$ interchangeably as the patch. It should be noted that, in general, the

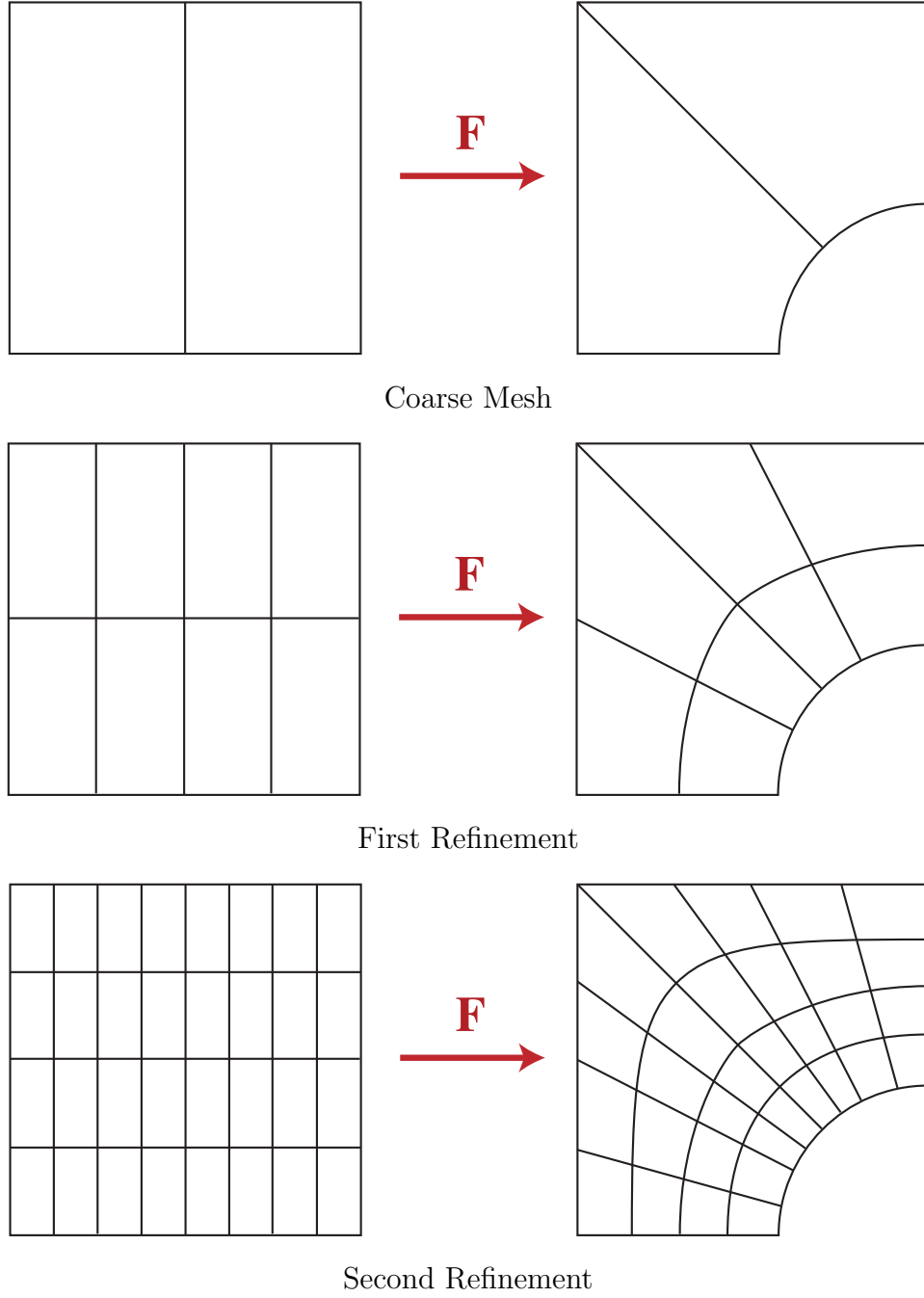


Figure 2: Illustration in the two-dimensional setting of how the parametric mapping \mathbf{F} is independent of the mesh family index h .

domain Ω cannot be represented using just a single patch. Instead, multiple patches must be employed. We will discuss further the multi-patch setting in Section 7.

We define on the parametric mesh a set of mesh faces $\widehat{\mathcal{F}}_h = \{\widehat{F}\}$ where \widehat{F} is a face of one or more elements in \mathcal{M}_h . We define the physical set of mesh faces as

$$\mathcal{F}_h = \{F = \mathbf{F}(\widehat{F}) : \widehat{F} \in \widehat{\mathcal{F}}_h\}$$

and we define the boundary mesh to be

$$\Gamma_h = \{F \in \mathcal{F}_h : F \subset \partial\Omega\}.$$

By construction,

$$\partial\Omega = \cup_{F \in \Gamma_h} \overline{F}.$$

Note that for each face $F \in \Gamma_h$ there is a unique $K \in \mathcal{K}_h$ such that F is a “face” of K (in the sense that F is the image of a face of Q , the pre-image of K). We hence define for such a face the mesh size

$$h_F := h_K.$$

One may also define h_F to be the wall-normal mesh-size as is done in [7]. Such a definition is more appropriate when stretched meshes are utilized in the presence of layers.

Throughout the paper, we will utilize the terminology “a constant independent of h ”. When we employ such terminology, we simply indicate that the constant will not depend on the given mesh and, in particular, its size. The constant may, however, depend on the domain, the shape regularity of the parametric mesh family, the polynomial degrees of the employed B-spline spaces, and global, mesh-invariant measures of the parametric mapping.

5 Discretization of Velocity and Pressure Fields

In this section, we define the B-spline spaces which we will utilize to discretize the velocity and pressure fields appearing in the generalized Stokes problem. These spaces are motivated by the recent theory of isogeometric discrete differential forms [15, 16] and may be interpreted as smooth generalizations of Raviart-Thomas elements [49]. We first define our discrete velocity and pressure spaces on the parametric domain $\widehat{\Omega} = (0, 1)^d$ and then define discrete spaces on the physical domain Ω using divergence- and integral-preserving transformations. We finish this section with a presentation of local approximation estimates and trace inequalities for our discrete velocity and pressure spaces.

5.1 Discrete Spaces on the Parametric Domain

Using the notation of the previous section and assuming that

$$\alpha := \min\{|\boldsymbol{\alpha}_l| : l = 1, \dots, d\} \geq 1,$$

we define the following two spaces:

$$\begin{aligned} \widehat{\mathcal{V}}_h &:= \begin{cases} S_{\boldsymbol{\alpha}_1, \boldsymbol{\alpha}_2-1}^{k_1, k_2-1} \times S_{\boldsymbol{\alpha}_1-1, \boldsymbol{\alpha}_2}^{k_1-1, k_2} & \text{if } d = 2, \\ S_{\boldsymbol{\alpha}_1, \boldsymbol{\alpha}_2-1, \boldsymbol{\alpha}_3-1}^{k_1, k_2-1, k_3-1} \times S_{\boldsymbol{\alpha}_1-1, \boldsymbol{\alpha}_2, \boldsymbol{\alpha}_3-1}^{k_1-1, k_2, k_3-1} \times S_{\boldsymbol{\alpha}_1-1, \boldsymbol{\alpha}_2-1, \boldsymbol{\alpha}_3}^{k_1-1, k_2-1, k_3} & \text{if } d = 3, \end{cases} \\ \widehat{\mathcal{Q}}_h &:= \begin{cases} S_{\boldsymbol{\alpha}_1-1, \boldsymbol{\alpha}_2-1}^{k_1-1, k_2-1} & \text{if } d = 2, \\ S_{\boldsymbol{\alpha}_1-1, \boldsymbol{\alpha}_2-1, \boldsymbol{\alpha}_3-1}^{k_1-1, k_2-1, k_3-1} & \text{if } d = 3. \end{cases} \end{aligned}$$

The space $\widehat{\mathcal{V}}_h$ comprises our set of discrete velocity fields while $\widehat{\mathcal{Q}}_h$ comprises our set of discrete pressure fields. Note that as $\alpha \geq 1$, our discrete velocity fields are \mathbf{H}^1 -conforming. If we allow $\alpha = 0$, our spaces collapse to standard Raviart-Thomas mixed finite elements [49]. In order to deal with no-penetration boundary conditions, we make use of the following constrained discrete spaces:

$$\begin{aligned} \widehat{\mathcal{V}}_{0,h} &:= \left\{ \widehat{\mathbf{v}}_h \in \widehat{\mathcal{V}}_h : \widehat{\mathbf{v}}_h \cdot \widehat{\mathbf{n}} = 0 \text{ on } \partial\widehat{\Omega} \right\}, \\ \widehat{\mathcal{Q}}_{0,h} &:= \left\{ \widehat{q}_h \in \widehat{\mathcal{Q}}_h : \int_{\widehat{\Omega}} \widehat{q}_h d\widehat{\mathbf{x}} = 0 \right\}. \end{aligned}$$

Above, $\widehat{\mathbf{n}}$ denotes the outward-facing normal to $\partial\widehat{\Omega}$. As specified in the introduction, we choose to enforce no-slip boundary condition weakly using Nitsche's method [48]. Due to the special relationship given by (12), the spaces $\widehat{\mathcal{V}}_{0,h}$ and $\widehat{\mathcal{Q}}_{0,h}$ along with the parametric divergence operator form the bounded discrete cochain complex

$$\widehat{\mathcal{V}}_{0,h} \xrightarrow{\widehat{\text{div}}} \widehat{\mathcal{Q}}_{0,h}$$

where $\widehat{\text{div}}$ is the divergence operator on the unit cube $\widehat{\Omega}$. In fact, we have a much stronger result due to the results of [15].

Proposition 5.1. *There exist L^2 -stable projection operators $\widehat{\Pi}_{\widehat{\mathcal{V}}_h}^0 : \mathbf{H}_0(\widehat{\text{div}}; \widehat{\Omega}) \rightarrow \widehat{\mathcal{V}}_{0,h}$ and $\widehat{\Pi}_{\widehat{\mathcal{Q}}_h}^0 : L_0^2(\widehat{\Omega}) \rightarrow \widehat{\mathcal{Q}}_{0,h}$ such that the following diagram commutes:*

$$\begin{array}{ccc} \mathbf{H}_0(\widehat{\text{div}}; \widehat{\Omega}) & \xrightarrow{\widehat{\text{div}}} & L_0^2(\widehat{\Omega}) \\ \widehat{\Pi}_{\widehat{\mathcal{V}}_h}^0 \downarrow & & \widehat{\Pi}_{\widehat{\mathcal{Q}}_h}^0 \downarrow \\ \widehat{\mathcal{V}}_{0,h} & \xrightarrow{\widehat{\text{div}}} & \widehat{\mathcal{Q}}_{0,h}. \end{array} \quad (22)$$

Furthermore, there exists a positive constant \widehat{C}_u independent of h such that

$$\|\widehat{\Pi}_{\widehat{\mathcal{V}}_h}^0 \widehat{\mathbf{v}}\|_{\mathbf{H}^1(\widehat{\Omega})} \leq \widehat{C}_u \|\widehat{\mathbf{v}}\|_{\mathbf{H}^1(\widehat{\Omega})}, \quad \forall \widehat{\mathbf{v}} \in \mathbf{H}_0(\widehat{\text{div}}; \widehat{\Omega}) \cap \mathbf{H}^1(\widehat{\Omega}). \quad (23)$$

5.2 Discrete Spaces on the Physical Domain

To define our discrete velocity and pressure spaces on the physical domain, we introduce the following pullback operators:

$$\iota_u(\mathbf{v}) := \det(D\mathbf{F})(D\mathbf{F})^{-1}(\mathbf{v} \circ \mathbf{F}), \quad \mathbf{v} \in \mathbf{H}_0(\text{div}; \Omega) \quad (24)$$

$$\iota_p(q) := \det(D\mathbf{F})(q \circ \mathbf{F}), \quad q \in L_0^2(\Omega) \quad (25)$$

where $D\mathbf{F}$ is the Jacobian matrix of the parametric mapping \mathbf{F} . The push-forward given by (24), popularly known as the Piola transform, has two important properties: (i) it preserves the nullity of normal components, (ii) it maps divergences to divergences. Hence, it maps divergence-free fields in parametric space to divergence-free fields in physical space, as illustrated in Fig. 3. On the other hand, the push-forward given by (25) has the property that it preserves the nullity of the integral operator. Due to these properties, we have the following commuting diagram:

$$\begin{array}{ccc} \mathbf{H}_0(\widehat{\text{div}}; \widehat{\Omega}) & \xrightarrow{\widehat{\text{div}}} & L_0^2(\widehat{\Omega}) \\ \iota_u \uparrow & & \uparrow \iota_p \\ \mathbf{H}_0(\text{div}; \Omega) & \xrightarrow{\text{div}} & L_0^2(\Omega). \end{array} \quad (26)$$

This motivates the use of the following discrete velocity and pressure spaces in the physical domain:

$$\begin{aligned} \mathcal{V}_{0,h} &:= \left\{ \mathbf{v} \in \mathbf{H}_0(\text{div}; \Omega) : \iota_u(\mathbf{v}) \in \widehat{\mathcal{V}}_{0,h} \right\}, \\ \mathcal{Q}_{0,h} &:= \left\{ q \in L_0^2(\Omega) : \iota_p(q) \in \widehat{\mathcal{Q}}_{0,h} \right\}. \end{aligned}$$

Furthermore, we define the projectors $\Pi_{\mathcal{V}_h}^0 : \mathbf{H}_0(\text{div}; \Omega) \rightarrow \mathcal{V}_{0,h}$ and $\Pi_{\mathcal{Q}_h}^0 : L^2(\Omega) \rightarrow \mathcal{Q}_{0,h}$ via the compositions

$$\Pi_{\mathcal{Q}_h}^0 := \iota_u^{-1} \circ \widehat{\Pi}_{\widehat{\mathcal{Q}}_h}^0 \circ \iota_u, \quad \Pi_{\mathcal{V}_h}^0 := \iota_p^{-1} \circ \widehat{\Pi}_{\widehat{\mathcal{V}}_h}^0 \circ \iota_p.$$

Employing the preceding results and terminology as well as the smoothness properties of the parametric mapping \mathbf{F} , we arrive at the following proposition.

Proposition 5.2. *The following diagram commutes:*

$$\begin{array}{ccc} \mathbf{H}_0(\text{div}; \Omega) & \xrightarrow{\text{div}} & L_0^2(\Omega) \\ \Pi_{\mathcal{V}_h}^0 \downarrow & & \downarrow \widehat{\Pi}_{\widehat{\mathcal{Q}}_h}^0 \\ \mathcal{V}_{0,h} & \xrightarrow{\text{div}} & \mathcal{Q}_{0,h}. \end{array} \quad (27)$$

Furthermore, there exists a positive constant C_u independent of h such that

$$\|\Pi_{\mathcal{V}_h}^0 \mathbf{v}\|_{\mathbf{H}^1(\Omega)} \leq C_u \|\mathbf{v}\|_{\mathbf{H}^1(\Omega)}, \quad \forall \mathbf{v} \in \mathbf{H}_0(\text{div}; \Omega) \cap \mathbf{H}^1(\Omega). \quad (28)$$

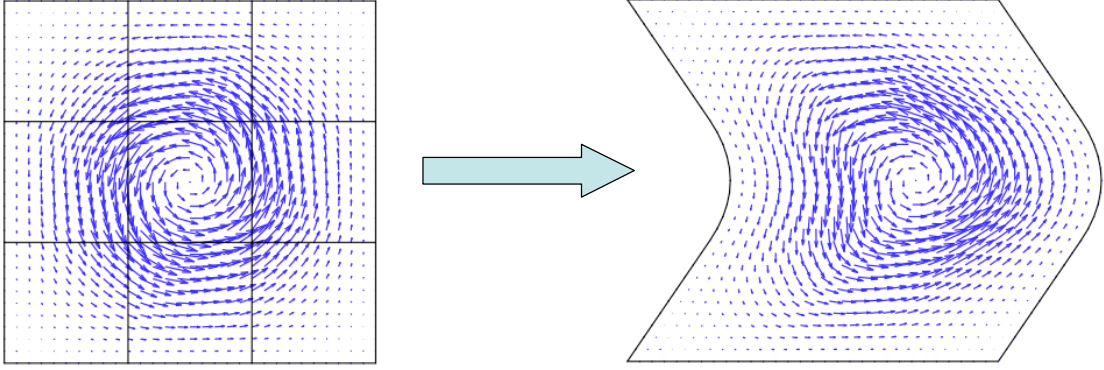


Figure 3: The Piola transform maps divergence-free fields in parametric space to divergence-free fields in physical space, as shown here for the case of a divergence-free B-spline.

We immediately have an inf-sup condition for our discrete velocity/pressure pair.

Proposition 5.3. *There exists a positive constant $\mathring{\beta}$ independent of h such that the following holds: for every $q_h \in \mathcal{Q}_{0,h}$, there exists a $\mathbf{v}_h \in \mathcal{V}_{0,h}$ such that:*

$$\operatorname{div} \mathbf{v}_h = q_h \quad (29)$$

and

$$\|\mathbf{v}_h\|_{\mathbf{H}^1(\Omega)} \leq \mathring{\beta}^{-1} \|q_h\|_{L^2(\Omega)}. \quad (30)$$

Hence,

$$\inf_{\substack{q_h \in \mathcal{Q}_{0,h} \\ q_h \neq 0}} \sup_{\mathbf{v}_h \in \mathcal{V}_{0,h}} \frac{(\operatorname{div} \mathbf{v}_h, q_h)_{L^2(\Omega)}}{\|\mathbf{v}_h\|_{\mathbf{H}^1(\Omega)} \|q_h\|_{L^2(\Omega)}} \geq \mathring{\beta}. \quad (31)$$

Proof. Let $q_h \in \mathcal{Q}_{0,h}$ be arbitrary. It is a classical result (see pg. 24 of [29], for example) that there exists a function $\mathbf{v} \in \mathbf{H}_0^1(\Omega)$ such that $\operatorname{div} \mathbf{v} = q_h$ and

$$\|\mathbf{v}\|_{\mathbf{H}^1(\Omega)} \leq \beta^{-1} \|q_h\|_{L^2(\Omega)}$$

where β is a positive constant independent of \mathbf{v} . Let $\mathbf{v}_h = \Pi_{\mathcal{V}_h}^0 \mathbf{v}$. Then, by Proposition 5.2, $\operatorname{div} \mathbf{v}_h = \operatorname{div} \Pi_{\mathcal{V}_h}^0 \mathbf{v} = \Pi_{\mathcal{Q}_h}^0 \operatorname{div} \mathbf{v} = q_h$ and

$$\|\mathbf{v}_h\|_{\mathbf{H}^1(\Omega)} \leq C_u \|\mathbf{v}\|_{\mathbf{H}^1(\Omega)} \leq C_u \beta^{-1} \|q_h\|_{L^2(\Omega)}.$$

Thus the theorem holds with $\mathring{\beta} = \frac{\beta}{C_u}$. □

We would like to state that such an inf-sup condition would not have held if we had elected to strongly enforce homogeneous tangential boundary conditions within the space $\mathcal{V}_{0,h}$. This is because

$$\operatorname{div} \{ \mathcal{V}_{0,h} \cap \mathbf{H}_0^1(\Omega) \} \subsetneq \mathcal{Q}_{0,h}.$$

Hence, there exists a $q_h \in \mathcal{Q}_{0,h}$ such that $q_h \neq 0$ and

$$\sup_{\mathbf{v}_h \in \mathcal{V}_{0,h} \cap \mathbf{H}_0^1(\Omega)} \frac{(\operatorname{div} \mathbf{v}_h, q_h)_{L^2(\Omega)}}{\|\mathbf{v}_h\|_{\mathbf{H}^1(\Omega)} \|q_h\|_{L^2(\Omega)}} = 0.$$

Hence, an alternative methodology must be employed if one wishes to strongly enforce homogeneous tangential boundary conditions within the space $\mathcal{V}_{0,h}$. For example, in [14], a special discrete pressure space was constructed in the two-dimensional setting by selectively reducing the dimensionality of $\mathcal{Q}_{0,h}$ using T-splines [5]. However, a proof of mesh-independent discrete stability remains absent with this choice of pressure space, and the convenient tensor-product structure of B-splines is lost.

We also have the following result.

Proposition 5.4. *If $\mathbf{v}_h \in \mathcal{V}_{0,h}$ satisfies*

$$(\operatorname{div} \mathbf{v}_h, q_h)_{L^2(\Omega)} = 0, \quad \forall q_h \in \mathcal{Q}_{0,h}, \quad (32)$$

then $\operatorname{div} \mathbf{v}_h \equiv 0$.

Proof. The proof holds trivially as div maps $\mathcal{V}_{0,h}$ onto $\mathcal{Q}_{0,h}$. □

Hence, by choosing $\mathcal{V}_{0,h}$ and $\mathcal{Q}_{0,h}$ as discrete velocity and pressure spaces, we arrive at a discretization that automatically returns velocity fields that are pointwise divergence-free.

5.3 Visualization of Basis Functions

We now visualize some of the basis functions associated with our chosen discrete velocity and pressure spaces. For ease of presentation, we confine ourselves to the two-dimensional setting. We also work with the unconstrained analogues of $\mathcal{V}_{0,h}$ and $\mathcal{Q}_{0,h}$, which we denote as \mathcal{V}_h and \mathcal{Q}_h . Let $k_1 = k_2 = 2$, and let Ξ_1 and Ξ_2 be equal to

$$\Xi_1 := \Xi_2 := \{0, 0, 0, 1/3, 2/3, 1, 1, 1\}.$$

These polynomial degrees and knot vectors define a parametric mesh \mathcal{M}_h and B-spline spaces $\widehat{\mathcal{V}}_h$ and $\widehat{\mathcal{Q}}_h$ over \mathcal{M}_h . To define the physical domain, we employ a biquadratic B-spline mapping. The control net defining this mapping (see Chapter 2 of [20]) and the resulting physical mesh \mathcal{K}_h are illustrated in Figure 4. In Figure 5, we have depicted

a “first-component” vector basis function of the discrete velocity space \mathcal{V}_h . Note that the basis function is C^1 -continuous along horizontal parametric lines and C^0 -continuous along vertical parametric lines. Further note that the directionality of the basis function is preserved under the map ι_u in the sense that the function is oriented in the direction of horizontal parametric lines in both parametric and physical space. In Figure 6, we have depicted a typical “second-component” vector basis function of \mathcal{V}_h . Note that the basis function is C^0 -continuous along horizontal parametric lines and C^1 -continuous along vertical parametric lines, and the directionality of the basis function is preserved under the map ι_u in the sense that the function is oriented in the direction of vertical parametric lines in both parametric and physical space. Finally, in Figure 7, we have depicted a representative basis function of the discrete pressure space \mathcal{Q}_h which is C^0 -continuous in both parametric and physical space.

5.4 Approximation Results and Trace Inequalities

Let us define

$$k' = \min_{l=1,\dots,d} |p_l - 1|. \quad (33)$$

Note that the discrete velocity and pressure spaces $\mathcal{V}_{0,h}$ and $\mathcal{Q}_{0,h}$ consist of mapped piecewise polynomials which are complete up to degree k' . Hence, k' may be thought of as the polynomial degree of our discretization technique. The following result details the local approximation properties of our discrete spaces. Its proof may be found in [15].

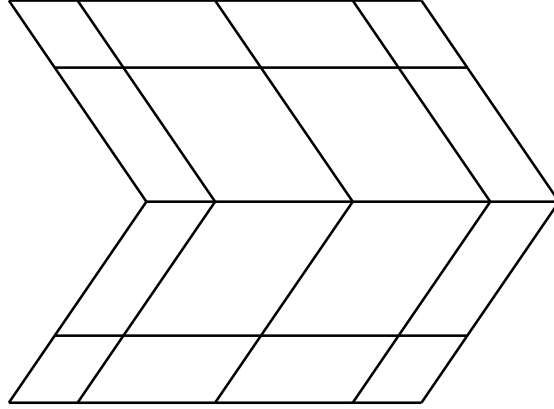
Proposition 5.5. *Let $K \in \mathcal{K}_h$ and \tilde{K} denote the support extension of K . For $0 \leq j \leq s \leq k' + 1$, we have*

$$\|\mathbf{v} - \Pi_{\mathcal{V}_h}^0 \mathbf{v}\|_{\mathbf{H}^j(K)} \leq Ch_K^{s-j} \|\mathbf{v}\|_{\mathbf{H}^s(\tilde{K})}, \quad \forall \mathbf{v} \in \mathbf{H}^s(\tilde{K}) \cap \mathbf{H}_0(\text{div}; \Omega) \quad (34)$$

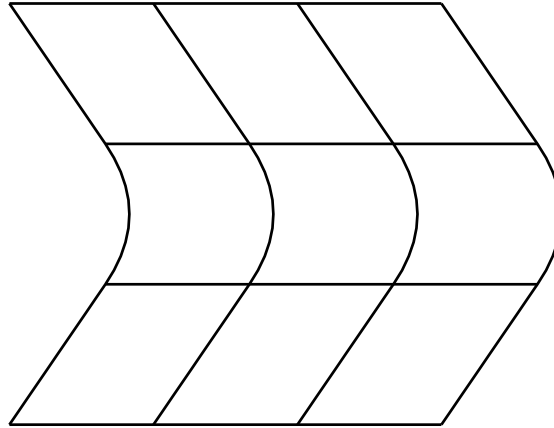
$$\|q - \Pi_{\mathcal{Q}_h}^0 q\|_{H^j(K)} \leq Ch_K^{s-j} \|q\|_{H^s(\tilde{K})}, \quad \forall q \in H^s(\tilde{K}) \cap L_0^2(\Omega) \quad (35)$$

where C denotes a positive constant, possibly different at each appearance, independent of h .

Hence, our discrete spaces deliver optimal rates of convergence from an approximation point of view. This being said, the results of Proposition 5.5 are riddled with inconvenient interpolation constants C which depend on, among other things, the polynomial degree and continuity of our approximation spaces. To attack the question of degree and continuity directly, Beirão da Veiga *et al.* derived interpolation estimates for B-splines with explicit dependence on degree and continuity in [21]. However, the derived estimates are only available for interpolations of Hermite-type. All of this seems to indicate that function analytic estimates have their limitations. Alternatively, one can use numerics to study the approximation properties of discrete spaces using the theory of Kolmogorov n -widths. This approach allows one to exactly



Control Mesh



Physical Mesh

Figure 4: The control net and physical mesh for the biquadratic B-spline surface with $\Xi_1 := \Xi_2 := \{0, 0, 0, 1/3, 2/3, 1, 1, 1\}$.

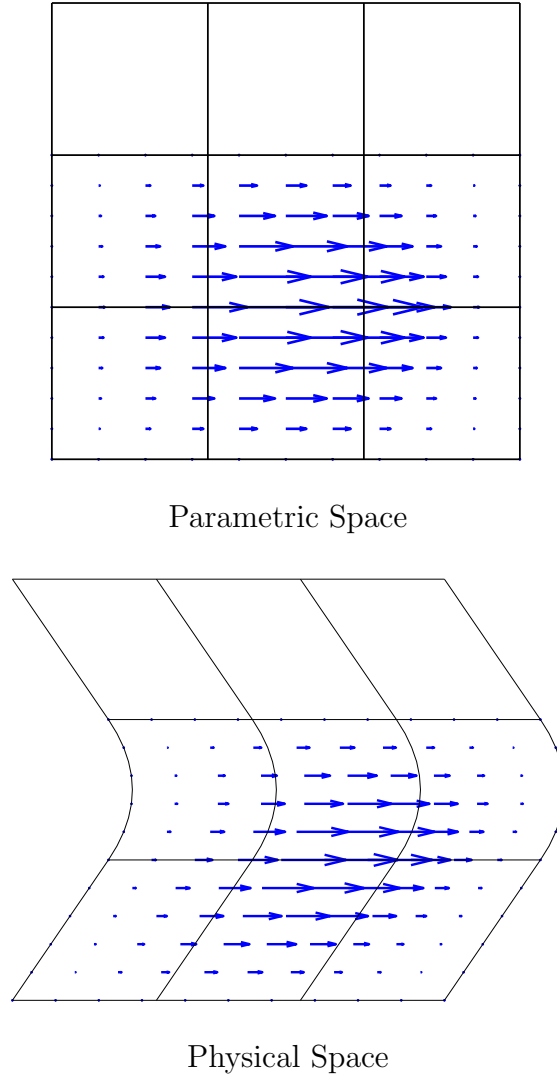
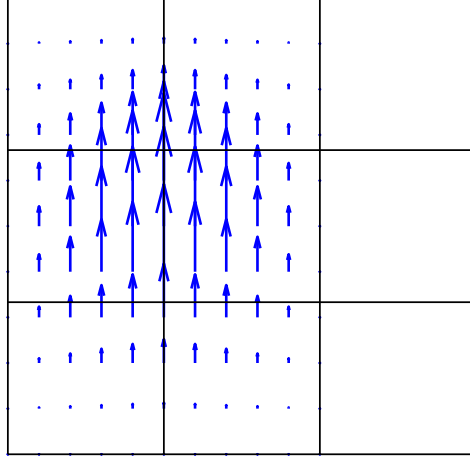
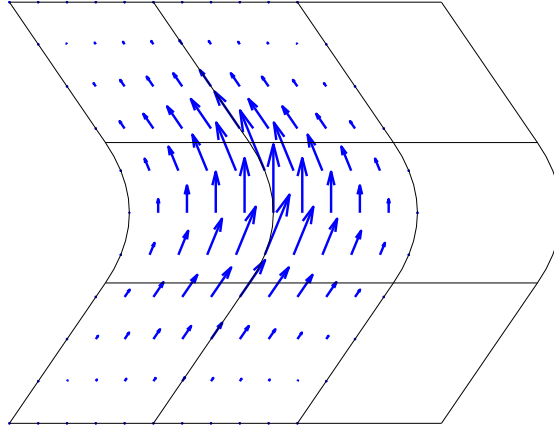


Figure 5: Vector plots of a representative first-component vector basis function of the discrete velocity space \mathcal{V}_h in both parametric and physical space.

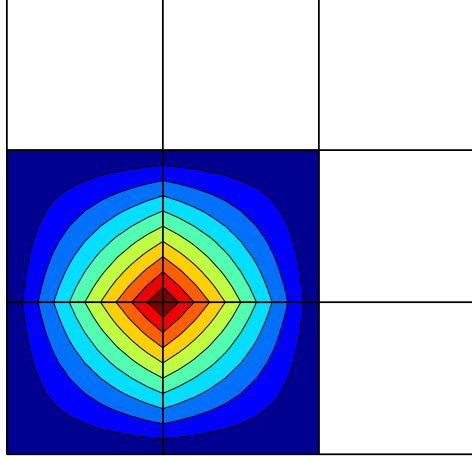


Parametric Space

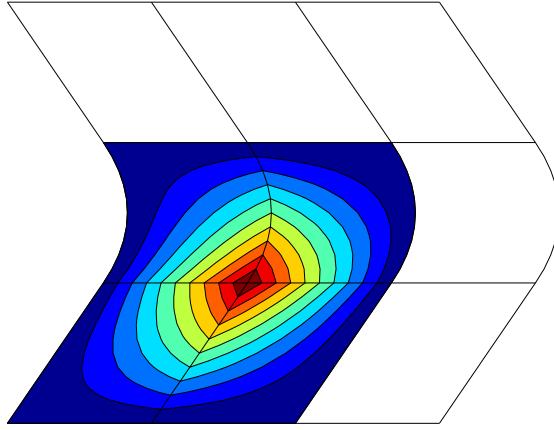


Physical Space

Figure 6: Vector plots of a representative second-component vector basis function of the discrete velocity space \mathcal{V}_h in both parametric and physical space.



Parametric Space



Physical Space

Figure 7: Contour plots of a representative basis function of the discrete pressure space \mathcal{Q}_h in both parametric and physical space.

compute the interpolation constants associated with variational projection through the solution of a generalized eigenproblem. The theory of Kolmogorov n -widths was used to study one-dimensional B-spline discretizations in [25]. This paper revealed that maximal continuity B-spline spaces harbor nearly optimal resolution properties and admit smaller interpolation constants than lower continuity spaces. Recently, the theory of Kolmogorov n -widths has been used to study multi-dimensional and compatible B-spline discretizations. This study has also revealed the advantage of employing B-splines of maximal continuity in the multi-dimensional setting. The results of this study will be presented in a forthcoming publication.

We will also need the following trace estimate in our proceeding mathematical analysis. Its proof can be found in [26].

Proposition 5.6. *Let $K \in \mathcal{K}_h$ and $Q = \mathbf{F}^{-1}(K)$. Then we have*

$$\|(\nabla^s \mathbf{v}_h) \mathbf{n}\|_{(L^2(\partial K))^d} \leq C_{trace} h_K^{-1} \|\mathbf{v}_h\|_{\mathbf{H}^1(K)}, \quad \forall \mathbf{v}_h \in \mathcal{V}_{0,h} \quad (36)$$

where C_{trace} denotes a positive constant independent of h .

In [26], it was shown that Proposition 5.6 holds with $C_{trace} \sim (k')^2$. However, our numerical experience has indicated that a corresponding global trace inequality holds with $C_{trace} \sim k'$ if B-splines of maximal continuity are utilized. This allows us to select a smaller penalty parameter when employing Nitsche's method. As we will see in the next section, our convergence estimates scale inversely with the square root of Nitsche's penalty parameter. Hence, we want to select Nitsche's penalty parameter as small as possible.

6 Approximation of the Generalized Stokes Problem

In this section, we approximate the homogeneous generalized Stokes problem using the discrete velocity and pressure spaces introduced in the previous section. We prove continuity, stability, and *a priori* error estimates for our discretization scheme in the single patch setting, and we explicitly track all of our estimates' dependencies on the problem parameters and Nitsche's penalty parameter.

6.1 Variational Formulation

We begin this section by presenting a discrete variational formulation for the generalized Stokes problem. Since members of $\mathcal{V}_{0,h}$ do not satisfy homogeneous tangential Dirichlet boundary conditions, we resort to Nitsche's method [48] to weakly enforce no-slip boundary conditions. This requires slightly more regularity on our problem data. Specifically, we assume

$$\boldsymbol{\nu} \in W^{1,\infty}(\Omega) := \{w \in L^\infty(\Omega) : \nabla w \in \mathbf{L}^\infty(\Omega)\}.$$

This assumption ensures the trace of ν on the boundary $\partial\Omega$ is well-defined. Now, let us define the following bilinear form:

$$a_h(\mathbf{w}, \mathbf{v}) = a(\mathbf{w}, \mathbf{v}) - \sum_{F \in \Gamma_h} \int_F 2\nu \left(((\nabla^s \mathbf{v}) \mathbf{n}) \cdot \mathbf{w} + ((\nabla^s \mathbf{w}) \mathbf{n}) \cdot \mathbf{v} - \frac{C_{pen}}{h_F} \mathbf{w} \cdot \mathbf{v} \right) ds. \quad (37)$$

In the above equation, $C_{pen} \geq 1$ denotes a specially chosen positive penalty constant which will be specified in the sequel. Our discrete formulation is written as follows.

$$(G) \left\{ \begin{array}{l} \text{Find } \mathbf{u}_h \in \mathcal{V}_{0,h} \text{ and } p_h \in \mathcal{Q}_{0,h} \text{ such that} \\ a_h(\mathbf{u}_h, \mathbf{v}_h) - b(p_h, \mathbf{v}_h) + b(q_h, \mathbf{u}_h) = (\mathbf{f}, \mathbf{v}_h)_{\mathbf{L}^2(\Omega)}, \\ \forall \mathbf{v}_h \in \mathcal{V}_{0,h}, q_h \in \mathcal{Q}_{0,h}. \end{array} \right. \quad (38)$$

Note that the mesh-dependent bilinear form given by (37) has three additional terms in comparison with the continuous bilinear form: a penalty term, a consistency term, and a stability term. All three of these terms will prove important in our proceeding mathematical analysis.

We have the following lemma detailing the consistency of our numerical method provided the exact solution satisfies a reasonable regularity condition.

Lemma 6.1. *Suppose that the unique weak solution (\mathbf{u}, p) of (W) satisfies the regularity condition $\mathbf{u} \in \mathbf{H}^{3/2+\epsilon}(\Omega)$ for some $\epsilon > 0$. Then:*

$$a_h(\mathbf{u}, \mathbf{v}_h) - b(p, \mathbf{v}_h) + b(q_h, \mathbf{u}) = (\mathbf{f}, \mathbf{v}_h)_{\mathbf{L}^2(\Omega)} \quad (39)$$

for all $\mathbf{v}_h \in \mathcal{V}_{0,h}$ and $q_h \in \mathcal{Q}_{0,h}$.

Proof. We trivially have

$$b(q_h, \mathbf{u}) = 0, \quad \forall q_h \in \mathcal{Q}_{0,h}.$$

Now let $\mathbf{v}_h \in \mathcal{V}_{0,h}$. By the trace theorem for fractional Sobolev spaces [57], the assumption $\mathbf{u} \in \mathbf{H}^{3/2+\epsilon}(\Omega)$ guarantees that $(\nabla^s \mathbf{u}) \mathbf{n}$ is well-defined along $\partial\Omega$ and $(\nabla^s \mathbf{u}) \mathbf{n} \in (L^2(\partial\Omega))^d$. Furthermore, $(\nabla^s \mathbf{v}_h) \mathbf{n}$ is well-defined along $\partial\Omega$ and $(\nabla^s \mathbf{v}_h) \mathbf{n} \in (L^2(\partial\Omega))^d$. Hence, the quantity $a_h(\mathbf{u}, \mathbf{v}_h)$ is well-defined. Utilizing integration by parts and the fact that \mathbf{u} satisfies homogeneous Dirichlet boundary conditions and \mathbf{v}_h satisfies homogeneous normal Dirichlet boundary conditions, we have

$$\begin{aligned} a_h(\mathbf{u}, \mathbf{v}_h) - b(p, \mathbf{v}_h) &= \int_{\Omega} (\sigma \mathbf{u} - \nabla \cdot (2\nu \nabla^s \mathbf{u}) + \mathbf{grad} p) \cdot \mathbf{v}_h d\mathbf{x} \\ &= \int_{\Omega} \mathbf{f} \cdot \mathbf{v}_h d\mathbf{x} \\ &= (\mathbf{f}, \mathbf{v}_h)_{\mathbf{L}^2(\Omega)} \end{aligned}$$

where integration is to be understood in the sense of distributions. This completes the proof of the lemma. \square

Consistency is the primary reason that we employed Nitsche's method instead of a naïve penalty method. Nitsche's method also admits adjoint consistency, and this will allow us to prove optimal L^2 estimates for our numerical method. This is in contrast with some standard discontinuous Galerkin techniques such as the Nonsymmetric Interior Penalty Galerkin (NIPG) method [50]. Furthermore, note that our method is consistent for velocity fields satisfying $\mathbf{u} \in \mathbf{H}^{3/2+\epsilon}(\Omega)$ for arbitrary $\epsilon > 0$. Thus, our method is consistent for such singular problems as flow over a backward facing step. As a direct result of consistency, we have the following orthogonality condition.

Corollary 6.1. *Let (\mathbf{u}_h, p_h) denote a solution of (G), and suppose that the unique weak solution (\mathbf{u}, p) of (W) satisfies the regularity condition $\mathbf{u} \in \mathbf{H}^{3/2+\epsilon}(\Omega)$ for some $\epsilon > 0$. Then:*

$$a_h(\mathbf{u} - \mathbf{u}_h, \mathbf{v}_h) - b(p - p_h, \mathbf{v}_h) + b(q_h, \mathbf{u} - \mathbf{u}_h) = 0 \quad (40)$$

for all $\mathbf{v}_h \in \mathcal{V}_{0,h}$ and $q_h \in \mathcal{Q}_{0,h}$.

Our discretization also enjoys the following pointwise mass conservation property which is a direct consequence of Proposition 5.4.

Corollary 6.2. *Let (\mathbf{u}_h, p_h) denote a solution of (G). Then:*

$$\operatorname{div} \mathbf{u}_h \equiv 0 \quad (41)$$

We would like to note that in the event the viscosity ν vanishes for uniformly positive σ , Problem (G) reduces a compatible discretization of incompressible Darcy flow subject to a no-penetration boundary condition. This reduction is contingent upon the weak specification of the no-slip condition. In this sense, weak boundary conditions are essential to the proper behavior of the discrete system under vanishing viscosity. Our proceeding stability and error analysis extends trivially to the case of vanishing viscosity. Furthermore, much like the solutions of Navier-Stokes flows, the generalized Stokes solution is characterized by the presence of a sharp boundary layer for small ν . The weak no-slip condition alleviates the necessity of highly-refined boundary layer meshes [6, 7, 8].

Remark 6.1. *If we wish to impose non-homogeneous tangential Dirichlet (e.g., prescribed slip) boundary conditions, we add the following expression to the right hand side of our discrete formulation:*

$$f_{BC}(\mathbf{v}_h) = \sum_{F \in \Gamma_h} \int_F 2\nu \left(-((\nabla^s \mathbf{v}_h) \mathbf{n}) \cdot \mathbf{u}_{BC} + \frac{C_{pen}}{h_F} \mathbf{u}_{BC} \cdot \mathbf{v}_h \right) d\mathbf{s} \quad (42)$$

where \mathbf{u}_{BC} is a vector function living on $\partial\Omega$ with prescribed tangential boundary value and zero normal boundary value. The imposition of non-homogeneous normal Dirichlet boundary conditions is executed strongly in the standard sense.

6.2 Continuity and Stability

We now establish continuity and stability estimates for our discrete formulation. Continuity and stability, in conjunction with consistency and regularity, will guarantee convergence. To obtain the estimates in this subsection, we will need to call upon standard tools from the discontinuous Galerkin community such as trace estimates, and we will also rely on the results presented in Proposition 5.2.

Before proceeding, let us assume throughout the remainder of the section that the reaction rate σ and the kinematic viscosity ν are constant over Ω . This will greatly simplify the presentation of our mathematical analysis. Nonetheless, our results extend to the more general setting of variable reaction and viscosity. Let us define the following weighted mesh-dependent norm:

$$\begin{aligned} \|\mathbf{v}\|_{\mathcal{V}(h)}^2 &:= \sigma \|\mathbf{v}\|_{\mathbf{H}(\text{div};\Omega)}^2 + 2\nu |\mathbf{v}|_{\mathbf{H}^1(\Omega)}^2 \\ &\quad + 2\nu \sum_{F \in \Gamma_h} h_F \|(\nabla^s \mathbf{v}) \mathbf{n}\|_{(L^2(F))^d}^2 + 2\nu \sum_{F \in \Gamma_h} \frac{C_{pen}}{h_F} \|\mathbf{v}\|_{(L^2(F))^d}^2. \end{aligned} \quad (43)$$

Note that this is a proper norm over our discrete velocity space due to the Poincaré inequality

$$\|\mathbf{v}\|_{\mathbf{H}^1(\Omega)} \leq C_{poin} |\mathbf{v}|_{\mathbf{H}^1(\Omega)}, \quad \forall \mathbf{v} \in \mathbf{H}^1(\Omega) \cap \mathbf{H}_0(\text{div};\Omega) \quad (44)$$

where C_{poin} is a positive constant which depends only on Ω . In fact, by Proposition 5.6 and the Poincaré inequality, there exists a positive constant C_{inv} independent of h , σ , ν , and C_{pen} such that

$$\|\mathbf{v}_h\|_{\mathcal{V}(h)}^2 \leq C_{inv} \left(\sigma \|\mathbf{v}_h\|_{\mathbf{H}(\text{div};\Omega)}^2 + 2\nu |\mathbf{v}_h|_{\mathbf{H}^1(\Omega)}^2 + 2\nu \sum_{F \in \Gamma_h} \frac{C_{pen}}{h_F} \|\mathbf{v}_h\|_{(L^2(F))^d}^2 \right) \quad (45)$$

for all $\mathbf{v}_h \in \mathcal{V}_{0,h}$. The above inequality dictates that our proposed norm acts as expected on the discrete subspace $\mathcal{V}_{0,h}$. That is, it is analogous to a weighted \mathbf{H}^1 -norm coupled with an appropriate penalty term to handle tangential boundary conditions. The use of a mesh-dependent norm is fairly standard in the discontinuous Galerkin community. It is also standard in the stabilized methods community. The use of a weighted norm is motivated by our desire to extract error estimates with an explicit dependence on the problem parameters σ and ν as well as the penalty constant C_{pen} . Let us define the following weighted L^2 -norm for the pressure space

$$\|q\|_{\mathcal{Q}}^2 := \frac{1}{\sigma + 2\nu} \|q\|_{L^2(\Omega)}^2, \quad \forall q \in L_0^2(\Omega). \quad (46)$$

Note that when $\nu = 0$, our norms reduce to σ -weighted $\mathbf{H}(\text{div})$ - and L^2 -norms. Hence, we recover the proper norms for Darcy flow in the limit of vanishing viscosity.

We have the following continuity result.

Lemma 6.2. *The following continuity statements hold:*

$$a_h(\mathbf{w}, \mathbf{v}) \leq C_{cont} \|\mathbf{w}\|_{\mathcal{V}(h)} \|\mathbf{v}\|_{\mathcal{V}(h)}, \quad \forall \mathbf{w}, \mathbf{v} \in \mathcal{V}_{0,h} \oplus \left(\mathbf{H}_0^1(\Omega) \cap \mathbf{H}^{3/2+\epsilon}(\Omega) \right) \quad (47)$$

$$b(p, \mathbf{v}) \leq \|p\|_{\mathcal{Q}} \|\mathbf{v}\|_{\mathcal{V}(h)}, \quad \forall p \in L_0^2(\Omega), \mathbf{v} \in \mathcal{V}_{0,h} \oplus \left(\mathbf{H}_0^1(\Omega) \cap \mathbf{H}^{3/2+\epsilon}(\Omega) \right) \quad (48)$$

where $\epsilon > 0$ is an arbitrary positive number and C_{cont} is a positive constant independent of h , σ , ν , C_{pen} , and ϵ .

Proof. To establish the first estimate, we write

$$a_h(\mathbf{w}, \mathbf{v}) = a(\mathbf{w}, \mathbf{v}) - \sum_{F \in \Gamma_h} \int_F 2\nu \left(((\nabla^s \mathbf{v}) \mathbf{n}) \cdot \mathbf{w} + ((\nabla^s \mathbf{w}) \mathbf{n}) \cdot \mathbf{v} - \frac{C_{pen}}{h_F} \mathbf{w} \cdot \mathbf{v} \right)$$

for some $\mathbf{w}, \mathbf{v} \in \mathcal{V}_{0,h} \oplus \left(\mathbf{H}_0^1(\Omega) \cap \mathbf{H}^{3/2+\epsilon}(\Omega) \right)$. We now bound $a_h(\cdot, \cdot)$ term by term. To begin, note immediately that

$$a(\mathbf{w}, \mathbf{v}) + 2\nu \sum_{F \in \Gamma_h} \int_F \frac{C_{pen}}{h_F} \mathbf{w} \cdot \mathbf{v} \leq \|\mathbf{w}\|_{\mathcal{V}(h)} \|\mathbf{v}\|_{\mathcal{V}(h)}.$$

Next, we write

$$\begin{aligned} \sum_{F \in \Gamma_h} \int_F 2\nu ((\nabla^s \mathbf{v}) \mathbf{n}) \cdot \mathbf{w} &\leq 2\nu \sum_{F \in \Gamma_h} (\|\mathbf{w}\|_{(L^2(F))^d} \|(\nabla^s \mathbf{v}) \mathbf{n}\|_{(L^2(F))^d}) \\ &\leq 2\nu \sqrt{\sum_{F \in \Gamma_h} h_F \|(\nabla^s \mathbf{v}) \mathbf{n}\|_{(L^2(F))^d}^2} \sqrt{\sum_{F \in \Gamma_h} h_F^{-1} \|\mathbf{w}\|_{(L^2(F))^d}^2} \\ &\leq \|\mathbf{w}\|_{\mathcal{V}(h)} \|\mathbf{v}\|_{\mathcal{V}(h)}. \end{aligned}$$

Similarly, we have

$$\sum_{F \in \Gamma_h} \int_F 2\nu ((\nabla^s \mathbf{w}) \mathbf{n}) \cdot \mathbf{v} \leq \|\mathbf{w}\|_{\mathcal{V}(h)} \|\mathbf{v}\|_{\mathcal{V}(h)}.$$

Collecting our bounds, we have

$$a_h(\mathbf{w}, \mathbf{v}) \leq C_{cont} \|\mathbf{w}\|_{\mathcal{V}(h)} \|\mathbf{v}\|_{\mathcal{V}(h)}$$

with $C_{cont} = 3$. To establish the second continuity result of the lemma, we first write

$$b(p, \mathbf{v}) \leq \|p\|_{L^2(\Omega)} \|\operatorname{div} \mathbf{v}\|_{L^2(\Omega)}.$$

The result is then a consequence of

$$\|p\|_{L^2(\Omega)} = (\sigma + 2\nu)^{1/2} \|p\|_{\mathcal{Q}}$$

and

$$\|\operatorname{div} \mathbf{v}\|_{L^2(\Omega)} \leq (\sigma + 2\nu)^{-1/2} \|\mathbf{v}\|_{\mathcal{V}(h)}.$$

□

Now we seek a coercivity estimate for the bilinear form $a_h(\cdot, \cdot)$. Note that we cannot obtain a general estimate with respect to the $\mathcal{V}(h)$ -norm because the bilinear form imposes no gradient control along $\partial\Omega$. On the other hand, (45) suggests that a coercivity estimate can be achieved if we restrict ourselves to the discrete space $\mathcal{V}_{0,h}$. To develop estimates which are independent of the problem parameters σ and ν , we further restrict ourselves to the divergence-free space

$$\mathring{\mathcal{V}}_{0,h} := \{\mathbf{v}_h \in \mathcal{V}_{0,h} : \operatorname{div} \mathbf{v}_h = 0\}.$$

To proceed, we must make two assumptions regarding the size of C_{pen} . First, in light of Proposition 5.6, we choose C_{pen} large enough such that

$$C_{pen} \geq 4h_K C_{poin}^2 C_{Korn} \frac{\|(\nabla^s \mathbf{v}_h) \mathbf{n}\|_{(L^2(\partial K))^d}^2}{\|\mathbf{v}_h\|_{\mathbf{H}^1(K)}^2}, \quad \forall K \in \mathcal{K}_h, \mathbf{v}_h \in \mathcal{V}_{0,h} \quad (49)$$

where C_{poin} is the Poincaré constant associated with (44) and C_{Korn} is the positive constant associated with the following Korn's inequality [11]:

$$\|\mathbf{w}\|_{\mathbf{H}^1(\Omega)}^2 \leq C_{Korn} \left(\|\nabla^s \mathbf{w}\|_{(L^2(\Omega))^{d \times d}}^2 + |\partial\Omega|^{-1/(d-1)} \|\mathbf{w}\|_{(L^2(\partial\Omega))^d}^2 \right), \quad \forall \mathbf{w} \in \mathbf{H}^1(\Omega).$$

Second, we assume that

$$C_{pen} \geq 4h_0 |\partial\Omega|^{-1/(d-1)} \quad (50)$$

where h_0 is the mesh size of the coarsest mesh \mathcal{K}_0 and $|\partial\Omega|$ denotes the area of $\partial\Omega$. This second assumption is necessary as rotation modes carry zero energy when $\sigma = 0$. Hence, weak boundary conditions are needed to control these modes in rotationally symmetric (or near rotationally symmetric) configurations. As such configurations are of significant engineering interest, we believe that any analysis results should cover these situations. Note that a constant C_{pen} satisfying the above assumption need not depend on h , σ , or ν . Rather, it only needs to depend on the size of the domain, the polynomial degree of the discretization, the parametric shape regularity, and global, mesh-invariant measures of the parametric mapping.

We have the following lemma governing the coercivity of our problem.

Lemma 6.3. *Suppose (49) and (50) are satisfied. Then we have*

$$a_h(\mathbf{w}_h, \mathbf{w}_h) \geq C_{coerc} \|\mathbf{w}_h\|_{\mathcal{V}(h)}^2, \quad \forall \mathbf{w}_h \in \mathring{\mathcal{V}}_{0,h} \quad (51)$$

where C_{coerc} is a positive constant independent of h , σ , ν , and C_{pen} .

Proof. Let $\mathbf{w}_h \in \mathring{\mathcal{V}}_{0,h}$ be arbitrary. We expand

$$\begin{aligned}
a_h(\mathbf{w}_h, \mathbf{w}_h) &= a(\mathbf{w}_h, \mathbf{w}_h) \\
&\quad - \sum_{F \in \Gamma_h} \int_F 2\nu \left(((\nabla^s \mathbf{w}_h) \mathbf{n}) \cdot \mathbf{w}_h + ((\nabla^s \mathbf{w}_h) \mathbf{n}) \cdot \mathbf{w}_h - \frac{C_{pen}}{h_F} \mathbf{w}_h \cdot \mathbf{w}_h \right) \\
&= \sigma \|\mathbf{w}_h\|_{\mathbf{H}(\text{div}; \Omega)}^2 + 2\nu \|\nabla^s \mathbf{w}_h\|_{(\mathbf{L}(\Omega))^{d \times d}}^2 + 2\nu \sum_{F \in \Gamma_h} \frac{C_{pen}}{h_F} \|\mathbf{w}_h\|_{(L^2(F))^d}^2 \\
&\quad - 4\nu \sum_{F \in \Gamma_h} \int_F ((\nabla^s \mathbf{w}_h) \mathbf{n}) \cdot \mathbf{w}_h
\end{aligned} \tag{52}$$

where we have used the divergence-free condition on \mathbf{w}_h to obtain $\|\mathbf{w}_h\|_{\mathbf{H}(\text{div}; \Omega)} = \|\mathbf{w}_h\|_{\mathbf{L}^2(\Omega)}$. We now use Cauchy-Schwarz to write

$$\begin{aligned}
&4\nu \sum_{F \in \Gamma_h} \int_F ((\nabla^s \mathbf{w}_h) \mathbf{n}) \cdot \mathbf{w}_h \leq \\
&2\nu \sum_{F \in \Gamma_h} \left(\frac{2h_F}{C_{pen}} \|(\nabla^s \mathbf{w}_h) \mathbf{n}\|_{(L^2(F))^d}^2 + \frac{C_{pen}}{2h_F} \|\mathbf{w}_h\|_{(L^2(F))^d}^2 \right).
\end{aligned} \tag{53}$$

Due to Assumption (49) and the Poincaré inequality, we have

$$\sum_{F \in \Gamma_h} \frac{2h_F}{C_{pen}} \|(\nabla^s \mathbf{w}_h) \mathbf{n}\|_{(L^2(F))^d}^2 \leq \sum_{K \in \mathcal{K}_h} \frac{1}{2C_{Korn}} |\mathbf{w}_h|_{\mathbf{H}^1(\Omega)}^2 \tag{54}$$

where C_{Korn} is the positive constant (only dependent on the domain Ω) associated with the Korn's inequality

$$|\mathbf{w}|_{\mathbf{H}^1(\Omega)}^2 \leq C_{Korn} \left(\|\nabla^s \mathbf{w}\|_{(L(\Omega))^{d \times d}}^2 + |\partial\Omega|^{-1/(d-1)} \|\mathbf{w}\|_{(L^2(\partial\Omega))^d}^2 \right), \quad \forall \mathbf{w} \in \mathbf{H}^1(\Omega). \tag{55}$$

Inserting (54) into (53) gives

$$\sum_{F \in \Gamma_h} \int_F 4\nu ((\nabla^s \mathbf{w}_h) \mathbf{n}) \cdot \mathbf{w}_h \leq 2\nu \sum_{F \in \Gamma_h} \left(\frac{1}{2C_{Korn}} |\mathbf{w}_h|_{\mathbf{H}^1(\Omega)}^2 + \frac{C_{pen}}{2h_F} \|\mathbf{w}_h\|_{(L^2(F))^d}^2 \right),$$

and by inserting the above inequality into (52) and employing (55), we obtain

$$\begin{aligned}
a_h(\mathbf{w}_h, \mathbf{w}_h) &\geq \sigma \|\mathbf{w}_h\|_{\mathbf{H}(\text{div}; \Omega)}^2 + \frac{\nu}{C_{Korn}} |\mathbf{w}_h|_{\mathbf{H}^1(\Omega)}^2 \\
&\quad + \sum_{F \in \Gamma_h} \nu \left(\frac{C_{pen}}{h_F} - \frac{2}{|\partial\Omega|^{1/(d-1)}} \right) \|\mathbf{w}_h\|_{(L^2(F))^d}^2.
\end{aligned}$$

Invoking Assumption (50), we have

$$a_h(\mathbf{w}_h, \mathbf{w}_h) \geq \sigma \|\mathbf{w}_h\|_{\mathbf{H}(\text{div}; \Omega)}^2 + \frac{\nu}{C_{Korn}} |\mathbf{w}_h|_{\mathbf{H}^1(\Omega)}^2 + \sum_{F \in \Gamma_h} \frac{\nu C_{pen}}{2h_F} \|\mathbf{w}_h\|_{(L^2(F))^d}^2$$

as

$$h_F \leq h \leq h_0.$$

The lemma then follows with $C_{coerc} = C_{inv}^{-1} \min \{0.25, 0.5 (C_{Korn})^{-1}\}$ where C_{inv} is the constant associated with (45). \square

We need one more stability estimate. We need to satisfy the Babuška-Brezzi inf-sup condition. Recall that we already proved an inf-sup condition for our discrete spaces in Section 5. However, for that inf-sup condition, we utilized the \mathbf{H}^1 -norm for the velocity space. Here, we must employ the stronger $\mathcal{V}(h)$ -norm. To arrive at an inf-sup condition for this stronger norm, we will proceed by employing three powerful tools: (1) commuting projectors, (2) trace inequalities, and (3) approximation estimates.

Lemma 6.4. *There exists a positive constant $\tilde{\beta}$ independent of h , σ , and ν such that the following holds: for every $q_h \in \mathcal{Q}_{0,h}$, there exists a $\mathbf{v}_h \in \mathcal{V}_{0,h}$ such that:*

$$\text{div } \mathbf{v}_h = q_h \tag{56}$$

and

$$\|\mathbf{v}_h\|_{\mathcal{V}(h)} \leq \frac{\sigma + 2\nu}{\tilde{\beta}} \|q_h\|_{\mathcal{Q}}. \tag{57}$$

Hence,

$$\inf_{q_h \in \mathcal{Q}_{0,h}, q_h \neq 0} \sup_{\mathbf{v}_h \in \mathcal{V}_{0,h}} \frac{(\text{div } \mathbf{v}_h, q_h)}{\|\mathbf{v}_h\|_{\mathcal{V}(h)} \|q_h\|_{\mathcal{Q}}} \geq \tilde{\beta}. \tag{58}$$

Furthermore, the inf-sup constant $\tilde{\beta}$ asymptotically scales inversely with the square root of C_{pen} .

Proof. Let $q_h \in \mathcal{Q}_{0,h}$ be arbitrary. Then we know there exists a function $\mathbf{v} \in \mathbf{H}_0^1(\Omega)$ such that $\text{div } \mathbf{v} = q_h$ and

$$2\nu \|\mathbf{v}\|_{\mathbf{H}^1(\Omega)}^2 \leq 2\nu \beta^{-2} \|q_h\|_{L^2(\Omega)}^2$$

where β is a positive constant independent of \mathbf{v} . Let $\mathbf{v}_h = \Pi_{\mathcal{V}_h}^0 \mathbf{v}$. Then, by Proposition 5.2, $\text{div } \mathbf{v}_h = \text{div } \Pi_{\mathcal{V}_h}^0 \mathbf{v} = \Pi_{\mathcal{Q}_h}^0 \text{div } \mathbf{v} = q_h$ and

$$2\nu \|\mathbf{v}_h\|_{\mathbf{H}^1(\Omega)}^2 \leq 2\nu C_u^2 \|\mathbf{v}\|_{\mathbf{H}^1(\Omega)}^2 \leq 2\nu C_u^2 \beta^{-2} \|q_h\|_{L^2(\Omega)}^2 \tag{59}$$

where $C_u > 0$ is a positive constant independent of h , σ , η , and C_{pen} . Similarly, we have

$$\sigma \|\mathbf{v}_h\|_{\mathbf{H}(\text{div}; \Omega)}^2 \leq \sigma C_u^2 \beta^{-2} \|q_h\|_{L^2(\Omega)}^2. \quad (60)$$

As \mathbf{v} satisfies homogeneous Dirichlet boundary conditions, we can apply the continuous trace inequality (see Theorem 3.2 of [26]) to obtain the expression

$$\begin{aligned} \sum_{F \in \Gamma_h} h_F^{-1} \|\mathbf{v}_h\|_{(L^2(F))^d}^2 &= \sum_{F \in \Gamma_h} h_F^{-1} \|\mathbf{v}_h - \mathbf{v}\|_{(L^2(F))^d}^2 \\ &\leq C_{tr}^2 \sum_{K \in \mathcal{K}_h} \left(h_K^{-2} \|\mathbf{v}_h - \mathbf{v}\|_{\mathbf{L}^2(K)}^2 + |\mathbf{v}_h - \mathbf{v}|_{\mathbf{H}^1(K)}^2 \right) \end{aligned}$$

where C_{tr} is a positive constant only dependent on the shape regularity of the mesh family $\{\mathcal{M}_h\}_{h \leq h_0}$ and global, mesh-invariant measures of the parametric mapping. Proposition 5.5 gives

$$\sum_{K \in \mathcal{K}_h} \left(h_K^{-2} \|\mathbf{v}_h - \mathbf{v}\|_{\mathbf{L}^2(K)}^2 + |\mathbf{v}_h - \mathbf{v}|_{\mathbf{H}^1(K)}^2 \right) \leq C_{bound}^2 \|\mathbf{v}\|_{\mathbf{H}^1(\Omega)}^2$$

where C_{bound} is a positive constant independent of h , σ , ν , and C_{pen} . Thus, we have

$$2\nu \sum_{F \in \Gamma_h} \frac{C_{pen}}{h_F} \|\mathbf{v}_h\|_{(L^2(F))^d}^2 \leq 2\nu C_{bound}^2 C_{tr}^2 C_{pen} \beta^{-2} \|q_h\|_{L^2(\Omega)}^2. \quad (61)$$

Combining (45), (59), (60), and (61), we have

$$\|\mathbf{v}_h\|_{\mathcal{V}(h)}^2 \leq C_{inv} \beta^{-2} (C_u^2 + C_{bound}^2 C_{tr}^2 C_{pen}) (\sigma + 2\nu) \|q_h\|_{L^2(\Omega)}^2.$$

Hence, (57) holds with

$$\tilde{\beta} = C_{inv}^{-1/2} (C_u^2 + C_{bound}^2 C_{tr}^2 C_{pen})^{-1/2} \beta.$$

□

The inverse dependence of the inf-sup constant $\tilde{\beta}$ on the square root of the penalty constant C_{pen} suggests that C_{pen} should be chosen as small as possible to satisfy coercivity. Indeed, we have numerically computed the inf-sup constant $\tilde{\beta}$ for a wide range of values of C_{pen} and found that the relationship $\tilde{\beta} \lesssim C_{pen}^{-1/2}$ is sharp (for reference, see the results listed in Table 1). We would like to note that this makes intuitive sense as we lose inf-sup stability entirely if we enforce the no-slip condition strongly.

By Lemmata 6.2, 6.3, and 6.4 and Brezzi's Theorem [12], we immediately have the following theorem establishing well-posedness.

Table 1: Dependence of the inf-sup constant $\tilde{\beta}$ on Nitsche's penalty constant C_{pen} for $k' = 1$, $h = 1/16$, and $\Omega = (0, 1)^2$.

C_{pen}	1	2	4	8	16	32	64
$\tilde{\beta}$	4.24e-1	3.89e-1	3.29e-1	2.50e-1	1.82e-1	1.30e-1	9.24e-2
order	-	-0.13	-0.24	-0.39	-0.46	-0.48	-0.49

Theorem 6.1. *Suppose that the assumptions of Lemma 6.3 hold true. Then, Problem (G) has a unique weak solution $(\mathbf{u}_h, p_h) \in \mathcal{V}_{0,h} \times \mathcal{Q}_{0,h}$. Furthermore,*

$$\|\mathbf{u}_h\|_{\mathcal{V}(h)} \leq \frac{1}{C_{coerc}} (\sigma + 2\nu C_{poin}^{-2})^{-1/2} \|\mathbf{f}\|_{\mathbf{L}^2(\Omega)}, \quad (62)$$

$$\|p_h\|_{\mathcal{Q}} \leq \frac{1}{\tilde{\beta}} (\sigma + 2\nu C_{poin}^{-2})^{-1/2} \left(1 + \frac{C_{cont}}{C_{coerc}}\right) \|\mathbf{f}\|_{\mathbf{L}^2(\Omega)}. \quad (63)$$

We would like to note that all of the continuity and stability estimates here hold when ν is identically zero and σ is positive. Hence, we have a unified stability analysis of Stokes flow and incompressible Darcy flow.

Remark 6.2. *Note that for the setting of constant viscosity, one has*

$$\nabla \cdot (2\nu \nabla^s \mathbf{u}) = \nu \Delta \mathbf{u}. \quad (64)$$

This inspires a different variational formulation than that presented here which is often the basis for numerical discretization (see, for example, [19]). However, these discretizations (and their accompanying mathematical analysis) are not extendable to the more difficult and physically relevant setting of variable viscosity, and they also cannot easily accommodate traction boundary conditions.

6.3 A Priori Error Estimates

We are now ready to derive *a priori* error estimates for our discrete formulation. We begin with the following lemma.

Lemma 6.5. *Let (\mathbf{u}, p) and (\mathbf{u}_h, p_h) denote the unique solutions of Problems (W) and (G) respectively. Furthermore, assume that $\mathbf{u} \in \mathbf{H}^{3/2+\epsilon}(\Omega)$ for some $\epsilon > 0$ and that the assumptions of Lemma 6.3 hold true. Then*

$$\|\mathbf{u} - \mathbf{u}_h\|_{\mathcal{V}(h)} \leq \left(1 + \frac{C_{cont}}{C_{coerc}}\right) \inf_{\mathbf{v}_h \in \mathcal{V}_{0,h}} \|\mathbf{u} - \mathbf{v}_h\|_{\mathcal{V}(h)} \quad (65)$$

and

$$\|p - p_h\|_{\mathcal{Q}} \leq \left(1 + \frac{1}{\tilde{\beta}}\right) \inf_{q_h \in \mathcal{Q}_{0,h}} \|p - q_h\|_{\mathcal{Q}} + \frac{C_{cont}}{\tilde{\beta}} \|\mathbf{u} - \mathbf{u}_h\|_{\mathcal{V}(h)} \quad (66)$$

where C_{cont} is the continuity constants given by Lemma 6.2, C_{coerc} is the coercivity constant given by Lemma 6.3, and $\tilde{\beta}$ is the inf-sup constant given by Lemma 6.4.

Proof. We first prove (65). We have that, for any $\mathbf{v}_h \in \mathcal{V}_{0,h}$ such that $\operatorname{div} \mathbf{v}_h = 0$,

$$\begin{aligned} \|\mathbf{v}_h - \mathbf{u}_h\|_{\mathcal{V}(h)}^2 &\leq \frac{1}{C_{coerc}} a(\mathbf{v}_h - \mathbf{u}_h, \mathbf{v}_h - \mathbf{u}_h) \\ &= \frac{1}{C_{coerc}} a(\mathbf{v}_h - \mathbf{u}, \mathbf{v}_h - \mathbf{u}_h) \\ &\leq \frac{C_{cont}}{C_{coerc}} \|\mathbf{v}_h - \mathbf{u}\|_{\mathcal{V}(h)} \|\mathbf{v}_h - \mathbf{u}_h\|_{\mathcal{V}(h)} \end{aligned} \quad (67)$$

where we employed the orthogonality given by Corollary 6.1 and the condition

$$\operatorname{div}(\mathbf{u}_h - \mathbf{v}_h) = 0$$

in the second line of the (67). Hence, we can write

$$\begin{aligned} \|\mathbf{u} - \mathbf{u}_h\|_{\mathcal{V}(h)} &\leq \inf_{\mathbf{v}_h \in \dot{\mathcal{V}}_{0,h}} (\|\mathbf{u} - \mathbf{v}_h\|_{\mathcal{V}(h)} + \|\mathbf{v}_h - \mathbf{u}_h\|_{\mathcal{V}(h)}) \\ &\leq \left(1 + \frac{C_{cont}}{C_{coerc}}\right) \inf_{\mathbf{v}_h \in \dot{\mathcal{V}}_{0,h}} \|\mathbf{u} - \mathbf{v}_h\|_{\mathcal{V}(h)}. \end{aligned} \quad (68)$$

We now prove (66). We have that, for any $q_h \in \mathcal{Q}_{0,h}$,

$$\begin{aligned} \|p_h - q_h\|_{\mathcal{Q}} &\leq \frac{1}{\tilde{\beta}} \sup_{\mathbf{w}_h \in \mathcal{V}_{0,h}} \frac{b(p_h - q_h, \mathbf{w}_h)}{\|\mathbf{w}_h\|_{\mathcal{V}(h)}} \\ &= \frac{1}{\tilde{\beta}} \sup_{\mathbf{w}_h \in \mathcal{V}_{0,h}} \frac{b(p - q_h, \mathbf{w}_h) - a(\mathbf{u} - \mathbf{u}_h, \mathbf{w}_h)}{\|\mathbf{w}_h\|_{\mathcal{V}(h)}} \\ &\leq \frac{1}{\tilde{\beta}} (\|p - q_h\|_{\mathcal{Q}} + C_{cont} \|\mathbf{u} - \mathbf{u}_h\|_{\mathcal{V}(h)}) \end{aligned} \quad (69)$$

where we again employed orthogonality in the second line above. Inequality (66) then follows in the same manner as (68) by a splitting of the pressure error and a usage of (69). \square

We have the following theorem giving us *a priori* convergence estimates which are optimal for the discrete velocity field and suboptimal, by one order, for the discrete pressure field.

Theorem 6.2. *Let (\mathbf{u}, p) and (\mathbf{u}_h, p_h) denote the unique solutions of Problems (W) and (G) respectively. Furthermore, assume that $(\mathbf{u}, p) \in \mathbf{H}^{j+1}(\Omega) \times H^j(\Omega)$ for some $j > 1/2$ and that the assumptions of Lemma 6.3 hold true. Then*

$$\|\mathbf{u} - \mathbf{u}_h\|_{\mathcal{V}(h)} \leq C_{\mathbf{u}} \left(1 + \frac{C_{cont}}{C_{coerc}}\right) \sqrt{\sigma h^{2s+2} + 2\nu h^{2s}} \|\mathbf{u}\|_{\mathbf{H}^{s+1}(\Omega)} \quad (70)$$

and

$$\|p - p_h\|_{\mathcal{Q}} \leq C_p \left(1 + \frac{1}{\tilde{\beta}}\right) (\sigma + 2\nu)^{-1/2} h^s \|p\|_{H^s(\Omega)} + \frac{C_{cont}}{\tilde{\beta}} \|\mathbf{u} - \mathbf{u}_h\|_{\mathcal{V}(h)} \quad (71)$$

for $s = \min\{k', j\}$ where k' is the polynomial degree of our discretization, $C_{\mathbf{u}}$ is a positive constant independent of h , σ , and ν which asymptotically scales with the square root of C_{pen} , and C_p is a positive constant independent of h , σ , ν , and C_{pen} .

Proof. We first prove (70). Recall the error estimate given by (65):

$$\|\mathbf{u} - \mathbf{u}_h\|_{\mathcal{V}(h)} \leq \left(1 + \frac{C_{cont}}{C_{coerc}}\right) \inf_{\mathbf{v}_h \in \hat{\mathcal{V}}_{0,h}} \|\mathbf{u} - \mathbf{v}_h\|_{\mathcal{V}(h)}.$$

Noting $\operatorname{div} \Pi_{\mathcal{V}_h}^0 \mathbf{u} = \Pi_{\mathcal{Q}_h}^0 \operatorname{div} \mathbf{u} = 0$, we can choose $\mathbf{v}_h = \Pi_{\mathcal{V}_h}^0 \mathbf{u}$ in the above expression to obtain

$$\begin{aligned} \|\mathbf{u} - \mathbf{u}_h\|_{\mathcal{V}(h)} &\leq \left(1 + \frac{C_{cont}}{C_{coerc}}\right) \|\mathbf{u} - \Pi_{\mathcal{V}_h}^0 \mathbf{u}\|_{\mathcal{V}(h)} \\ &= C_{co} \sqrt{T_1 + T_2 + T_3 + T_4} \end{aligned} \quad (72)$$

where we have assigned $C_{co} = \left(1 + \frac{C_{cont}}{C_{coerc}}\right)$ and

$$T_1 = \sigma \|\mathbf{u} - \Pi_{\mathcal{V}_h}^0 \mathbf{u}\|_{\mathbf{H}(\operatorname{div}; \Omega)}^2 = \sigma \|\mathbf{u} - \Pi_{\mathcal{V}_h}^0 \mathbf{u}\|_{\mathbf{L}^2(\Omega)}^2 \quad (73)$$

$$T_2 = 2\nu \|\mathbf{u} - \Pi_{\mathcal{V}_h}^0 \mathbf{u}\|_{\mathbf{H}^1(\Omega)}^2 \quad (74)$$

$$T_3 = 2\nu \sum_{F \in \Gamma_h} h_F \|(\nabla^s (\mathbf{u} - \Pi_{\mathcal{V}_h}^0 \mathbf{u})) \mathbf{n}\|_{(L^2(F))^d}^2 \quad (75)$$

$$T_4 = 2\nu \sum_{F \in \Gamma_h} C_{pen} h_F^{-1} \|\mathbf{u} - \Pi_{\mathcal{V}_h}^0 \mathbf{u}\|_{(L^2(F))^d}^2. \quad (76)$$

To handle the face integral in (75), we recruit the multiplicative trace inequality for fractional Sobolev spaces [57] and Young's inequality element-wise to obtain the bound

$$\begin{aligned} &\sum_{F \in \Gamma_h} C_{pen} h_F \|(\nabla^s (\mathbf{u} - \Pi_{\mathcal{V}_h}^0 \mathbf{u})) \mathbf{n}\|_{(L^2(F))^d}^2 \leq \\ &(C_{trc,1})^2 \sum_{K \in \mathcal{K}_h} \left(\|\mathbf{u} - \Pi_{\mathcal{V}_h}^0 \mathbf{u}\|_{\mathbf{H}^1(K)}^2 + h_K^{2q} \|\mathbf{u} - \Pi_{\mathcal{V}_h}^0 \mathbf{u}\|_{\mathbf{H}^{q+1}(\Omega)}^2 \right) \end{aligned}$$

where $1/2 < q \leq s$ and $C_{trc,1}$ is a positive constant independent of h , σ , ν , and C_{pen} . To handle the face integral in (76), we recruit the standard continuous trace

inequality element-wise to obtain the bound

$$\sum_{F \in \Gamma_h} C_{pen} h_F^{-1} \|\mathbf{u} - \Pi_{\mathcal{V}_h}^0 \mathbf{u}\|_{(L^2(F))^d}^2 \leq (C_{trc,2})^2 \sum_{K \in \mathcal{K}_h} \left(h_K^{-2} \|\mathbf{u} - \Pi_{\mathcal{V}_h}^0 \mathbf{u}\|_{\mathbf{L}^2(K)}^2 + \|\mathbf{u} - \Pi_{\mathcal{V}_h}^0 \mathbf{u}\|_{\mathbf{H}^1(K)}^2 \right)$$

where $C_{trc,2}$ is a positive constant independent of h , σ , and ν which varies linearly with the square root of C_{pen} . It should be noted the two constants $C_{trc,1}$ and $C_{trc,2}$ necessarily depend on the shape regularity of the mesh family $\{\mathcal{Q}\}_{h \leq h_0}$ and the parametric mapping which together give the shape regularity of the mesh family $\{\mathcal{K}\}_{h \leq h_0}$. See [26] for more details. Inserting the above two inequalities into (72) and then applying Proposition 5.5, we immediately acquire the bound

$$\|\mathbf{u} - \Pi_{\mathcal{V}_h}^0 \mathbf{u}\|_{\mathcal{V}(h)} \leq C_{\mathbf{u}} C_{co} \sqrt{\sigma h^{2s+2} + 2\nu h^{2s}} \|\mathbf{u}\|_{\mathbf{H}^{s+1}(\Omega)}$$

for $C_{\mathbf{u}}$ a positive constant independent of h , σ , and ν with the same functional dependency on the penalty parameter as $C_{trc,2}$.

The proof for (71) is much more immediate. Choosing $q_h = \Pi_{\mathcal{Q}_h}^0 p$ in the error estimate given by (66), one obtains

$$\|p - p_h\|_{\mathcal{Q}} \leq \left(1 + \frac{1}{\tilde{\beta}}\right) \|p - \Pi_{\mathcal{Q}_h}^0 p\|_{\mathcal{Q}} + \frac{C_{cont}}{\tilde{\beta}} \|\mathbf{u} - \mathbf{u}_h\|_{\mathcal{V}(h)}.$$

Inequality (71) follows by an application of Proposition 5.5 to bound the pressure interpolation error. \square

Since we have the bound

$$2\nu |\cdot|_{\mathbf{H}^1(\Omega)} \lesssim \|\cdot\|_{\mathcal{V}(h)},$$

the above theorem also provides optimal convergence rates for the velocity field in the \mathbf{H}^1 -norm. If we assume slightly more regularity for the pressure space, we have the following proposition.

Proposition 6.1. *Let (\mathbf{u}, p) and (\mathbf{u}_h, p_h) denote the unique solutions of Problems (W) and (G) respectively. Furthermore, assume that $(\mathbf{u}, p) \in \mathbf{H}^{j+1}(\Omega) \times H^{j+1}(\Omega)$ for some $j > 1/2$ and that the assumptions of Lemma 6.3 hold true. Then*

$$\|p - p_h\|_{\mathcal{Q}} \leq C_{p,e} \left(1 + \frac{1}{\tilde{\beta}}\right) (\sigma + 2\nu)^{-1/2} h^{s+1} \|p\|_{H^{s+1}(\Omega)} + \frac{C_{cont}}{\tilde{\beta}} \|\mathbf{u} - \mathbf{u}_h\|_{\mathcal{V}(h)} \quad (77)$$

for $s = \min\{k', j\}$ where $C_{p,e}$ is a positive constant independent of h , σ , ν , and C_{pen} .

Observe that the pressure error estimate given by the above proposition is still suboptimal due to the presence of the velocity error, which converges with order s for general viscous flows. Let us further note that the preceding theorem and proposition are trivially extended to the setting of vanishing viscosity. In this case, the velocity error actually converges with order $s + 1$, giving optimal *a priori* error estimates for both the discrete pressure field and discrete velocity field for incompressible Darcy flow.

Under an elliptic regularity assumption, we can obtain optimal estimates for the velocity field in the \mathbf{L}^2 -norm by utilizing a standard duality argument. Given the unique solutions (\mathbf{u}, p) and (\mathbf{u}_h, p_h) of Problems (W) and (G), let us consider the following ancillary problem, written in strong form.

$$(A) \left\{ \begin{array}{ll} \text{Find } (\boldsymbol{\psi}, r) \in \mathbf{H}_0^1(\Omega) \times L_0^2(\Omega) \text{ such that} & \\ \sigma \boldsymbol{\psi} - \nabla \cdot (2\nu \nabla^s \boldsymbol{\psi}) + \mathbf{grad} r = \mathbf{u} - \mathbf{u}_h & \text{in } \Omega \quad (78) \\ \operatorname{div} \boldsymbol{\psi} = 0 & \text{in } \Omega \quad (79) \\ \boldsymbol{\psi} = \mathbf{0} & \text{on } \partial\Omega. \quad (80) \end{array} \right.$$

The above problem has a unique weak solution $(\boldsymbol{\psi}, r)$. Before proceeding, note that we can formally take the divergence of (78) to obtain

$$\Delta r = 0, \quad \text{in } \Omega. \quad (81)$$

Since r has zero average, it follows, at least from our formal argument, that $r = 0$. This argument can be made rigorous by a suitable use of convolutions and passing to the limit. Now suppose that $\boldsymbol{\psi} \in \mathbf{H}^2(\Omega)$. We can then multiply the left and right hand sides of (78) by $\sigma \boldsymbol{\psi} + \nabla \cdot (2\nu \nabla^s \boldsymbol{\psi})$ to acquire the result

$$\|\sigma \boldsymbol{\psi}\|_{\mathbf{L}^2(\Omega)}^2 + \|\nabla \cdot (2\nu \nabla^s \boldsymbol{\psi})\|_{\mathbf{L}^2(\Omega)}^2 = (\mathbf{u} - \mathbf{u}_h, \sigma \boldsymbol{\psi} + \nabla \cdot (2\nu \nabla^s \boldsymbol{\psi}))_{\mathbf{L}^2(\Omega)}. \quad (82)$$

A simple application of Cauchy-Schwarz and the triangle inequality gives

$$\begin{aligned} & \|\sigma \boldsymbol{\psi}\|_{\mathbf{L}^2(\Omega)}^2 + \|\nabla \cdot (2\nu \nabla^s \boldsymbol{\psi})\|_{\mathbf{L}^2(\Omega)}^2 = \\ & \|\mathbf{u} - \mathbf{u}_h\|_{\mathbf{L}^2(\Omega)} (\|\sigma \boldsymbol{\psi}\|_{\mathbf{L}^2(\Omega)} + \|\nabla \cdot (2\nu \nabla^s \boldsymbol{\psi})\|_{\mathbf{L}^2(\Omega)}) \end{aligned} \quad (83)$$

Since $x^2 + y^2 \geq \frac{1}{2}(x + y)^2$, we can divide both sides by $\|\sigma \boldsymbol{\psi}\|_{\mathbf{L}^2(\Omega)} + \|\nabla \cdot (2\nu \nabla^s \boldsymbol{\psi})\|_{\mathbf{L}^2(\Omega)}$ to obtain

$$\frac{1}{2} (\|\sigma \boldsymbol{\psi}\|_{\mathbf{L}^2(\Omega)} + \|\nabla \cdot (2\nu \nabla^s \boldsymbol{\psi})\|_{\mathbf{L}^2(\Omega)}) \leq \|\mathbf{u} - \mathbf{u}_h\|_{\mathbf{L}^2(\Omega)}. \quad (84)$$

As $\boldsymbol{\psi}$ satisfies normal and tangential homogeneous Dirichlet boundary conditions and ν is assumed positive, we can employ a combination of Korn's inequalities and Poincaré inequalities to obtain a standard elliptic regularity result of the form

$$\|\boldsymbol{\psi}\|_{\mathbf{H}^2(\Omega)} \leq C_A \nu^{-1} \|\mathbf{u} - \mathbf{u}_h\|_{\mathbf{L}^2(\Omega)}. \quad (85)$$

where C_A is a positive constant which only depends on the domain Ω . In view of the above discussion, we have the following theorem.

Theorem 6.3. *Let (\mathbf{u}, p) and (\mathbf{u}_h, p_h) denote the unique solutions of Problems (W) and (G) respectively, and let $(\boldsymbol{\psi}, r)$ denote the unique solution of Problem (A). Furthermore, assume that $(\mathbf{u}, p) \in \mathbf{H}^{j+1}(\Omega) \times H^j(\Omega)$ for some $j \geq 1$, that $\boldsymbol{\psi} \in \mathbf{H}^2(\Omega)$, and that the assumptions of Lemma 6.3 hold true. Then*

$$\|\mathbf{u} - \mathbf{u}_h\|_{\mathbf{L}^2(\Omega)} \leq C_l h^{s+1} \|\mathbf{u}\|_{\mathbf{H}^{s+1}(\Omega)} \quad (86)$$

for $s = \min\{k', j\}$ where C_l is a positive constant independent of h , σ , and ν which asymptotically scales with the square root of C_{pen} .

Proof. Since by assumption $(\boldsymbol{\psi}, r) \in \mathbf{H}^2(\Omega) \times H^1(\Omega)$, consistency and symmetry give

$$a_h(\mathbf{v}, \boldsymbol{\psi}) - b(r, \mathbf{v}) = (\mathbf{u} - \mathbf{u}_h, \mathbf{v})_{\mathbf{L}^2(\Omega)}$$

for all $\mathbf{v} \in \mathcal{V}_h$. Let us take $\mathbf{v} = \mathbf{u} - \mathbf{u}_h$. We then have

$$\|\mathbf{u} - \mathbf{u}_h\|_{\mathbf{L}^2(\Omega)}^2 = a_h(\mathbf{u} - \mathbf{u}_h, \boldsymbol{\psi}).$$

as $\operatorname{div}(\mathbf{u} - \mathbf{u}_h) = 0$ (or $r = 0$ by our preceding discussion). By using the orthogonality given by Corollary 6.1, we can write

$$\begin{aligned} \|\mathbf{u} - \mathbf{u}_h\|_{\mathbf{L}^2(\Omega)}^2 &= a_h(\mathbf{u} - \mathbf{u}_h, \boldsymbol{\psi} - \Pi_{\mathcal{V}_h}^0 \boldsymbol{\psi}) \\ &\leq C_{cont} \|\mathbf{u} - \mathbf{u}_h\|_{\mathcal{V}(h)} \|\boldsymbol{\psi} - \Pi_{\mathcal{V}_h}^0 \boldsymbol{\psi}\|_{\mathcal{V}(h)}. \end{aligned} \quad (87)$$

We bound the interpolation error by utilizing a similar argument to that used to prove (77), obtaining

$$\|\boldsymbol{\psi} - \Pi_{\mathcal{V}_h}^0 \boldsymbol{\psi}\|_{\mathcal{V}(h)} \leq C_{interp} (\sigma^{1/2} h^2 + \nu^{1/2} h) \|\boldsymbol{\psi}\|_{\mathbf{H}^2(\Omega)}$$

for C_{interp} a positive constant independent of h , σ , and ν which asymptotically scales with the the square root of C_{pen} . We can now employ the elliptic regularity condition (85) to arrive at

$$\|\boldsymbol{\psi} - \Pi_{\mathcal{V}_h}^0 \boldsymbol{\psi}\|_{\mathcal{V}(h)} \leq C_A C_{interp} (\sigma^{1/2} \nu^{-1} h^2 + \nu^{-1/2} h) \|\mathbf{u} - \mathbf{u}_h\|_{\mathbf{L}^2(\Omega)}. \quad (88)$$

Inserting (88) into (87) results in

$$\|\mathbf{u} - \mathbf{u}_h\|_{\mathbf{L}^2(\Omega)} \leq C_A C_{interp} C_{cont} (\sigma^{1/2} \nu^{-1} h^2 + \nu^{-1/2} h) \|\mathbf{u} - \mathbf{u}_h\|_{\mathcal{V}(h)}.$$

Immediately invoking the error estimate given by Theorem 6.2, we obtain

$$\|\mathbf{u} - \mathbf{u}_h\|_{\mathbf{L}^2(\Omega)} \leq C_{temp} \left(1 + \sqrt{Da_h}\right)^2 h^{s+1} \|\mathbf{u}\|_{\mathbf{H}^{s+1}(\Omega)} \quad (89)$$

where C_{temp} is a positive constant independent of h , σ , and ν which asymptotically scales with the square root of C_{pen} and

$$Da_h = \frac{\sigma h^2}{\nu}.$$

However, we also have the following estimate due to Theorem 6.2:

$$\|\mathbf{u} - \mathbf{u}_h\|_{\mathbf{L}^2(\Omega)} \leq C_{\mathbf{u}} \left(1 + \frac{C_{cont}}{C_{coerc}}\right) (1 + (Da_h)^{-1})^{1/2} h^{s+1} \|\mathbf{u}\|_{\mathbf{H}^{s+1}(\Omega)}. \quad (90)$$

The desired result follows by taking the minimum of (89) and (90). \square

This concludes our *a priori* error analysis. Note that, for reasonably regular exact solutions, we have obtained optimal estimates for the velocity field in both the strong $\mathcal{V}(h)$ -norm as well as the weaker \mathbf{H}^1 - and \mathbf{L}^2 -norms. The estimates are additionally robust with respect to the fluid coefficients σ and ν . On the other hand, we have obtained pressure error estimates which are suboptimal by one order. This is reminiscent of error estimates for stabilized equal-order interpolations of the Stokes equations and is not unexpected as both our discrete velocity and pressure spaces consist of mapped piecewise polynomials which are only complete up to degree k' . However, our later numerical studies suggest the conservative nature of these estimates by revealing, for simple model problems, optimal convergence rates for the pressure field. Ongoing work is being dedicated to the theoretical confirmation of these convergence rates. Note that our analysis covers typical singular solutions of the generalized Stokes equations. Later in this chapter, we will numerically study the effectiveness of our method for a selection of singular Stokes problems. Finally, we would like to mention that our velocity error estimates are completely independent of the pressure field. This property does not hold for discretizations which preserve the incompressibility in only a discrete sense.

Remark 6.3. *In opposition to standard Bubnov-Galerkin methods, the constant*

$$(1 + C_{cont} (C_{coerc})^{-1})$$

appearing in (65) cannot be reduced to just $C_{cont} (C_{coerc})^{-1}$.

Remark 6.4. *At this point, suitable requirements guaranteeing elliptic regularity for domains obtained by NURBS mappings are unknown. One anticipates that such requirements should be less stringent than those associated with polyhedral domains (namely, convexity) because of enhanced smoothness. In our view, this is an interesting area of research.*

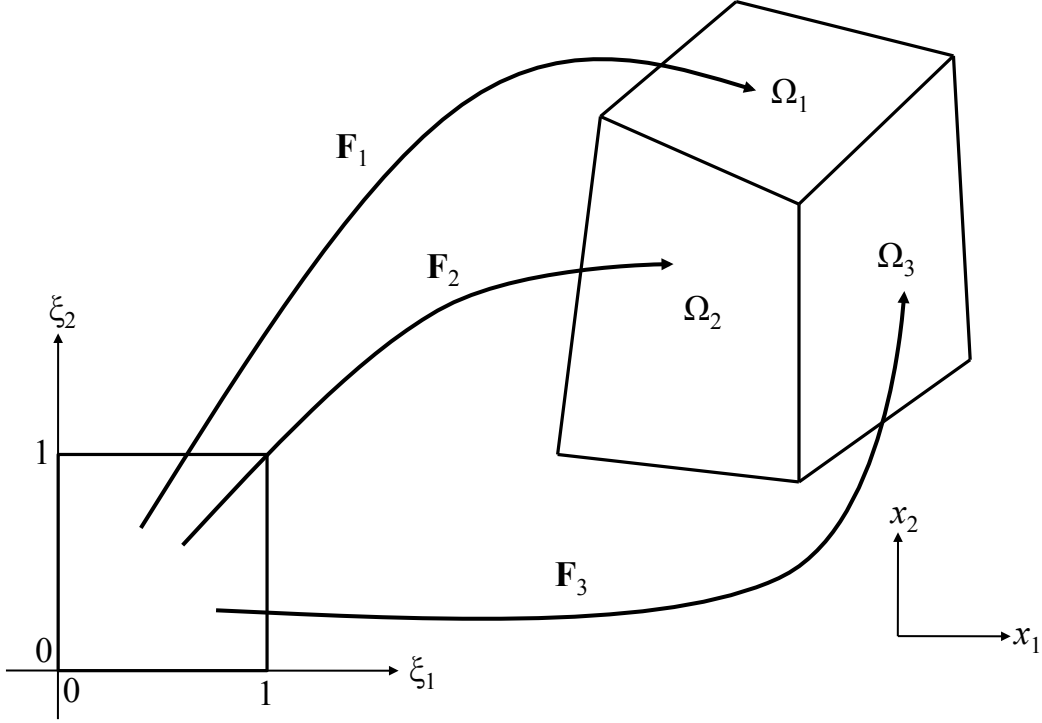


Figure 8: Example multi-patch construction in \mathbb{R}^2 .

7 Extension to Multi-Patch Domains

As was mentioned previously in Subsection 4.3, most geometries of scientific and engineering interest cannot be represented by a single patch. Instead, the multi-patch concept must be invoked. We assume that there exist n_p sufficiently smooth parametric mappings $\mathbf{F}_i : (0, 1)^d \rightarrow \mathbb{R}^d$ such that the subdomains

$$\Omega_i = \mathbf{F}_i \left(\widehat{\Omega} \right), \quad i = 1, \dots, n_p$$

are non-overlapping and

$$\overline{\Omega} = \cup_{i=1}^{n_p} \overline{\Omega_i}.$$

We refer to each subdomain Ω_i (and its pre-image) as a patch. For a visual depiction of a multi-patch construction in \mathbb{R}^2 , see Figure 8. We build discrete velocity and pressure spaces over each patch Ω_i , $i = 1, \dots, n_p$ in the same manner as in the previous sections except that we do not yet enforce boundary conditions, and we denote these spaces as $\mathcal{V}_h(\Omega_i)$ and $\mathcal{Q}_h(\Omega_i)$.

To proceed further, we must make some assumptions. First of all, we assume that if two disjoint patches Ω_i and Ω_j have the property that $\partial\Omega_i \cap \partial\Omega_j \neq \emptyset$, then this intersection consists strictly of patch faces, edges, and corners. More succinctly, two patches cannot intersect along an isolated portion of a face (or edge) interior. Second,

we assume that the mappings $\{\mathbf{F}_i\}_{i=1}^{n_p}$ are compatible in the following sense: if two patches Ω_i and Ω_j share a face, then \mathbf{F}_i and \mathbf{F}_j parametrize that face identically up to changes in orientation. Third, we assume that if two patches Ω_i and Ω_j share a face, the B-spline meshes associated with the patches are identical along that face. This guarantees our mesh is conforming. Finally, we assume for simplicity that $k_1 = \dots = k_d = k^*$ for all patches. The mixed polynomial degree case introduces additional complications that are beyond the scope of this work. We would like to note that all four assumptions hold if we employ a conforming NURBS multi-patch construction. See, for example, Chapter 2 of [20].

We define our global discrete velocity and pressure spaces as follows:

$$\mathcal{V}_{0,h} := \{\mathbf{v}_h \in \mathbf{H}_0(\text{div}; \Omega) : \mathbf{v}_h|_{\Omega_i} \in \mathcal{V}_h(\Omega_i), \forall i = 1, \dots, n_p\}, \quad (91)$$

$$\mathcal{Q}_{0,h} := \{q_h \in L_0^2(\Omega) : q_h|_{\Omega_i} \in \mathcal{Q}_h(\Omega_i), \forall i = 1, \dots, n_p\}. \quad (92)$$

The space $\mathcal{V}_{0,h}$ is easily constructed due to our preceding four assumptions and use of open knot vectors. Specifically, we set to zero the coefficient of any basis function whose normal is nonzero along $\partial\Omega$, and along shared faces between patches, we (i) equivalence the coefficients of any basis functions whose normal values are nonzero and equal in magnitude and direction and (ii) set opposite the coefficients of any basis functions whose normal values are nonzero, equal in magnitude, and opposite in direction. We note that this is precisely the same procedure as is used to construct Raviart-Thomas spaces on conforming finite element meshes. We simply have patches instead of elements. It is easily shown that the spaces $\mathcal{V}_{0,h}$ and $\mathcal{Q}_{0,h}$, along with the divergence operator, form the bounded discrete cochain complex

$$\mathcal{V}_{0,h} \xrightarrow{\text{div}} \mathcal{Q}_{0,h}.$$

However, functions in $\mathcal{V}_{0,h}$ do not necessarily lie in $\mathbf{H}^1(\Omega)$ as tangential continuity is not enforced across patch interfaces. Hence, we need to account for this lack of continuity when designing a discretization scheme for the generalized Stokes equations. We employ the symmetric interior penalty method [1, 24, 62], a standard technique in the discontinuous Galerkin community, to weakly enforce tangential continuity between adjacent patches.

We now establish some preliminary notation. Let $\mathcal{K}_h(\Omega_i)$ and $\mathcal{F}_h(\Omega_i)$ denote the sets of physical mesh elements and faces associated with patch Ω_i . We denote the global set of mesh elements as \mathcal{K}_h and the global set of mesh faces as \mathcal{F}_h . As in the single patch setting, we define the boundary mesh to be

$$\Gamma_h = \{F \in \mathcal{F}_h(\Omega_i), i = 1, \dots, n_p : F \subset \partial\Omega\}, \quad (93)$$

and we define the interface mesh to be

$$\mathcal{I}_h = \{F \in \mathcal{F}_h(\Omega_i), i = 1, \dots, n_p : F \in \mathcal{F}_h(\Omega_j), i \neq j \text{ and } F \notin \Gamma_h\}. \quad (94)$$

For each face $F \in \mathcal{I}_h$ belonging to the interface mesh, there exist two unique adjacent elements $K^+, K^- \in \mathcal{K}_h$ such that $F \in \partial K^+$ and $F \in \partial K^-$. We define for such a face the mesh size

$$h_F := \frac{1}{2} (h_{K^+} + h_{K^-}). \quad (95)$$

Let ϕ be an arbitrary scalar-, vector-, or matrix-valued piecewise smooth function, and let us denote by ϕ^+ and ϕ^- the traces of ϕ on F as taken from within the interior of K^+ and K^- respectively. We define the mean value of ϕ at $\mathbf{x} \in F$ as

$$\{\!\!\{\phi}\!\!\} := \frac{1}{2} (\phi^+ + \phi^-). \quad (96)$$

Further, for a generic multiplication operator \odot , we define the jump of $\phi \odot \mathbf{n}$ at $\mathbf{x} \in F$ as

$$[\![\phi \odot \mathbf{n}]\!] := \phi^+ \odot \mathbf{n}_{K^+} + \phi^- \odot \mathbf{n}_{K^-} \quad (97)$$

where $\mathbf{n}_{K^{+/-}}$ denotes the outward facing normal on the boundary $\partial K^{+/-}$ of element $K^{+/-}$.

With the above notation established, let us define the following bilinear form:

$$\begin{aligned} a_h^*(\mathbf{w}, \mathbf{v}) = & \sum_{i=1}^{n_p} \left((2\nu \nabla^s \mathbf{w}, \nabla^s \mathbf{v})_{(L^2(\Omega_i))^{d \times d}} + (\sigma \mathbf{w}, \mathbf{v})_{\mathbf{L}^2(\Omega_i)} \right) \\ & - \sum_{F \in \mathcal{I}_h} \int_F 2\nu (\{\!\!\{\nabla^s \mathbf{v}\}\!\!\} : [\![\mathbf{w} \otimes \mathbf{n}]\!] + \{\!\!\{\nabla^s \mathbf{w}\}\!\!\} : [\![\mathbf{v} \otimes \mathbf{n}]\!]) \, ds \\ & + \sum_{F \in \mathcal{I}_h} \int_F 2\nu \left(\frac{2C_{pen}}{h_F} [\![\mathbf{w} \otimes \mathbf{n}]\!] : [\![\mathbf{v} \otimes \mathbf{n}]\!] \right) \, ds \\ & - \sum_{F \in \Gamma_h} \int_F 2\nu \left(((\nabla^s \mathbf{v}) \mathbf{n}) \cdot \mathbf{w} + ((\nabla^s \mathbf{w}) \mathbf{n}) \cdot \mathbf{v} - \frac{C_{pen}}{h_F} \mathbf{w} \cdot \mathbf{v} \right) \, ds. \end{aligned} \quad (98)$$

Above, $C_{pen} > 0$ denotes the same positive penalty constant as before. Our discrete formulation over the multi-patch domain then reads as follows.

$$(MP) \left\{ \begin{array}{l} \text{Find } \mathbf{u}_h \in \mathcal{V}_{0,h} \text{ and } p_h \in \mathcal{Q}_{0,h} \text{ such that} \\ \quad a_h^*(\mathbf{u}_h, \mathbf{v}_h) - b(p_h, \mathbf{v}_h) + b(q_h, \mathbf{u}_h) = (\mathbf{f}, \mathbf{v}_h)_{\mathbf{L}^2(\Omega)} \\ \text{for all } \mathbf{v}_h \in \mathcal{V}_{0,h} \text{ and } q_h \in \mathcal{Q}_{0,h}. \end{array} \right. \quad (99)$$

As in the single patch setting, the discrete formulation detailed above returns a point-wise divergence-free velocity field. However, we do not have a convergence analysis available as we do not yet have a multi-patch analogue of Proposition 5.2. We anticipate this will take new theoretical developments. Nonetheless, we have utilized the above formulation in practice and observed it returns optimal convergence rates for both velocity and pressure fields.

8 Numerical Verification of Convergence Estimates

In this section, we numerically verify our convergence estimates using a collection of problems with exact solutions. Throughout, we choose Nitsche's penalty constant as

$$C_{pen} = 5(k' + 1)$$

where k' is the polynomial degree of a given discretization. We have found that this choice leads to stable numerical formulations for the generalized Stokes equations. Furthermore, unless otherwise specified, we employ uniform parametric meshes, linear parametric mappings, and B-spline spaces of maximal continuity.

8.1 Two-Dimensional Manufactured Solution

As a first numerical experiment, we consider a two-dimensional manufactured solution that was originally presented in [14]. Let

$$\Omega \equiv (0, 1)^2$$

and

$$\mathbf{f} \equiv \sigma \bar{\mathbf{u}} - \nabla \cdot (2\nu \nabla^s \bar{\mathbf{u}}) + \nabla \bar{p}$$

with

$$\bar{\mathbf{u}} = \begin{bmatrix} 2e^x(-1+x)^2x^2(y^2-y)(-1+2y) \\ (-e^x(-1+x)x(-2+x(3+x))(-1+y)^2y^2) \end{bmatrix}$$

and

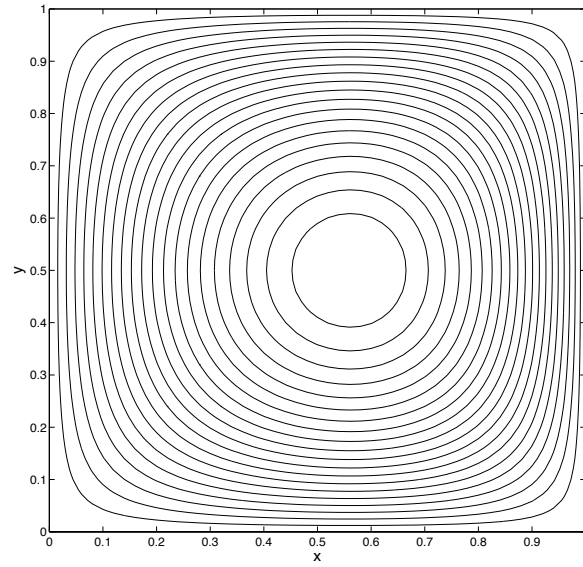
$$\begin{aligned} \bar{p} = & (-424 + 156e + (y^2 - y)(-456 + e^x(456 + x^2(228 - 5(y^2 - y)) + \\ & 2x(-228 + (y^2 - y)) + 2x^3(-36 + (y^2 - y)) + x^4(12 + (y^2 - y))))). \end{aligned}$$

Homogeneous boundary conditions are applied along the boundary $\partial\Omega$, and the pressure is enforced to satisfy $\int_{\Omega} p d\mathbf{x} = 0$. The unique solution to the generalized Stokes equation with the prescribed forcing is then clearly $(\mathbf{u}, p) = (\bar{\mathbf{u}}, \bar{p})$. The streamlines and pressure contours associated with the exact solution are plotted in Figure 9. Note from the streamline plot that the velocity solution has a simple vortex structure.

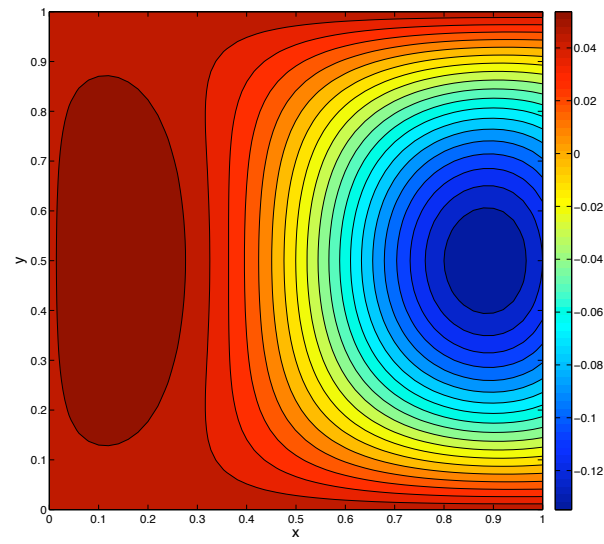
For the above constructed solution, we have computed convergence rates for divergence-conforming B-spline discretizations of varying mesh size and polynomial degree. Furthermore, we have computed convergence rates for a variety of Damköhler numbers

$$Da = \frac{\sigma L^2}{\nu}$$

where L is a length parameter which we henceforth specify as one. These convergence rates are provided in Tables 2, 3, and 4. Note immediately from the tables that our theoretically derived error estimates are confirmed. Second, note that the L^2 -norm of the pressure error optimally converges like $O(h^{k'+1})$, which is an improvement



(a)



(b)

Figure 9: Generalized Stokes manufactured solution in 2-D: (a) Flow velocity streamlines, (b) Pressure contours.

Table 2: Generalized Stokes convergence rates in 2-D: $Da = 0$

Polynomial degree $k' = 1$

h	1/4	1/8	1/16	1/32	1/64
$\ \mathbf{u} - \mathbf{u}_h\ _{\mathcal{V}(h)}$	7.75e-2	3.96e-2	1.98e-2	9.90e-3	4.95e-3
order	-	0.97	1.00	1.00	1.00
$ \mathbf{u} - \mathbf{u}_h _{\mathbf{H}^1(\Omega)}$	5.48e-2	2.80e-2	1.40e-2	7.00e-3	3.50e-3
order	-	0.97	1.00	1.00	1.00
$\ \mathbf{u} - \mathbf{u}_h\ _{\mathbf{L}^2(\Omega)}$	2.77e-3	8.16e-4	2.28e-4	6.10e-5	1.58e-5
order	-	1.76	1.84	1.90	1.95
$\ p - p_h\ _{L^2(\Omega)}$	5.04e-3	1.38e-3	3.49e-4	8.72e-5	2.18e-5
order	-	1.87	1.98	2.00	2.00

Polynomial degree $k' = 2$

h	1/4	1/8	1/16	1/32	1/64
$\ \mathbf{u} - \mathbf{u}_h\ _{\mathcal{V}(h)}$	1.37e-2	3.30e-3	8.03e-4	1.98e-4	4.92e-5
order	-	2.06	2.04	2.02	2.01
$ \mathbf{u} - \mathbf{u}_h _{\mathbf{H}^1(\Omega)}$	9.70e-3	2.33e-3	5.68e-4	1.40e-4	3.48e-5
order	-	2.06	2.04	2.02	2.01
$\ \mathbf{u} - \mathbf{u}_h\ _{\mathbf{L}^2(\Omega)}$	2.94e-4	3.84e-5	5.03e-6	6.47e-7	8.21e-8
order	-	2.94	2.93	2.96	2.98
$\ p - p_h\ _{L^2(\Omega)}$	1.18e-3	1.19e-4	1.17e-5	1.19e-6	1.27e-7
order	-	3.31	3.35	3.30	3.23

Polynomial degree $k' = 3$

h	1/4	1/8	1/16	1/32	1/64
$\ \mathbf{u} - \mathbf{u}_h\ _{\mathcal{V}(h)}$	1.39e-3	1.81e-4	2.33e-5	3.01e-6	3.85e-7
order	-	2.94	2.96	2.95	2.97
$ \mathbf{u} - \mathbf{u}_h _{\mathbf{H}^1(\Omega)}$	9.83e-4	1.28e-4	1.65e-5	2.10e-6	2.66e-7
order	-	2.94	2.96	2.97	2.98
$\ \mathbf{u} - \mathbf{u}_h\ _{\mathbf{L}^2(\Omega)}$	3.05e-5	2.34e-6	1.59e-7	1.03e-8	6.55e-10
order	-	3.70	3.88	3.95	3.98
$\ p - p_h\ _{L^2(\Omega)}$	1.10e-4	5.64e-6	3.45e-7	2.19e-8	1.39e-9
order	-	4.29	4.03	3.98	3.98

Table 3: Generalized Stokes convergence rates in 2-D: $Da = 1$

Polynomial degree $k' = 1$

h	1/4	1/8	1/16	1/32	1/64
$\ \mathbf{u} - \mathbf{u}_h\ _{\mathcal{V}(h)}$	7.75e-2	3.96e-2	1.98e-2	9.90e-3	4.95e-3
order	-	0.97	1.00	1.00	1.00
$ \mathbf{u} - \mathbf{u}_h _{\mathbf{H}^1(\Omega)}$	5.47e-2	2.80e-2	1.40e-2	7.00e-3	3.50e-3
order	-	0.97	1.00	1.00	1.00
$\ \mathbf{u} - \mathbf{u}_h\ _{\mathbf{L}^2(\Omega)}$	2.75e-3	8.09e-4	2.26e-4	6.05e-5	1.57e-5
order	-	1.76	1.84	1.90	1.95
$\ p - p_h\ _{L^2(\Omega)}$	5.04e-3	1.37e-3	3.48e-4	8.72e-5	2.18e-5
order	-	1.88	1.98	2.00	2.00

Polynomial degree $k' = 2$

h	1/4	1/8	1/16	1/32	1/64
$\ \mathbf{u} - \mathbf{u}_h\ _{\mathcal{V}(h)}$	1.37e-2	3.30e-3	8.03e-4	1.98e-4	4.92e-5
order	-	2.06	2.04	2.02	2.01
$ \mathbf{u} - \mathbf{u}_h _{\mathbf{H}^1(\Omega)}$	9.70e-3	2.33e-3	5.68e-4	1.40e-4	3.48e-5
order	-	2.06	2.04	2.02	2.01
$\ \mathbf{u} - \mathbf{u}_h\ _{\mathbf{L}^2(\Omega)}$	2.94e-4	3.84e-5	5.03e-6	6.47e-7	8.21e-8
order	-	2.94	2.93	2.96	2.98
$\ p - p_h\ _{L^2(\Omega)}$	1.18e-3	1.19e-4	1.17e-5	1.19e-6	1.27e-7
order	-	3.31	3.35	3.30	3.23

Polynomial degree $k' = 3$

h	1/4	1/8	1/16	1/32	1/64
$\ \mathbf{u} - \mathbf{u}_h\ _{\mathcal{V}(h)}$	1.39e-3	1.81e-4	2.35e-5	3.01e-6	3.85e-7
order	-	2.94	2.95	2.96	2.97
$ \mathbf{u} - \mathbf{u}_h _{\mathbf{H}^1(\Omega)}$	9.83e-4	1.28e-4	1.65e-5	2.10e-6	2.66e-7
order	-	2.94	2.96	2.97	2.98
$\ \mathbf{u} - \mathbf{u}_h\ _{\mathbf{L}^2(\Omega)}$	3.05e-5	2.34e-6	1.59e-7	1.03e-8	6.55e-10
order	-	3.70	3.88	3.95	3.98
$\ p - p_h\ _{L^2(\Omega)}$	1.10e-4	5.64e-6	3.45e-7	2.19e-8	1.39e-9
order	-	4.29	4.03	3.98	3.98

Table 4: Generalized Stokes convergence rates in 2-D: $Da = 1000$

Polynomial degree $k' = 1$

h	1/4	1/8	1/16	1/32	1/64
$\ \mathbf{u} - \mathbf{u}_h\ _{\mathcal{V}(h)}$	3.13e-3	1.33e-3	6.36e-4	3.14e-4	1.57e-4
order	-	1.23	1.06	1.02	1.00
$ \mathbf{u} - \mathbf{u}_h _{\mathbf{H}^1(\Omega)}$	5.50e-2	2.78e-2	1.39e-2	6.98e-3	3.49e-3
order	-	0.98	1.00	0.99	1.00
$\ \mathbf{u} - \mathbf{u}_h\ _{\mathbf{L}^2(\Omega)}$	1.93e-3	4.79e-4	1.22e-4	3.20e-5	8.38e-6
order	-	2.01	1.97	1.93	1.93
$\ p - p_h\ _{L^2(\Omega)}$	3.37e-3	7.97e-4	1.96e-4	4.89e-5	1.22e-5
order	-	2.08	2.02	2.00	2.00

Polynomial degree $k' = 2$

h	1/4	1/8	1/16	1/32	1/64
$\ \mathbf{u} - \mathbf{u}_h\ _{\mathcal{V}(h)}$	5.24e-4	1.11e-4	2.58e-5	6.30e-6	1.55e-6
order	-	2.24	2.11	2.03	2.02
$ \mathbf{u} - \mathbf{u}_h _{\mathbf{H}^1(\Omega)}$	9.85e-3	2.32e-3	5.67e-4	1.40e-4	3.48e-5
order	-	2.08	2.03	2.02	2.01
$\ \mathbf{u} - \mathbf{u}_h\ _{\mathbf{L}^2(\Omega)}$	2.83e-4	3.80e-5	5.01e-6	6.46e-7	8.21e-8
order	-	2.90	2.92	2.96	2.98
$\ p - p_h\ _{L^2(\Omega)}$	4.69e-4	5.36e-5	6.42e-6	7.97e-7	9.98e-8
order	-	3.13	3.06	3.01	3.00

Polynomial degree $k' = 3$

h	1/4	1/8	1/16	1/32	1/64
$\ \mathbf{u} - \mathbf{u}_h\ _{\mathcal{V}(h)}$	5.31e-5	6.12e-6	7.57e-7	9.56e-8	1.22e-8
order	-	3.12	3.02	2.99	2.97
$ \mathbf{u} - \mathbf{u}_h _{\mathbf{H}^1(\Omega)}$	9.74e-4	1.26e-4	1.64e-5	2.10e-6	2.66e-7
order	-	2.95	2.94	2.97	2.98
$\ \mathbf{u} - \mathbf{u}_h\ _{\mathbf{L}^2(\Omega)}$	3.04e-5	2.33e-6	1.59e-7	1.03e-8	6.55e-10
order	-	3.71	3.89	3.95	3.98
$\ p - p_h\ _{L^2(\Omega)}$	7.56e-5	4.60e-6	3.19e-7	2.12e-8	1.37e-9
order	-	4.04	3.89	3.91	3.95

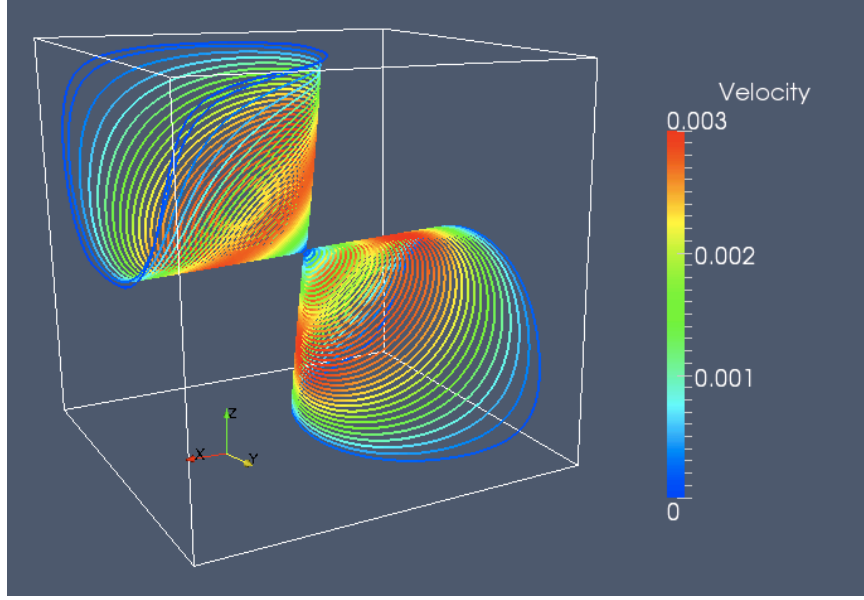


Figure 10: Generalized Stokes manufactured solution in 3-D: Flow velocity streamlines colored by velocity magnitude.

over our theoretically derived estimate. Third, note that our methodology is robust with respect to the Damköhler number. That is, the errors for our discretization are virtually independent of the Damköhler number. In fact, our pressure error decreases with increasing Damköhler number. Finally, it should be mentioned that (a) the \mathbf{H}^1 error of the velocity field approaches the \mathbf{H}^1 best approximation error as k' is increased, and (b) the L^2 error of the pressure field approaches the L^2 best approximation error as k' is increased.

8.2 Three-Dimensional Manufactured Solution

As a second numerical experiment, we consider a three-dimensional manufactured solution representing a vortical filament. Let

$$\Omega \equiv (0, 1)^3$$

and

$$\mathbf{f} \equiv \sigma \bar{\mathbf{u}} - \nabla \cdot (2\nu \nabla^s \bar{\mathbf{u}}) + \nabla \bar{p}$$

with

$$\bar{\mathbf{u}} = \mathbf{curl} \bar{\boldsymbol{\phi}},$$

$$\bar{\boldsymbol{\phi}} = \begin{bmatrix} x(x-1)y^2(y-1)^2z^2(z-1)^2 \\ 0 \\ x^2(x-1)^2y^2(y-1)^2z(z-1) \end{bmatrix},$$

Table 5: Generalized Stokes convergence rates in 3-D: $Da = 0$

Polynomial degree $k' = 1$					
h	1/2	1/4	1/8	1/16	1/32
$\ \mathbf{u} - \mathbf{u}_h\ _{V(h)}$	2.59e-2	1.27e-2	5.91e-3	2.81e-3	1.36e-3
order	-	1.03	1.10	1.07	1.05
$ \mathbf{u} - \mathbf{u}_h _{\mathbf{H}^1(\Omega)}$	1.51e-2	7.64e-3	3.77e-3	1.87e-3	9.34e-4
order	-	0.98	1.02	1.01	1.00
$\ \mathbf{u} - \mathbf{u}_h\ _{\mathbf{L}^2(\Omega)}$	1.35e-3	3.68e-4	1.03e-4	2.81e-5	7.40e-6
order	-	1.88	1.84	1.87	1.93
$\ p - p_h\ _{L^2(\Omega)}$	5.41e-2	1.48e-2	3.58e-3	8.85e-4	2.26e-4
order	-	1.87	2.05	2.02	1.97

Polynomial degree $k' = 2$					
h	1/2	1/4	1/8	1/16	1/32
$\ \mathbf{u} - \mathbf{u}_h\ _{V(h)}$	6.50e-3	1.54e-3	4.10e-4	9.51e-5	2.15e-5
order	-	2.08	1.91	2.11	2.15
$ \mathbf{u} - \mathbf{u}_h _{\mathbf{H}^1(\Omega)}$	3.71e-3	9.90e-4	2.79e-4	6.59e-5	1.50e-5
order	-	1.91	1.83	2.08	2.14
$\ \mathbf{u} - \mathbf{u}_h\ _{\mathbf{L}^2(\Omega)}$	1.97e-4	4.25e-5	7.38e-6	8.67e-7	9.18e-8
order	-	2.21	2.53	3.09	3.23
$\ p - p_h\ _{L^2(\Omega)}$	1.50e-2	1.59e-3	2.00e-4	2.56e-5	3.26e-6
order	-	3.24	2.99	2.97	2.97

and

$$\bar{p} = \sin(\pi x) \sin(\pi y) - \frac{4}{\pi^2}.$$

Again, homogeneous boundary conditions are applied along the boundary $\partial\Omega$, and the pressure is enforced to satisfy $\int_{\Omega} p d\mathbf{x} = 0$. The unique solution to the generalized Stokes equation with the prescribed forcing is then $(\mathbf{u}, p) = (\bar{\mathbf{u}}, \bar{p})$. Streamlines associated with the exact solution are plotted in Figure 10. Note that the streamlines wrap around a single diagonal vortex filament.

As in the two-dimensional setting, we have computed convergence rates for a variety of divergence-conforming B-spline discretizations and Damköhler numbers

$$Da = \frac{\sigma L^2}{\nu}$$

where L is a length parameter which we again specify as equal to one. These convergence rates are summarized in Tables 5, 6, and 7. Note immediately from the tables that our theoretically derived error estimates are confirmed. Second, note that the L^2 -norm of the pressure error optimally converges like $O(h^{k'+1})$, which is an improvement over our theoretically derived estimate. Third, note that our method is robust

Table 6: Generalized Stokes convergence rates in 3-D: $Da = 1$

Polynomial degree $k' = 1$

h	1/2	1/4	1/8	1/16	1/32
$\ \mathbf{u} - \mathbf{u}_h\ _{\mathcal{V}(h)}$	2.59e-2	1.28e-2	5.91e-3	2.81e-3	1.36e-3
order	-	1.02	1.11	1.07	1.05
$ \mathbf{u} - \mathbf{u}_h _{\mathbf{H}^1(\Omega)}$	1.51e-2	7.64e-3	3.77e-3	1.87e-3	9.33e-4
order	-	0.98	1.02	1.01	1.00
$\ \mathbf{u} - \mathbf{u}_h\ _{\mathbf{L}^2(\Omega)}$	1.34e-3	3.66e-4	1.02e-4	2.79e-5	7.34e-6
order	-	1.87	1.84	1.87	1.93
$\ p - p_h\ _{L^2(\Omega)}$	5.41e-2	1.48e-2	3.58e-3	8.85e-4	2.21e-4
order	-	1.87	2.05	2.02	2.00

Polynomial degree $k' = 2$

h	1/2	1/4	1/8	1/16	1/32
$\ \mathbf{u} - \mathbf{u}_h\ _{\mathcal{V}(h)}$	6.50e-3	1.54e-3	4.10e-4	9.50e-5	2.15e-5
order	-	2.08	1.91	2.11	2.14
$ \mathbf{u} - \mathbf{u}_h _{\mathbf{H}^1(\Omega)}$	3.71e-3	9.89e-4	2.79e-4	6.59e-5	1.50e-5
order	-	1.91	1.83	2.08	2.14
$\ \mathbf{u} - \mathbf{u}_h\ _{\mathbf{L}^2(\Omega)}$	1.97e-4	4.24e-5	7.38e-6	8.64e-7	9.18e-8
order	-	2.22	2.52	3.09	3.23
$\ p - p_h\ _{L^2(\Omega)}$	1.50e-2	1.59e-3	2.00e-4	2.56e-5	3.26e-6
order	-	3.24	2.99	2.97	2.97

Table 7: Generalized Stokes convergence rates in 3-D: $Da = 1000$

Polynomial degree $k' = 1$

h	1/2	1/4	1/8	1/16	1/32
$\ \mathbf{u} - \mathbf{u}_h\ _{\mathcal{V}(h)}$	1.55e-3	5.16e-4	2.04e-4	9.07e-5	4.32e-5
order	-	1.59	1.34	1.17	1.07
$ \mathbf{u} - \mathbf{u}_h _{\mathbf{H}^1(\Omega)}$	1.56e-2	7.57e-3	3.74e-3	1.86e-3	9.31e-4
order	-	1.04	1.02	1.01	1.00
$\ \mathbf{u} - \mathbf{u}_h\ _{\mathbf{L}^2(\Omega)}$	1.16e-3	2.58e-4	6.29e-5	1.59e-5	4.11e-6
order	-	2.17	2.04	1.98	1.95
$\ p - p_h\ _{L^2(\Omega)}$	5.41e-2	1.48e-2	3.57e-3	8.84e-4	2.20e-4
order	-	1.87	2.05	2.01	2.01

Polynomial degree $k' = 2$

h	1/2	1/4	1/8	1/16	1/32
$\ \mathbf{u} - \mathbf{u}_h\ _{\mathcal{V}(h)}$	2.98e-4	5.25e-5	1.06e-5	2.42e-6	5.84e-7
order	-	2.50	2.31	2.13	2.05
$ \mathbf{u} - \mathbf{u}_h _{\mathbf{H}^1(\Omega)}$	3.79e-3	8.56e-4	2.08e-4	5.14e-5	1.28e-5
order	-	2.15	2.04	2.02	2.01
$\ \mathbf{u} - \mathbf{u}_h\ _{\mathbf{L}^2(\Omega)}$	1.88e-4	2.84e-5	3.74e-6	4.97e-7	6.06e-8
order	-	2.73	2.93	2.91	3.04
$\ p - p_h\ _{L^2(\Omega)}$	1.50e-2	1.59e-3	2.00e-4	2.56e-5	3.26e-6
order	-	3.24	2.99	2.97	2.97

with respect to the Damköhler number. Finally, let us remark the exact velocity field is recovered for discretizations of degree $k' \geq 3$.

8.3 Two-Dimensional Problem with a Singular Solution

To examine how our discretization performs in the presence of singularities, we consider Stokes flow in the L-shaped domain $\Omega = (-1, 1)^2 \setminus ([0, 1) \times (-1, 0])$. The flow problem in consideration is depicted in Figure 11(a). Homogeneous Dirichlet boundary conditions are applied along $\Gamma_D = \{(0, y) : y \in (-1, 0)\} \cup \{(x, 0) : x \in (0, 1)\}$, Neumann boundary conditions are applied along $\Gamma_N = \partial\Omega \setminus \Gamma_D$, and we set $\sigma = 0$, $\nu = 1$, and $\mathbf{f} = \mathbf{0}$. As in [60], the Neumann boundary conditions are chosen such that the exact solution is

$$\mathbf{u} = \begin{bmatrix} r^\lambda((1+\lambda)\sin(\theta)\psi(\theta) + \cos(\theta)\psi'(\theta)) \\ r^\lambda(-(1+\lambda)\cos(\theta)\psi(\theta) + \sin(\theta)\psi'(\theta)) \end{bmatrix}$$

and

$$p = -r^{\lambda-1}((1+\lambda)^2\phi'(\theta) + \phi'''(\theta))/(1-\lambda)$$

where (r, θ) are polar coordinates with respect to the origin $(0, 0)$,

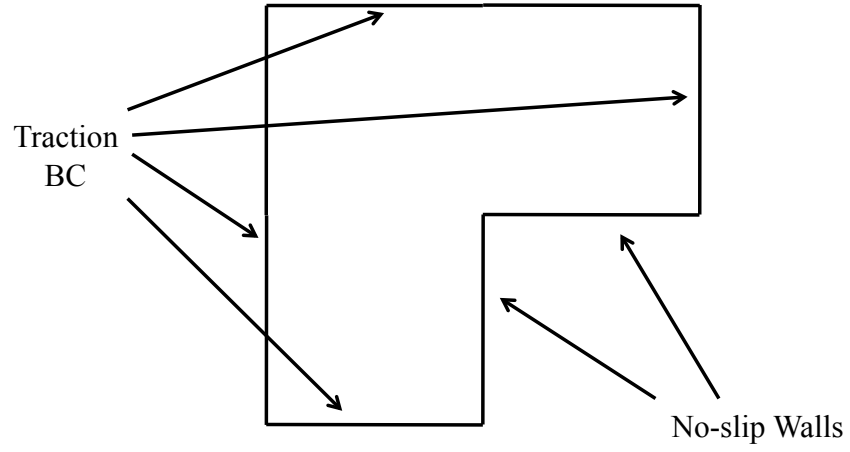
$$\begin{aligned} \phi &= \sin((1+\lambda)\theta)\cos(\lambda\omega)/(1+\lambda) - \cos((1+\lambda)\theta) \\ &\quad - \sin((1-\lambda)\theta)\cos(\lambda\omega)/(1-\lambda) + \cos((1-\lambda)\theta), \end{aligned}$$

$\omega = \frac{3}{2}\phi$, and $\lambda \approx 0.54448373678246$ is the smallest positive root of

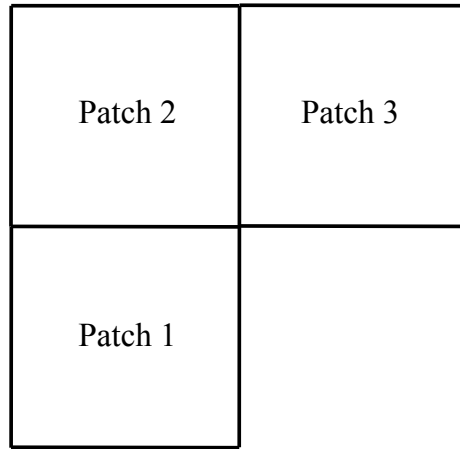
$$\sin(\lambda\omega) + \lambda\sin(\omega) = 0.$$

This singular solution is illustrated in Figure 12. Note that $(\mathbf{u}, p) \in \mathbf{H}^{1+\lambda}(\Omega) \times H^\lambda(\Omega)$. This is the strongest corner singularity for the Stokes operator in the L-shaped domain, and, as such, this numerical example models typical singular behavior observed in the vicinity of reentrant corners.

To compute this flow example using our discretization technique, we must resort to a multi-patch construction. We utilize the three-patch construction illustrated in Figure 11(b). Each patch is mapped from the parametric domain using an affine parametrization. As discussed in Section 7, we impose normal continuity strongly between patches and tangential continuity weakly using the symmetric interior penalty method. We have computed convergence rates for a variety of divergence-conforming B-spline discretizations and reported our results in Table 8. Note from the table that the $\mathcal{V}(h)$ -norm of the velocity field and the L^2 -norm of the pressure field are approaching the optimal convergence rates of $O(h^\lambda)$ as $h \rightarrow 0$. Furthermore, note the velocity and pressure errors improve with increasing polynomial degree. This is somewhat counterintuitive as we also increase smoothness with polynomial degree. This being said, such a property has also been observed in the context of Maxwell's equations [15]. While we only employed uniform meshes for the computations reported here, one could of course obtain more satisfactory results with geometrically graded meshes [30, 31].

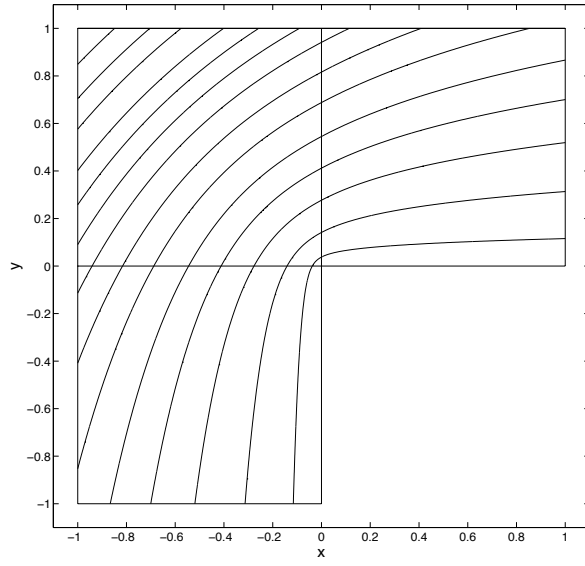


(a)

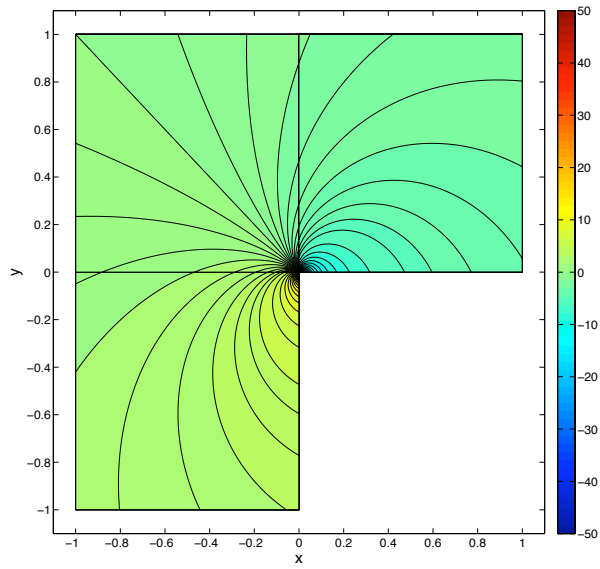


(b)

Figure 11: Singular Stokes solution in 2-D: (a) Problem setup, (b) Multi-patch construction.



(a)



(b)

Figure 12: Singular Stokes solution in 2-D: (a) Flow velocity streamlines, (b) Pressure contours.

Table 8: Singular Stokes convergence rates in 2-D

Polynomial degree $k' = 1$

h	1/2	1/4	1/8	1/16	1/32
$\ \mathbf{u} - \mathbf{u}_h\ _{\mathcal{V}(h)}$	2.29e0	1.61e0	1.13e0	7.73e-1	5.33e-1
order	-	0.51	0.51	0.55	0.54
$\ p - p_h\ _{L^2(\Omega)}$	1.30e0	9.40e-1	6.62e-1	4.66e-1	3.32e-1
order	-	0.47	0.51	0.51	0.49

Polynomial degree $k' = 2$

h	1/2	1/4	1/8	1/16	1/32
$\ \mathbf{u} - \mathbf{u}_h\ _{\mathcal{V}(h)}$	1.50e0	1.05e0	7.25e-1	5.00e-1	3.46e-1
order	-	0.51	0.53	0.54	0.53
$\ p - p_h\ _{L^2(\Omega)}$	8.56e-1	6.39e-1	4.50e-1	3.20e-1	2.36e-1
order	-	0.42	0.51	0.49	0.44

Polynomial degree $k' = 3$

h	1/2	1/4	1/8	1/16	1/32
$\ \mathbf{u} - \mathbf{u}_h\ _{\mathcal{V}(h)}$	1.15e0	8.36e-1	5.79e-1	4.00e-1	2.78e-1
order	-	0.46	0.53	0.53	0.52
$\ p - p_h\ _{L^2(\Omega)}$	6.05e-1	4.90e-1	3.54e-1	2.57e-1	1.91e-1
order	-	0.30	0.47	0.46	0.43

8.4 Cylindrical Couette Flow

Couette flow is often used as a “sanity check” for Stokes and Navier-Stokes discretizations. Cylindrical Couette flow is a more realistic problem which describes the flow between two concentric rotating cylinders. Here, we consider generalized Stokes flow between a fixed outer cylinder and a rotating inner cylinder. The problem setup is illustrated in Figure 13. No external forcing is applied. In the absence of Darcy drag forces (*i.e.*, $\sigma = 0$), the velocity field for this flow assumes the form

$$\mathbf{u} = \begin{bmatrix} u_\theta(r) \sin(\theta) \\ u_\theta(r) \cos(\theta) \end{bmatrix}$$

where

$$u_\theta(r) = Ar + \frac{B}{r},$$

(r, θ) are polar coordinates with respect to the center of the cylinders, and

$$A = -\Omega_{in} \frac{\delta^2}{1 - \delta^2}, \quad B = \Omega_{in} \frac{r_{in}^2}{(1 - \delta^2)}, \quad \Omega_{in} = \frac{U}{r_{in}}, \quad \delta = \frac{r_{in}}{r_{out}}.$$

We have depicted this velocity field in Figure 14(a). In the presence of Darcy drag forces, the character of the flow field changes considerably. Notably, the motion of the fluid is confined to a small boundary layer attached to the inner cylinder. This motion explicitly takes the form

$$\mathbf{u} = \begin{bmatrix} u_\theta(r) \sin(\theta) \\ u_\theta(r) \cos(\theta) \end{bmatrix}$$

where

$$u_\theta(r) = U \frac{I_1(\gamma r) K_1(\gamma r_{out}) - I_1(\gamma r_{out}) K_1(\gamma r)}{I_1(\gamma r_{in}) K_1(\gamma r_{out}) - I_1(\gamma r_{out}) K_1(\gamma r_{in})},$$

$\gamma = \sqrt{\sigma/\nu}$, and I_1 and K_1 are modified Bessel functions of the first and second kind respectively. Note that γ^{-1} acts as a length scale, and the width of the boundary layer attached to the inner cylinder is proportional to γ^{-1} . We have depicted a velocity field corresponding to $\gamma = \sqrt{50}$ in Figure 14(b). Finally, under the constraint that

$$\int_{\Omega} p d\mathbf{x} = 0,$$

the pressure field is identically zero for both the Stokes limit as well as the generalized Stokes setting. In what follows, we assume $r_{in} = 1$, $r_{out} = 2$, and $U = 1$.

We have computed convergence rates for a variety of divergence-conforming B-spline discretizations and for $\gamma = 0$ and $\gamma = \sqrt{50}$. To represent the annular domain in our computations, we employed the polar mapping

$$\mathbf{F}(\xi_1, \xi_2) = \begin{bmatrix} ((r_{out} - r_{in})\xi_2 + r_{in}) \sin(2\pi\xi_1) \\ ((r_{out} - r_{in})\xi_2 + r_{in}) \cos(2\pi\xi_1) \end{bmatrix}, \forall (\xi_1, \xi_2) \in (0, 1)^2 \quad (100)$$

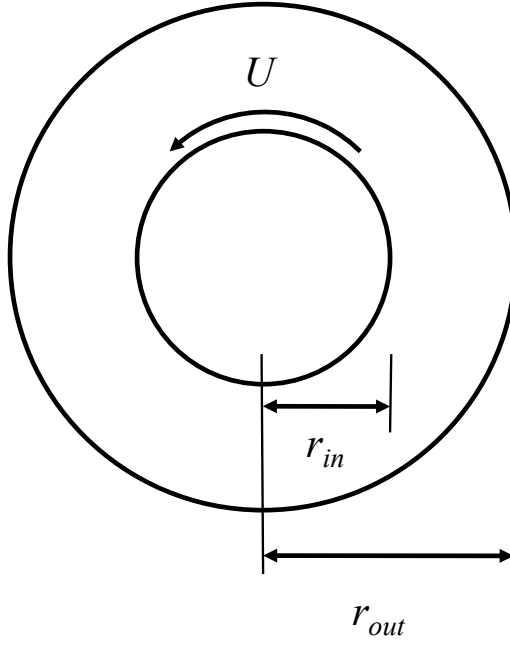
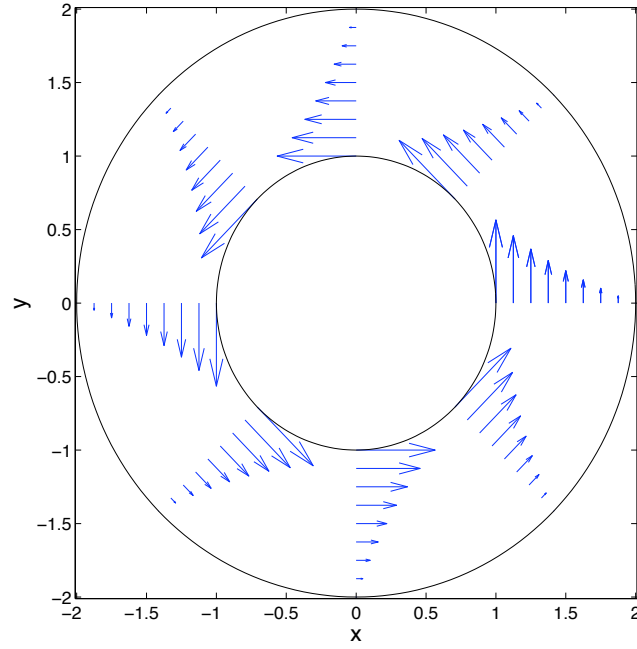


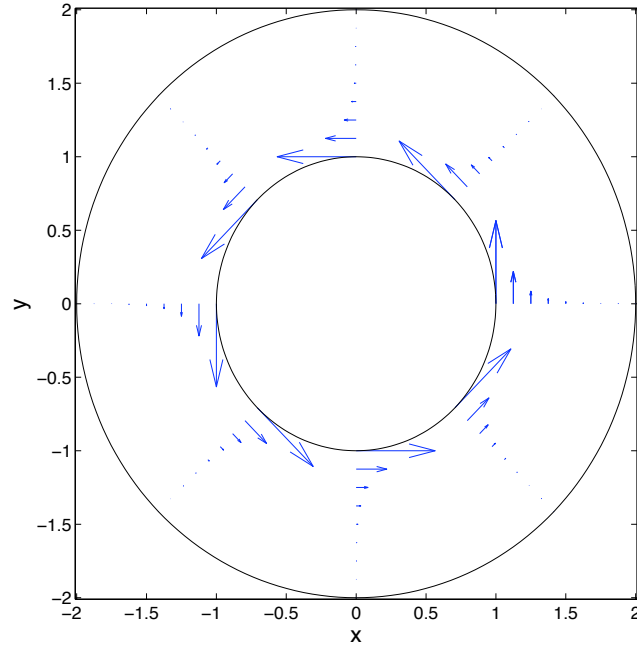
Figure 13: Cylindrical Couette flow: Problem setup.

and periodic B-splines of maximal continuity in the ξ_1 -direction (see Section 2 of [25]). It should be emphasized that we do not use the polar form of the generalized Stokes equations. Rather, we utilize the polar mapping to define our divergence-conforming B-splines in physical space and then employ the Cartesian-based variational formulation discussed in this chapter. The results of our computations are summarized in Tables 9 and 10. Note from the tables that all of our theoretically derived error estimates are confirmed, though the results corresponding to $\gamma = \sqrt{50}$ have a more substantial pre-asymptotic range due to the presence of a boundary layer. Additionally, note that we obtain null pressure fields and axisymmetric velocity fields with null radial component.

We repeated our computations using the multi-patch NURBS construction illustrated in Figure 16. Each of the four patches are built through a sufficient rotation of the canonical quadratic single-element NURBS patch described in Figure 17, and we have tabulated the location and weights of the control points of the canonical quadratic patch in Figure 11. The resulting NURBS parametrization is identical to the polar parametrization in the radial direction and different in the angular direction. We define our B-spline discretization scheme on the multi-patch NURBS construction using the procedure outlined in Section 7 with normal continuity being enforced strongly between patches and tangential continuity being enforced weakly. Surprisingly, we found we obtained exactly the same velocity and pressure fields using the multi-patch NURBS construction as we did with the polar mapping. This property is

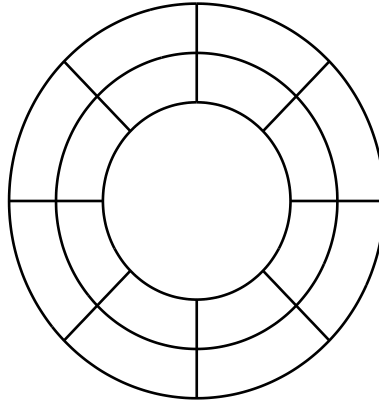


(a)

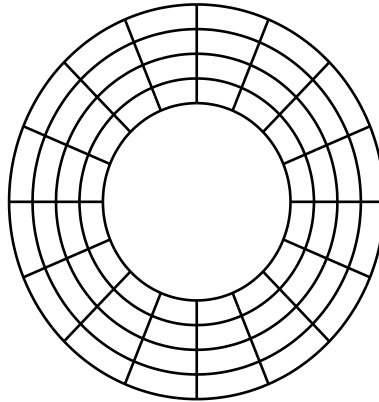


(b)

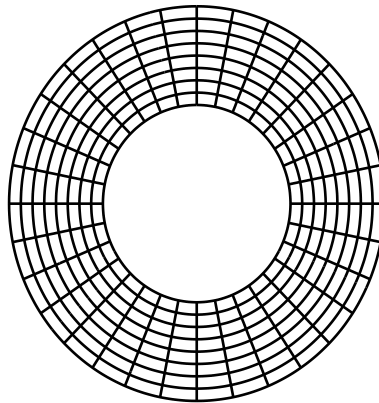
Figure 14: Cylindrical Couette flow: (a) Flow velocity arrows for $\gamma = 0$, (b) Flow velocity arrows for $\gamma = \sqrt{50}$.



$$h/h_0 = 1/2$$



$$h/h_0 = 1/4$$



$$h/h_0 = 1/8$$

Figure 15: Cylindrical Couette flow: Sequence of polar meshes.

Table 9: Cylindrical Couette flow convergence rates: $\gamma = 0$

Polynomial degree $k' = 1$

h/h_0	1/2	1/4	1/8	1/16	1/32
$\ \mathbf{u} - \mathbf{u}_h\ _{\mathcal{V}(h)}$	5.42e-1	2.63e-1	1.26e-1	6.12e-2	2.99e-2
order	-	1.04	1.06	1.04	1.03
$\ \mathbf{u} - \mathbf{u}_h\ _{\mathbf{H}^1(\Omega)}$	4.48e-1	2.32e-1	1.17e-1	5.86e-2	2.93e-2
order	-	0.95	0.99	1.00	1.00
$\ \mathbf{u} - \mathbf{u}_h\ _{\mathbf{L}^2(\Omega)}$	5.00e-2	1.53e-2	4.28e-3	1.14e-3	2.94e-4
order	-	1.71	1.84	1.91	1.96
$\ u_r - (u_r)_h\ _{L^2(\Omega)}$	0	0	0	0	0
$\ p - p_h\ _{L^2(\Omega)}$	0	0	0	0	0

Polynomial degree $k' = 2$

h/h_0	1/2	1/4	1/8	1/16	1/32
$\ \mathbf{u} - \mathbf{u}_h\ _{\mathcal{V}(h)}$	9.77e-2	2.42e-2	5.64e-3	1.32e-3	3.14e-4
order	-	2.01	2.10	2.10	2.07
$\ \mathbf{u} - \mathbf{u}_h\ _{\mathbf{H}^1(\Omega)}$	7.68e-2	2.00e-2	4.92e-3	1.21e-3	2.99e-4
order	-	1.94	2.02	2.02	2.02
$\ \mathbf{u} - \mathbf{u}_h\ _{\mathbf{L}^2(\Omega)}$	4.43e-3	6.03e-4	8.13e-5	1.07e-5	1.38e-6
order	-	2.88	2.89	2.93	2.95
$\ u_r - (u_r)_h\ _{L^2(\Omega)}$	0	0	0	0	0
$\ p - p_h\ _{L^2(\Omega)}$	0	0	0	0	0

Polynomial degree $k' = 3$

h/h_0	1/2	1/4	1/8	1/16	1/32
$\ \mathbf{u} - \mathbf{u}_h\ _{\mathcal{V}(h)}$	2.01e-2	2.67e-3	3.27e-4	4.01e-5	4.98e-6
order	-	2.91	3.03	3.03	3.01
$\ \mathbf{u} - \mathbf{u}_h\ _{\mathbf{H}^1(\Omega)}$	1.52e-2	2.13e-3	2.84e-4	3.72e-5	4.80e-6
order	-	2.84	2.91	2.93	2.95
$\ \mathbf{u} - \mathbf{u}_h\ _{\mathbf{L}^2(\Omega)}$	6.59e-4	5.69e-5	4.82e-6	3.50e-7	2.33e-8
order	-	3.53	3.56	3.78	3.91
$\ u_r - (u_r)_h\ _{L^2(\Omega)}$	0	0	0	0	0
$\ p - p_h\ _{L^2(\Omega)}$	0	0	0	0	0

Table 10: Cylindrical Couette flow convergence rates: $\gamma = \sqrt{50}$

Polynomial degree $k' = 1$

h/h_0	1/2	1/4	1/8	1/16	1/32
$\ \mathbf{u} - \mathbf{u}_h\ _{V(h)}$	8.06e-1	4.59e-1	2.30e-1	1.10e-1	5.28e-2
order	-	0.81	1.00	1.06	1.06
$ \mathbf{u} - \mathbf{u}_h _{\mathbf{H}^1(\Omega)}$	3.75e0	2.44e0	1.35e0	6.93e-1	3.49e-1
order	-	0.62	0.85	0.96	0.99
$\ \mathbf{u} - \mathbf{u}_h\ _{\mathbf{L}^2(\Omega)}$	2.43e-1	9.90e-2	3.16e-2	9.24e-3	2.56e-3
order	-	1.30	1.65	1.77	1.85
$\ u_r - (u_r)_h\ _{L^2(\Omega)}$	0	0	0	0	0
$\ p - p_h\ _{L^2(\Omega)}$	0	0	0	0	0

Polynomial degree $k' = 2$

h/h_0	1/2	1/4	1/8	1/16	1/32
$\ \mathbf{u} - \mathbf{u}_h\ _{V(h)}$	3.97e-1	1.30e-1	3.28e-2	7.56e-3	1.74e-3
order	-	1.61	1.99	2.12	2.12
$ \mathbf{u} - \mathbf{u}_h _{\mathbf{H}^1(\Omega)}$	1.96e0	6.99e-1	1.86e-1	4.57e-2	1.12e-2
order	-	1.49	1.91	2.03	2.03
$\ \mathbf{u} - \mathbf{u}_h\ _{\mathbf{L}^2(\Omega)}$	9.86e-2	2.00e-2	2.73e-3	3.66e-4	4.86e-5
order	-	2.30	2.87	2.90	2.91
$\ u_r - (u_r)_h\ _{L^2(\Omega)}$	0	0	0	0	0
$\ p - p_h\ _{L^2(\Omega)}$	0	0	0	0	0

Polynomial degree $k' = 3$

h/h_0	1/2	1/4	1/8	1/16	1/32
$\ \mathbf{u} - \mathbf{u}_h\ _{V(h)}$	1.69e-1	3.15e-2	4.01e-3	4.80e-4	5.86e-5
order	-	2.42	2.97	3.06	3.03
$ \mathbf{u} - \mathbf{u}_h _{\mathbf{H}^1(\Omega)}$	8.54e-1	1.67e-1	2.25e-2	2.95e-3	3.86e-4
order	-	2.35	2.89	2.93	2.93
$\ \mathbf{u} - \mathbf{u}_h\ _{\mathbf{L}^2(\Omega)}$	3.31e-2	3.56e-3	3.03e-4	2.55e-5	1.83e-6
order	-	3.22	3.55	3.57	3.80
$\ u_r - (u_r)_h\ _{L^2(\Omega)}$	0	0	0	0	0
$\ p - p_h\ _{L^2(\Omega)}$	0	0	0	0	0

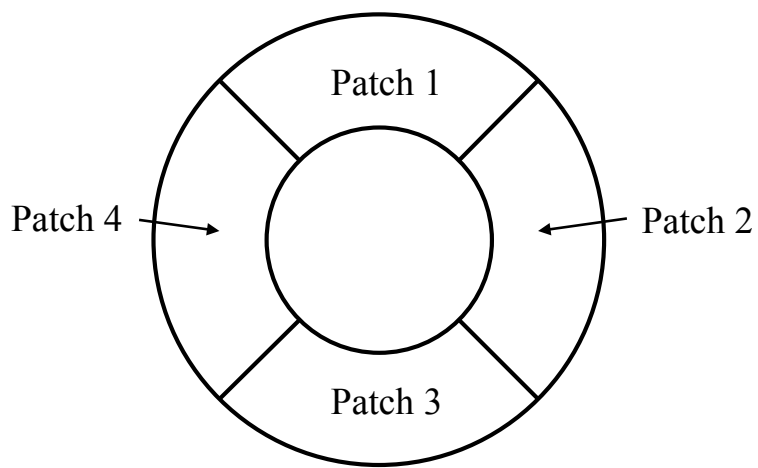


Figure 16: Cylindrical Couette flow: NURBS multi-patch construction

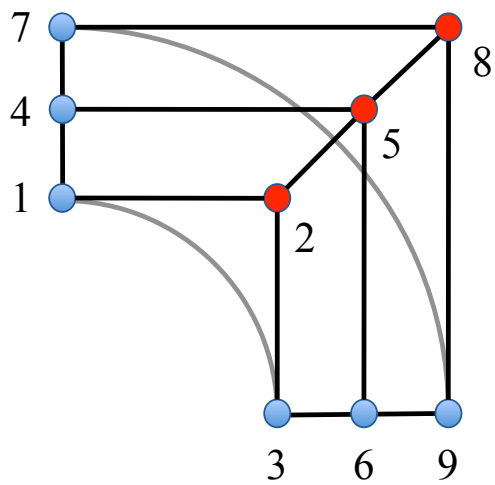


Figure 17: Cylindrical Couette flow: Patch template control points

Table 11: Cylindrical Couette flow: Patch template control points.

Control Point	x	y	w
1	0	1	1
2	1	1	$1/\sqrt{2}$
3	1	0	1
4	0	$3/2$	1
5	$3/2$	$3/2$	$1/\sqrt{2}$
6	$3/2$	0	1
7	0	2	1
8	2	2	$1/\sqrt{2}$
9	2	0	1

purely a consequence of the Piola transform. To shed some light on this observation, let us consider a parametric velocity field of the form $\widehat{\mathbf{v}} = \{v(\xi_2), 0\}^T$. Then, the image of this velocity field under the Piola transform, denoted as \mathbf{v} , has the property that

$$\operatorname{div} \mathbf{v} = \frac{1}{J} \widehat{\operatorname{div} \widehat{\mathbf{v}}} = 0$$

where J is the determinant of the Jacobian matrix $D\mathbf{F}$. Moreover, the vector \mathbf{v} is oriented in the direction of parametric lines defined by $\xi_2 = C$ where C is an arbitrary constant. Hence, if ξ_1 represents the angular direction and ξ_2 represents the radial direction, this implies that divergence-free lateral velocity fields in parametric space are mapped to axisymmetric angular velocity fields in physical space regardless of the specification of \mathbf{F} . Unfortunately, this argument applies only to angular velocity fields and we are not generally able to obtain axisymmetric pressure and radial velocity fields using the multi-patch NURBS construction.

8.5 Annular Poiseuille Flow

Poiseuille flow is another problem which is often utilized as a “sanity check” for Stokes and Navier-Stokes discretizations. Here, we consider generalized Stokes Poiseuille flow of a viscous fluid between two concentric cylinders. The problem setup is illustrated in Figure 18. No-slip and no-penetration boundary conditions are imposed along the cylinder surfaces, and periodic boundary conditions are imposed along the axial direction. An external axial pressure gradient is applied to drive the fluid. In the absence of Darcy drag forces, the velocity field for annular Poiseuille flow assumes the form

$$\mathbf{u} = \begin{bmatrix} 0 \\ 0 \\ u_z(r) \end{bmatrix}$$

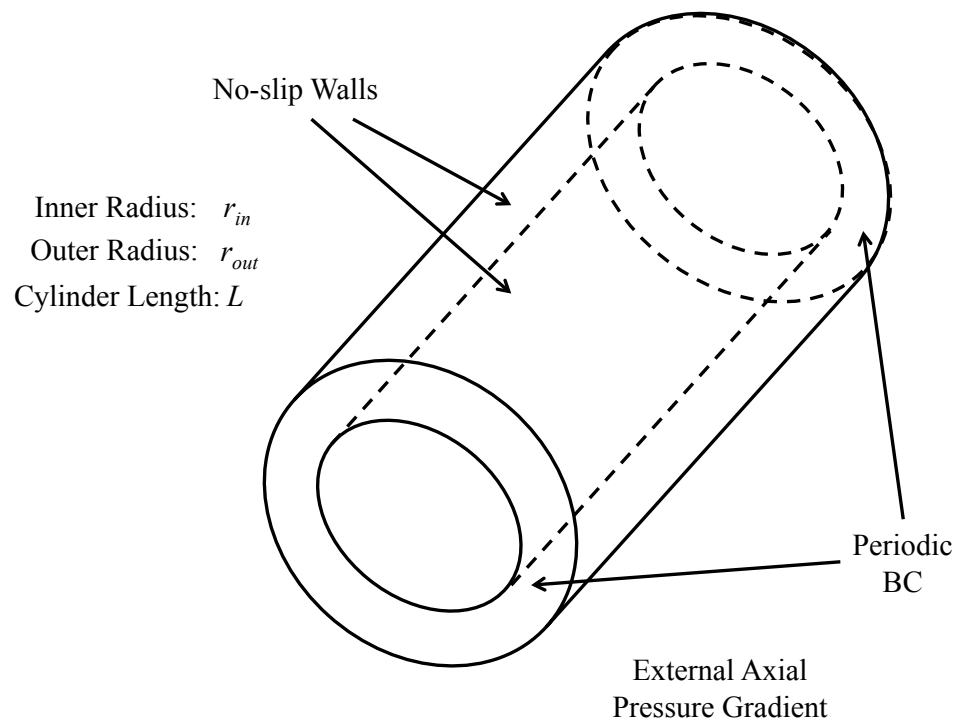


Figure 18: Annular Poiseuille flow: Problem setup.

where

$$u_z(r) = -\frac{\Delta p}{4\nu L} \left(r_{in}^2 - r^2 + \frac{r_{out}^2 - r_{in}^2}{\ln(r_{out}/r_{in})} \ln(r/r_{in}) \right)$$

(r, θ) are polar coordinates with respect to the center of the cylinders, and $-\Delta p/L$ is the applied pressure gradient. In the presence of Darcy drag, the velocity field takes the form

$$\mathbf{u} = \begin{bmatrix} 0 \\ 0 \\ u_z(r) \end{bmatrix}$$

where

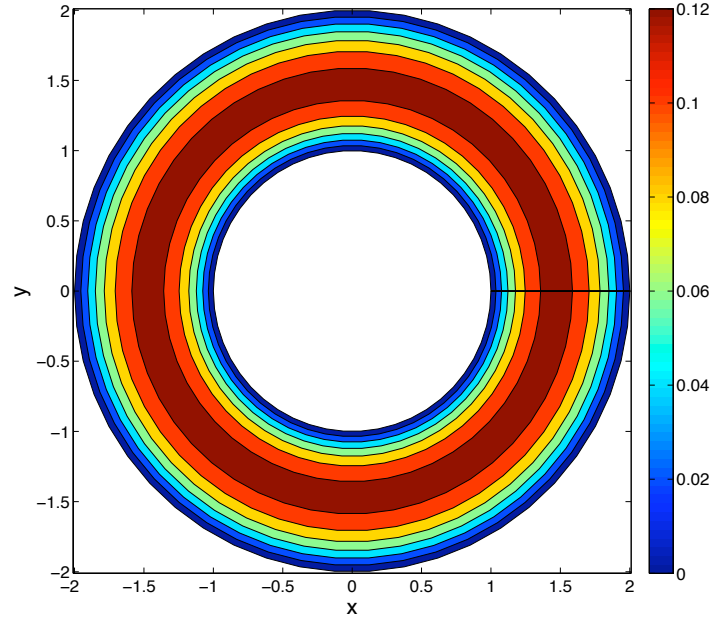
$$u_z(r) = -\frac{\Delta p}{\sigma L} \left(\frac{K_0(\gamma r) (I_0(\gamma r_{out}) - I_0(\gamma r_{in})) - I_0(\gamma r) (K_0(\gamma r_{out}) - K_0(\gamma r_{in}))}{K_0(\gamma r_{out}) I_0(\gamma r_{in}) - K_0(\gamma r_{in}) I_0(\gamma r_{out})} \right) - \frac{\Delta p}{\sigma L},$$

$\gamma = \sqrt{\sigma/\nu}$, and I_0 and K_0 are modified Bessel functions of the first and second kind respectively. We have illustrated velocity fields corresponding to $\gamma = 0$ and $\gamma = \sqrt{50}$ in Figure 19. As was the case for cylindrical Couette flow, γ^{-1} acts as a length scale, and there is a boundary layer attached to the inner cylinder with width proportional to γ^{-1} . Finally, under the constraint that

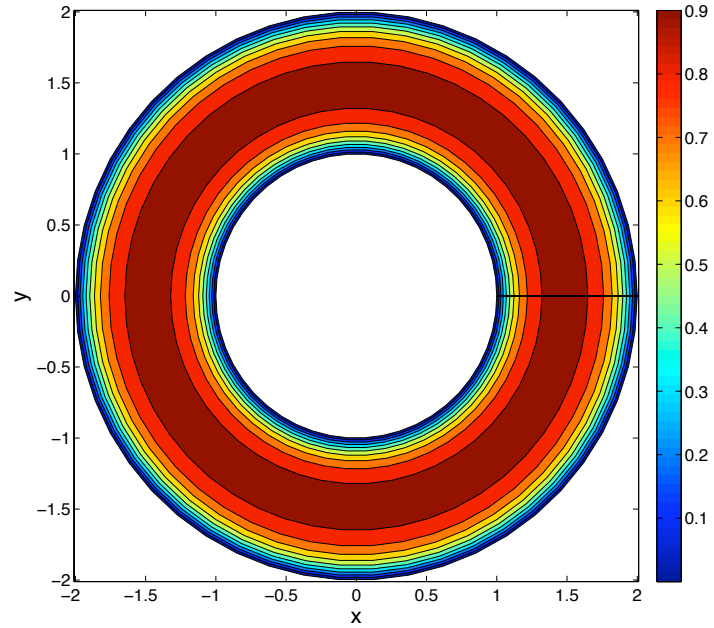
$$\int_{\Omega} p d\mathbf{x} = 0,$$

the pressure field is identically zero for both the Stokes limit as well as the generalized Stokes setting. In what follows, we assume $r_{in} = 1$, $r_{out} = 2$, $L = 1$, and $\Delta p = -1$.

We have computed convergence rates for a variety of divergence-conforming B-spline discretizations and for $\gamma = 0$ and $\gamma = \sqrt{50}$. We have employed both the polar mapping and the NURBS multi-patch construction described in the previous subsection to represent the annular domain in our computations with the axial direction parametrized using a simple linear mapping. Periodic B-splines of maximal continuity were employed in the axial direction. The results of our computations for $\gamma = 0$ are summarized in Tables 12 and 13. Note immediately that all of our theoretically derived error estimates are confirmed. Additionally, note that we obtain null pressure fields, radial velocity fields, and angular velocity fields for all cases considered. This being said, observe that we obtain slightly smaller axial velocity errors with the polar mapping than we do with the NURBS multi-patch construction. This is because we maintain exact axisymmetry with the polar mapping but not with the NURBS multi-patch construction. The results of our computations for $\gamma = \sqrt{50}$ are summarized in Tables 14 and 15. Again, note that our theoretically derived error estimates are confirmed, and our results for the polar mapping induce slightly smaller axial velocity errors than our results for the NURBS multi-patch construction.



(a)



(b)

Figure 19: Annular Poiseuille flow: Axial velocity contours along an axial slice for (a) $\gamma = 0$ and (b) $\gamma = \sqrt{50}$.

Table 12: Annular Poiseuille flow convergence rates for $\gamma = 0$: Polar meshes

Polynomial degree $k' = 1$

h/h_0	1/2	1/4	1/8	1/16	1/32
$\ \mathbf{u} - \mathbf{u}_h\ _{V(h)}$	5.30e-1	2.47e-1	1.19e-1	5.80e-2	2.86e-2
order	-	1.10	1.05	1.04	1.02
$\ \mathbf{u} - \mathbf{u}_h\ _{\mathbf{H}^1(\Omega)}$	4.56e-1	2.28e-1	1.14e-1	5.67e-2	2.83e-2
order	-	1.00	1.00	1.01	1.00
$\ \mathbf{u} - \mathbf{u}_h\ _{\mathbf{L}^2(\Omega)}$	5.49e-2	1.62e-2	4.34e-3	1.12e-3	2.84e-4
order	-	1.76	1.90	1.95	1.98
$\ u_r - (u_r)_h\ _{L^2(\Omega)}$	0	0	0	0	0
$\ u_\theta - (u_\theta)_h\ _{L^2(\Omega)}$	0	0	0	0	0
$\ p - p_h\ _{L^2(\Omega)}$	0	0	0	0	0

Polynomial degree $k' = 2$

h/h_0	1/2	1/4	1/8	1/16	1/32
$\ \mathbf{u} - \mathbf{u}_h\ _{V(h)}$	5.67e-2	1.23e-2	2.83e-3	6.73e-4	1.64e-4
order	-	2.20	2.12	2.07	2.04
$\ \mathbf{u} - \mathbf{u}_h\ _{\mathbf{H}^1(\Omega)}$	4.49e-2	1.07e-2	2.61e-3	6.45e-4	1.60e-4
order	-	2.07	2.04	2.02	2.01
$\ \mathbf{u} - \mathbf{u}_h\ _{\mathbf{L}^2(\Omega)}$	2.41e-3	3.49e-4	4.64e-5	5.97e-6	7.58e-7
order	-	2.79	2.91	2.96	2.98
$\ u_r - (u_r)_h\ _{L^2(\Omega)}$	0	0	0	0	0
$\ u_\theta - (u_\theta)_h\ _{L^2(\Omega)}$	0	0	0	0	0
$\ p - p_h\ _{L^2(\Omega)}$	0	0	0	0	0

Polynomial degree $k' = 3$

h/h_0	1/2	1/4	1/8	1/16	1/32
$\ \mathbf{u} - \mathbf{u}_h\ _{V(h)}$	1.86e-3	2.14e-4	2.54e-5	3.11e-6	3.87e-7
order	-	3.12	3.07	3.03	3.01
$\ \mathbf{u} - \mathbf{u}_h\ _{\mathbf{H}^1(\Omega)}$	1.37e-3	1.74e-4	2.26e-5	2.93e-6	3.75e-7
order	-	2.98	2.94	2.95	2.97
$\ \mathbf{u} - \mathbf{u}_h\ _{\mathbf{L}^2(\Omega)}$	5.38e-5	5.05e-6	4.03e-7	2.80e-8	1.83e-9
order	-	3.41	3.65	3.85	3.94
$\ u_r - (u_r)_h\ _{L^2(\Omega)}$	0	0	0	0	0
$\ u_\theta - (u_\theta)_h\ _{L^2(\Omega)}$	0	0	0	0	0
$\ p - p_h\ _{L^2(\Omega)}$	0	0	0	0	0

Table 13: Annular Poiseuille flow convergence rates for $\gamma = 0$: NURBS

Polynomial degree $k' = 1$

h/h_0	1/2	1/4	1/8	1/16	1/32
$\ \mathbf{u} - \mathbf{u}_h\ _{V(h)}$	5.30e-1	2.47e-1	1.19e-1	5.80e-2	2.86e-2
order	-	1.10	1.05	1.04	1.02
$ \mathbf{u} - \mathbf{u}_h _{\mathbf{H}^1(\mathcal{K}_h)}$	4.57e-1	2.28e-1	1.14e-1	5.67e-2	2.83e-2
order	-	1.00	1.00	1.01	1.00
$\ \mathbf{u} - \mathbf{u}_h\ _{\mathbf{L}^2(\Omega)}$	5.51e-2	1.63e-2	4.35e-3	1.12e-3	2.84e-4
order	-	1.76	1.91	1.96	1.98
$\ u_r - (u_r)_h\ _{L^2(\Omega)}$	0	0	0	0	0
$\ u_\theta - (u_\theta)_h\ _{L^2(\Omega)}$	0	0	0	0	0
$\ p - p_h\ _{L^2(\Omega)}$	0	0	0	0	0

Polynomial degree $k' = 2$

h/h_0	1/2	1/4	1/8	1/16	1/32
$\ \mathbf{u} - \mathbf{u}_h\ _{V(h)}$	5.69e-2	1.23e-2	2.83e-3	6.75e-4	1.64e-4
order	-	2.21	2.12	2.07	2.04
$ \mathbf{u} - \mathbf{u}_h _{\mathbf{H}^1(\mathcal{K}_h)}$	4.51e-2	1.07e-2	2.61e-3	6.46e-4	1.61e-4
order	-	2.08	2.04	2.01	2.00
$\ \mathbf{u} - \mathbf{u}_h\ _{\mathbf{L}^2(\Omega)}$	2.52e-3	3.55e-4	4.70e-5	6.04e-6	7.66e-7
order	-	2.83	2.92	2.96	2.98
$\ u_r - (u_r)_h\ _{L^2(\Omega)}$	0	0	0	0	0
$\ u_\theta - (u_\theta)_h\ _{L^2(\Omega)}$	0	0	0	0	0
$\ p - p_h\ _{L^2(\Omega)}$	0	0	0	0	0

Polynomial degree $k' = 3$

h/h_0	1/2	1/4	1/8	1/16	1/32
$\ \mathbf{u} - \mathbf{u}_h\ _{V(h)}$	1.91e-3	2.38e-4	2.73e-5	3.33e-6	4.13e-7
order	-	3.00	3.12	3.04	3.01
$ \mathbf{u} - \mathbf{u}_h _{\mathbf{H}^1(\mathcal{K}_h)}$	1.44e-3	2.03e-4	2.48e-5	3.16e-6	4.03e-7
order	-	2.83	3.03	2.97	2.97
$\ \mathbf{u} - \mathbf{u}_h\ _{\mathbf{L}^2(\Omega)}$	8.00e-5	1.21e-5	6.41e-7	4.00e-8	2.53e-9
order	-	2.72	4.24	4.00	3.98
$\ u_r - (u_r)_h\ _{L^2(\Omega)}$	0	0	0	0	0
$\ u_\theta - (u_\theta)_h\ _{L^2(\Omega)}$	0	0	0	0	0
$\ p - p_h\ _{L^2(\Omega)}$	0	0	0	0	0

Table 14: Annular Poiseuille flow convergence rates for $\gamma = \sqrt{50}$: Polar meshes

Polynomial degree $k' = 1$

h/h_0	1/2	1/4	1/8	1/16	1/32
$\ \mathbf{u} - \mathbf{u}_h\ _{\mathcal{V}(h)}$	1.73e-1	9.88e-2	4.91e-2	2.35e-2	1.13e-2
order	-	0.81	1.01	1.06	1.06
$ \mathbf{u} - \mathbf{u}_h _{\mathbf{H}^1(\Omega)}$	8.20e-1	5.29e-1	2.90e-1	1.48e-1	7.46e-2
order	-	0.65	0.87	0.97	0.99
$\ \mathbf{u} - \mathbf{u}_h\ _{\mathbf{L}^2(\Omega)}$	4.88e-2	2.12e-2	6.69e-3	1.94e-3	5.37e-4
order	-	1.20	1.66	1.79	1.85
$\ u_r - (u_r)_h\ _{L^2(\Omega)}$	0	0	0	0	0
$\ u_\theta - (u_\theta)_h\ _{L^2(\Omega)}$	0	0	0	0	0
$\ p - p_h\ _{L^2(\Omega)}$	0	0	0	0	0

Polynomial degree $k' = 2$

h/h_0	1/2	1/4	1/8	1/16	1/32
$\ \mathbf{u} - \mathbf{u}_h\ _{\mathcal{V}(h)}$	8.77e-2	2.59e-2	6.37e-3	1.46e-3	3.37e-4
order	-	1.76	2.02	2.13	2.12
$ \mathbf{u} - \mathbf{u}_h _{\mathbf{H}^1(\Omega)}$	4.34e-1	1.39e-1	3.63e-2	8.86e-3	2.16e-3
order	-	1.64	1.94	2.03	2.04
$\ \mathbf{u} - \mathbf{u}_h\ _{\mathbf{L}^2(\Omega)}$	2.32e-2	3.98e-3	5.33e-4	7.14e-5	9.46e-6
order	-	2.54	2.90	2.90	2.92
$\ u_r - (u_r)_h\ _{L^2(\Omega)}$	0	0	0	0	0
$\ u_\theta - (u_\theta)_h\ _{L^2(\Omega)}$	0	0	0	0	0
$\ p - p_h\ _{L^2(\Omega)}$	0	0	0	0	0

Polynomial degree $k' = 3$

h/h_0	1/2	1/4	1/8	1/16	1/32
$\ \mathbf{u} - \mathbf{u}_h\ _{\mathcal{V}(h)}$	2.95e-2	5.72e-3	7.10e-4	8.48e-5	1.04e-5
order	-	2.37	3.01	3.07	3.03
$ \mathbf{u} - \mathbf{u}_h _{\mathbf{H}^1(\Omega)}$	1.48e-1	3.03e-2	4.02e-3	5.27e-4	6.88e-5
order	-	2.29	2.91	2.93	2.94
$\ \mathbf{u} - \mathbf{u}_h\ _{\mathbf{L}^2(\Omega)}$	5.23e-3	6.40e-4	5.59e-5	4.63e-6	3.27e-7
order	-	3.03	3.52	3.59	3.82
$\ u_r - (u_r)_h\ _{L^2(\Omega)}$	0	0	0	0	0
$\ u_\theta - (u_\theta)_h\ _{L^2(\Omega)}$	0	0	0	0	0
$\ p - p_h\ _{L^2(\Omega)}$	0	0	0	0	0

Table 15: Annular Poiseuille flow convergence rates for $\gamma = \sqrt{50}$: NURBS

Polynomial degree $k' = 1$

h/h_0	1/2	1/4	1/8	1/16	1/32
$\ \mathbf{u} - \mathbf{u}_h\ _{\mathcal{V}(h)}$	1.73e-1	9.88e-2	4.91e-2	2.35e-2	1.13e-2
order	-	0.81	1.01	1.06	1.06
$ \mathbf{u} - \mathbf{u}_h _{\mathbf{H}^1(\Omega)}$	8.20e-1	5.29e-1	2.90e-1	1.49e-1	7.46e-2
order	-	0.65	0.87	0.96	1.00
$\ \mathbf{u} - \mathbf{u}_h\ _{\mathbf{L}^2(\Omega)}$	4.89e-2	2.12e-2	6.70e-3	1.95e-3	5.37e-4
order	-	1.21	1.66	1.78	1.86
$\ u_r - (u_r)_h\ _{L^2(\Omega)}$	0	0	0	0	0
$\ u_\theta - (u_\theta)_h\ _{L^2(\Omega)}$	0	0	0	0	0
$\ p - p_h\ _{L^2(\Omega)}$	0	0	0	0	0

Polynomial degree $k' = 2$

h/h_0	1/2	1/4	1/8	1/16	1/32
$\ \mathbf{u} - \mathbf{u}_h\ _{\mathcal{V}(h)}$	8.77e-2	2.59e-2	6.38e-3	1.46e-3	3.37e-4
order	-	1.76	2.02	2.13	2.12
$ \mathbf{u} - \mathbf{u}_h _{\mathbf{H}^1(\Omega)}$	4.34e-1	1.39e-1	3.63e-2	8.86e-3	2.16e-3
order	-	1.64	1.94	2.03	2.04
$\ \mathbf{u} - \mathbf{u}_h\ _{\mathbf{L}^2(\Omega)}$	2.32e-2	3.98e-3	5.33e-4	7.14e-5	9.46e-6
order	-	2.54	2.90	2.90	2.92
$\ u_r - (u_r)_h\ _{L^2(\Omega)}$	0	0	0	0	0
$\ u_\theta - (u_\theta)_h\ _{L^2(\Omega)}$	0	0	0	0	0
$\ p - p_h\ _{L^2(\Omega)}$	0	0	0	0	0

Polynomial degree $k' = 3$

h/h_0	1/2	1/4	1/8	1/16	1/32
$\ \mathbf{u} - \mathbf{u}_h\ _{\mathcal{V}(h)}$	2.95e-2	5.72e-3	7.10e-4	8.48e-5	1.04e-5
order	-	2.37	3.01	3.07	3.03
$ \mathbf{u} - \mathbf{u}_h _{\mathbf{H}^1(\Omega)}$	1.48e-1	3.03e-2	4.02e-3	5.27e-4	6.88e-5
order	-	2.29	2.91	2.93	2.94
$\ \mathbf{u} - \mathbf{u}_h\ _{\mathbf{L}^2(\Omega)}$	5.23e-3	6.40e-4	5.59e-5	4.63e-6	3.27e-7
order	-	3.03	3.52	3.59	3.82
$\ u_r - (u_r)_h\ _{L^2(\Omega)}$	0	0	0	0	0
$\ u_\theta - (u_\theta)_h\ _{L^2(\Omega)}$	0	0	0	0	0
$\ p - p_h\ _{L^2(\Omega)}$	0	0	0	0	0

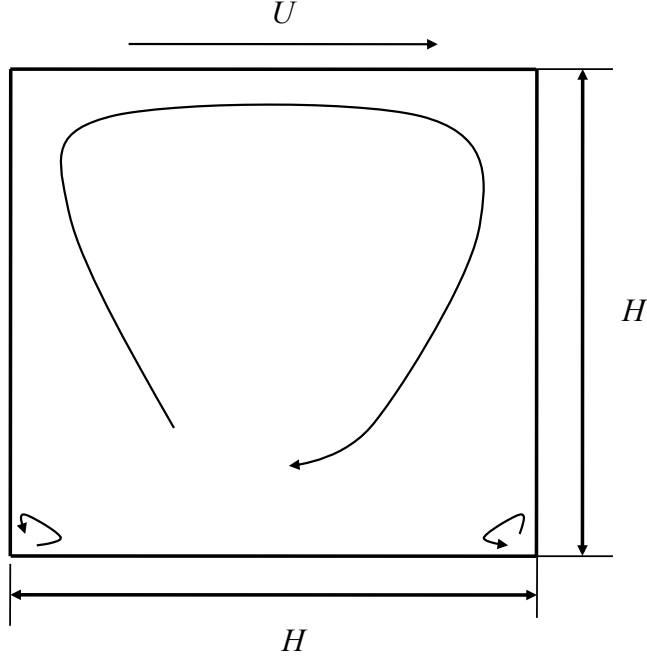


Figure 20: Lid-driven Stokes flow in a two-dimensional cavity: Problem setup.

9 Benchmark Problems

In this section, we investigate the effectiveness of our methodology as applied to two standard Stokes benchmark problems: two-dimensional and three-dimensional lid-driven cavity flow. In addition, we investigate the effectiveness of our methodology for a Darcy-dominated generalized Stokes flow problem characterized by sharp boundary layers. As in the last subsection, we choose Nitsche’s penalty constant as $C_{pen} = 5(k' + 1)$ in all of the following numerical tests, and we employ uniform parametric meshes, linear parametric mappings, and B-spline spaces of maximal continuity.

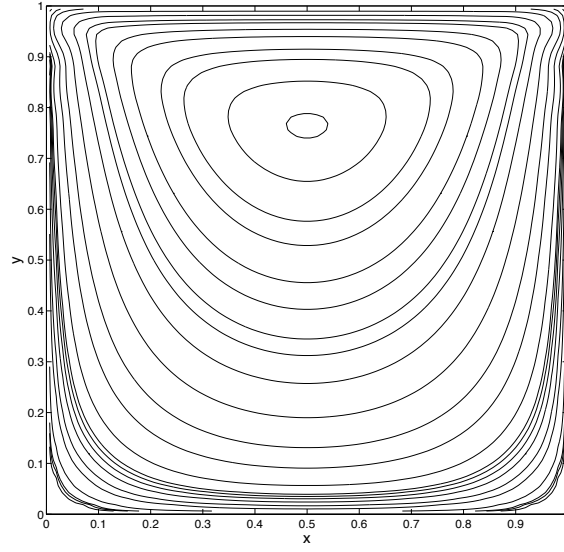
9.1 Two-Dimensional Lid-Driven Cavity Flow

Two-dimensional lid-driven cavity flow is one of the classical verification tests for numerical discretizations of incompressible flow. The setup for this flow problem is elaborated in Figure 20. The reaction coefficient σ and the applied forcing \mathbf{f} are set to be zero. The left, right, and bottom sides of the cavity are fixed no-slip walls while the top side of the cavity is a wall which slides to the right with velocity magnitude U . For the computations here, H and U are set to be 1. The pressure and stress fields associated with this flow experience corner singularities which impede the convergence of numerical methods and expose unstable velocity/pressure pairs. In fact, the exact velocity solution does not even lie in $\mathbf{H}^1(\Omega)$. Instead, it lies in the Sobolev space

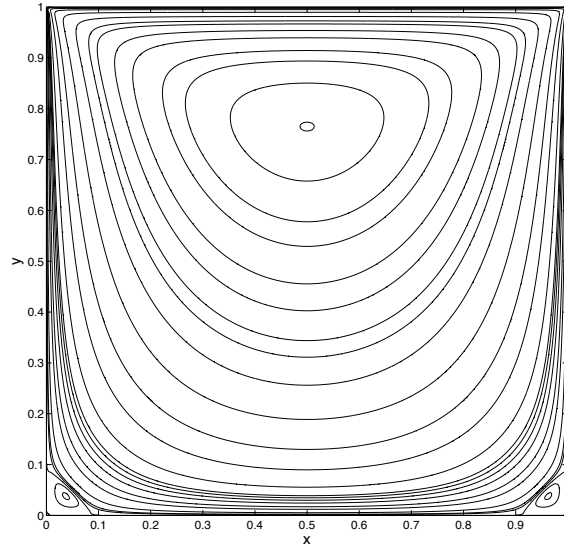
$\mathbf{W}^{1,q}(\Omega)$ where $1 < q < 2$. The velocity field is additionally characterized by a primary vortex near the center of the cavity and an infinite sequence of so-called Moffatt eddies of decreasing size and intensity in the lower left and right corners of the cavity [47]. Of primary interest is how well our discretization procedure approximates the smooth portions of the flow. Of secondary interest is how well our discretization procedure resolves the corner singularities. We do not, however, employ any special techniques such as singular finite elements to handle the singularities.

We have computed approximations of two-dimensional lid-driven cavity flow using divergence-conforming B-spline discretizations of varying mesh size and polynomial degrees $k' = 1, 2, 3$. The computed streamlines for two of these approximations are presented in Figure 21. The streamlines corresponding to the approximation defined on the fine mesh ($k' = 1, h = 1/128$) are virtually indistinguishable from well-accepted benchmark solutions [51]. The streamlines corresponding to the approximation defined on the coarse mesh ($k' = 1, h = 1/16$) closely resemble the fine mesh streamlines in the interior of the domain. In the four corners of the domain, the approximation on the coarse mesh exhibits visible numerical error due to lack of resolution. These results indicate that our methodology suffers from minimal pollution error [4]. It is hypothesized that this is due to the local stability and approximation properties of B-splines. To further highlight how well the approximation on the coarse mesh approximates the solution in the interior of the domain, we have plotted the value of the first component of the velocity field along the vertical center line in Figure 22(a) and the value of the second component along the horizontal center line in Figure 22(b) for the both the coarse mesh and fine mesh solutions. It should be mentioned that we have captured the first Moffatt eddy in the two lower corners with both meshes, and we have observed a second Moffatt eddy for meshes of size $h \leq 1/256$.

We finish our discussion of the two-dimensional lid-driven cavity problem by analyzing how well our methodology resolves the corner singularities. To do so, we compare the results of our methodology with the highly accurate pseudospectral results given in [10]. These pseudospectral results were obtained using a subtraction of the leading terms of the asymptotic solution of the Stokes equations in the vicinity of the corners in order to exactly represent the corner singularities. In Table 16, we compare the vorticity ($\omega = \text{curl} \mathbf{u}$) given by our numerical methodology with the pseudospectral vorticity near the upper right corner of the cavity. We see that the vorticity associated with our numerical methodology slowly converges to the converged pseudospectral solution. We further compare our computed vorticities with the vorticity obtained with a highly-refined finite difference solution [32]. We find that, for $k' = 1$, our solutions are more accurate than the finite difference solution for $h \leq 1/64$, and for $k' = 2$, our solutions are more accurate than the finite difference solution for $h \leq 1/32$. For $k' = 3$, our solutions are more accurate than the finite difference solution at all resolutions.

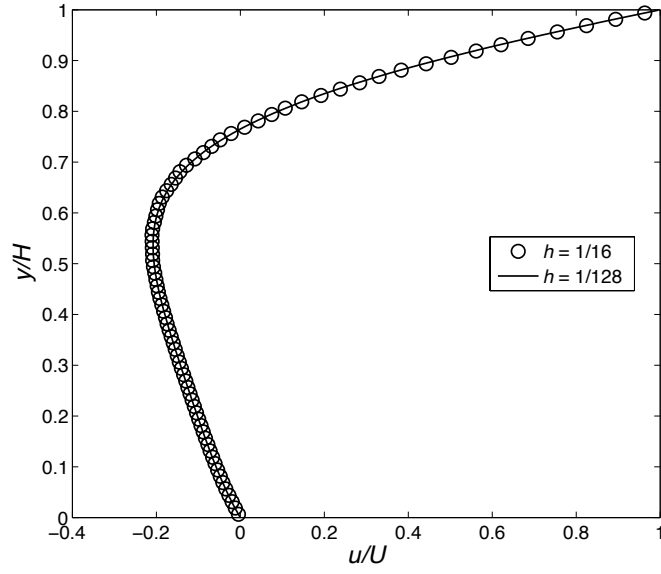


(a)

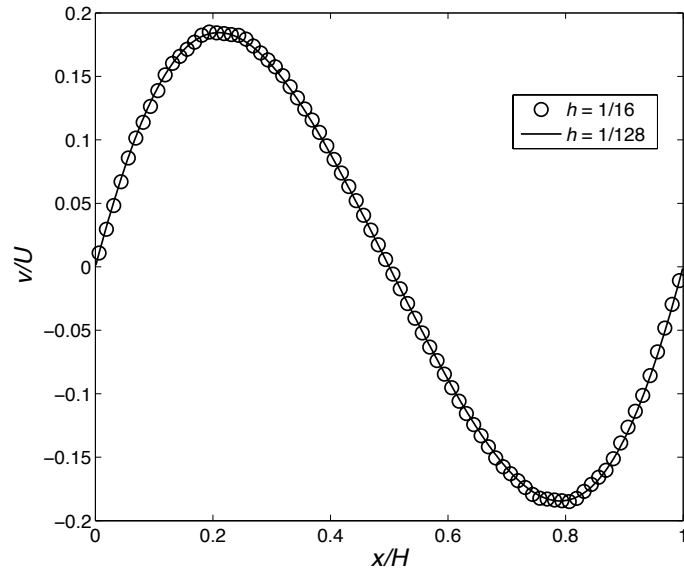


(b)

Figure 21: Lid-driven Stokes flow in a two-dimensional cavity: (a) Computed flow velocity streamlines for $k' = 1$ and $h = 1/16$, (b) Computed flow velocity streamlines for $k' = 1$ and $h = 1/128$.



(a)



(b)

Figure 22: Lid-driven Stokes flow in a two-dimensional cavity: (a) Value of the first component of the velocity field along the vertical center line for $k' = 1$, (b) Value of the second component of the velocity field along the horizontal center line for $k' = 1$.

Table 16: Lid-driven Stokes flow in a two-dimensional cavity: Convergence of vorticity at the point $(\mathbf{x} = (1, 0.95))$.

Polynomial degree $k' = 1$

Method	ω
B-spline, $h = 1/16$	-0.80995
B-spline, $h = 1/32$	14.34482
B-spline, $h = 1/64$	19.04468
B-spline, $h = 1/128$	23.29179
B-spline, $h = 1/256$	25.32238
Pseudospectral (Ref. [10])	27.27901
Finite Difference (Ref. [32])	18.08

Polynomial degree $k' = 2$

Method	ω
B-spline, $h = 1/16$	11.06384
B-spline, $h = 1/32$	31.81761
B-spline, $h = 1/64$	32.81972
B-spline, $h = 1/128$	26.48645
B-spline, $h = 1/256$	27.34395
Pseudospectral (Ref. [10])	27.27901
Finite Difference (Ref. [32])	18.08

Polynomial degree $k' = 3$

Method	ω
B-spline, $h = 1/16$	29.86220
B-spline, $h = 1/32$	25.00897
B-spline, $h = 1/64$	29.92944
B-spline, $h = 1/128$	28.75895
B-spline, $h = 1/256$	27.52637
Pseudospectral (Ref. [10])	27.27901
Finite Difference (Ref. [32])	18.08

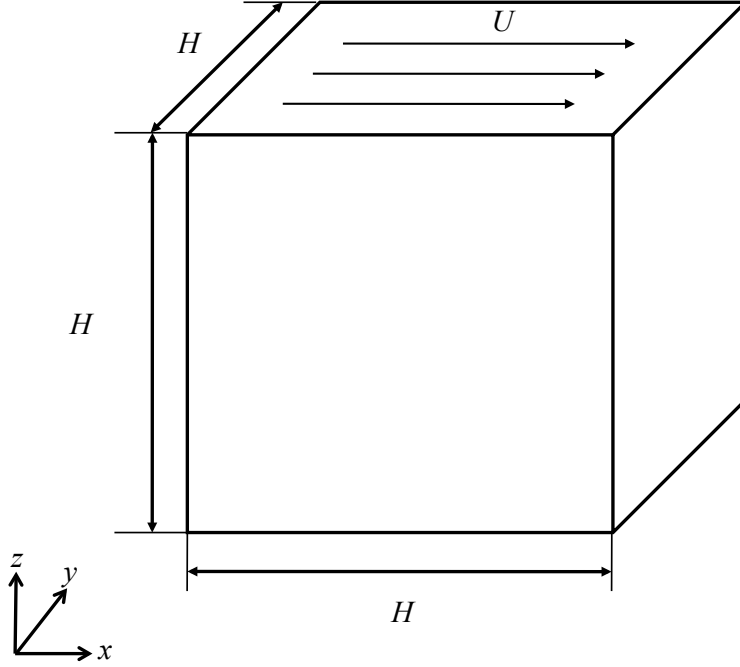


Figure 23: Lid-driven Stokes flow in a three-dimensional cavity: Problem setup.

9.2 Three-Dimensional Lid-Driven Cavity Flow

While three-dimensional lid-driven cavity flow is encountered much less often in the literature than its two-dimensional counterpart, we believe it is still an interesting test case for numerical discretizations of incompressible flow. In the three-dimensional setting, cavity flow is characterized by the presence of both edge and corner singularities. The problem setup is illustrated in Figure 23. Again, for the computations here, σ and \mathbf{f} are set to be zero. Every side of the cavity except the top is assumed to be a stationary no-slip wall, and the top side of the cavity is assumed to be a wall which slips to the right with velocity magnitude U . The streamlines resulting from a simulation of three-dimensional lid-driven cavity flow using divergence-conforming B-splines of degree $k' = 2$ on a mesh with 32×32 elements are illustrated in Figure 24. Note that the three-dimensional streamlines resemble the two-dimensional streamlines along the slice $y/H = 1/2$. To examine how well our discretization technique performs on coarse meshes, we have compared the centerline values of our velocity field along the slice $y/H = 1/2$ for both a coarse and fine mesh approximation in Figure 25. From the figure, we see that the coarse and fine mesh centerline velocity fields are nearly indistinguishable. This indicates that our methodology suffers from minimal pollution error.

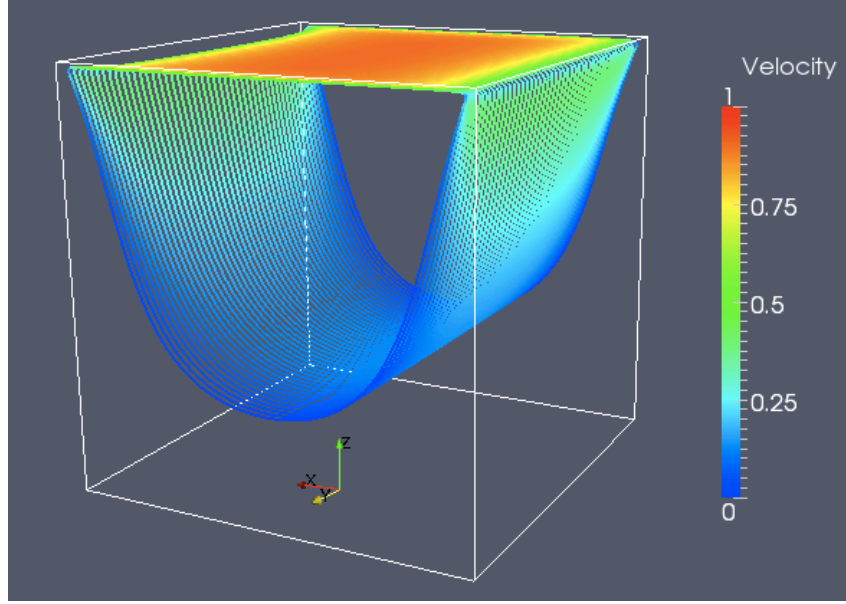


Figure 24: Lid-driven Stokes flow in a three-dimensional cavity: Computed flow velocity streamlines for $k' = 2$ and $h = 1/32$ colored by velocity magnitude.

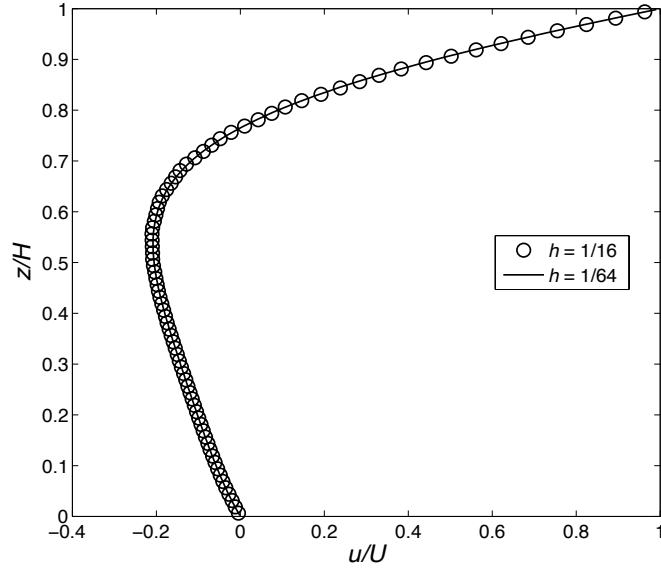
9.3 Darcy-Dominated Flow with Sharp Boundary Layers

As a final numerical example, we consider a reaction-dominated generalized Stokes problem subject to sharp boundary layers. The problem is posed on the unit square. Homogeneous no-slip and no-penetration boundary conditions are enforced along the boundary of the square, and an external forcing of the form

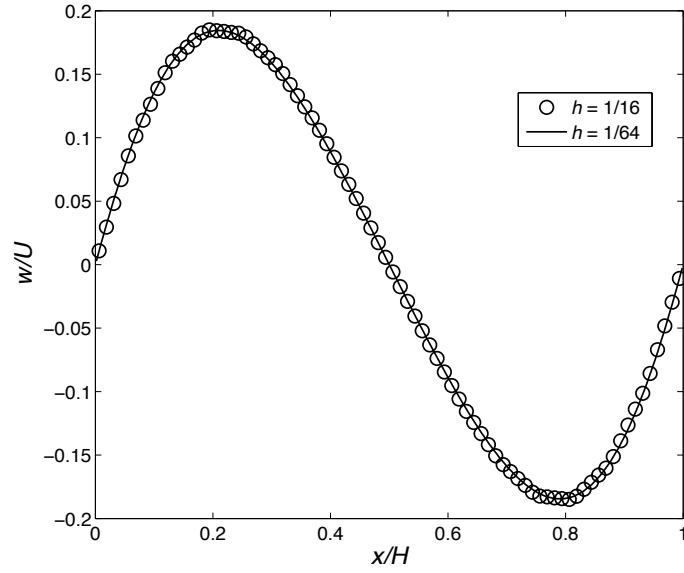
$$\mathbf{f} = \begin{bmatrix} \sin(\pi x) \cos(\pi y) \\ -\cos(\pi x) \sin(\pi y) \end{bmatrix}$$

is applied. The reaction term σ is set to be equal to 1 while the viscosity ν is set to be equal to 10^{-6} . With these choices, the resulting flow field has a vortical structure in the interior of the domain and sharp boundary layers along the entire boundary of the domain.

We have simulated this flow problem using both our discretization technique as well as the \mathbf{Q}_2/Q_1 Taylor-Hood velocity/pressure pair [36]. The Taylor-Hood velocity/pressure pair is one of the most popular finite elements for generalized Stokes flow, but it is known not to be robust in the Darcy limit. Specifically, the accuracy of the \mathbf{Q}_2/Q_1 Taylor-Hood velocity field reduces to first-order in the Darcy limit [33]. This is due to a lack of strong coercivity (in the kernel) with respect to the $\mathbf{H}(\text{div}; \Omega)$ -norm. We have visualized the computed velocity vectors corresponding to divergence-free B-splines of degree $k' = 1$ and the \mathbf{Q}_2/Q_1 Taylor-Hood velocity-pressure pair on a 16×16 element mesh in Figures 26(a) and (b). These two quiver plots seem to indicate that the two discrete flow fields are nearly identical except in a small region near



(a)



(b)

Figure 25: Lid-driven Stokes flow in a three-dimensional cavity: (a) Value of the first component of the velocity field along the line $(x/H, y/H) = (1/2, 1/2)$ for $k' = 1$, (b) Value of the third component of the velocity field along the line $(y/H, z/H) = (1/2, 1/2)$ for $k' = 1$.

the boundary of the domain. However, when we view only the first-component of the velocity field as in Figures 27 and 28, we see that the divergence-free B-spline solution is monotone while the Taylor-Hood solution suffers from spurious oscillations. Finally, we have visualized the divergence of the discrete flow field corresponding to the Taylor-Hood solution in Figure 29. From this figure, we see that the Taylor-Hood solution is characterized by strong expansion and compression in the four corners of the domain. When coupled with a transport solver, this ultimately leads to methods with unphysical species production [46]. On the other hand, the discrete flow field corresponding to the B-spline solution is pointwise divergence-free.

10 Conclusions

In this paper, new divergence-conforming B-spline discretizations have been presented for the generalized Stokes equations. A collection of stability and error estimates have been derived which are robust with respect to the parameters of generalized Stokes flow, and these theoretical results have been confirmed and supplemented by numerical simulations of problems with known analytical solutions. These discretizations have been also applied to the simulation of a number of benchmark problems where the advantages of the new methodology over classical methods have been highlighted. In future work, we plan to extend the present developments to the Navier-Stokes equations and generalize to locally-refined meshes.

Acknowledgements

John A. Evans and Thomas J.R. Hughes were partially supported by the Office of Naval Research under contract number N00014-08-0992 and by the National Science Foundation under Grant No. 0700204. John A. Evans was additionally partially supported by the Department of Energy Computational Science Graduate Fellowship, provided under grant number DE-FG02-97ER25308. This support is gratefully acknowledged.

References

- [1] D N Arnold. An interior penalty finite element method with discontinuous elements. *SIAM Journal on Numerical Analysis*, 19:742–760, 1982.
- [2] D N Arnold and J Qin. Quadratic velocity/linear pressure Stokes elements. In R Vichnevetsky and R S Steplemen, editors, *Advances in Computer Methods for Partial Differential Equations VII*, 1992.

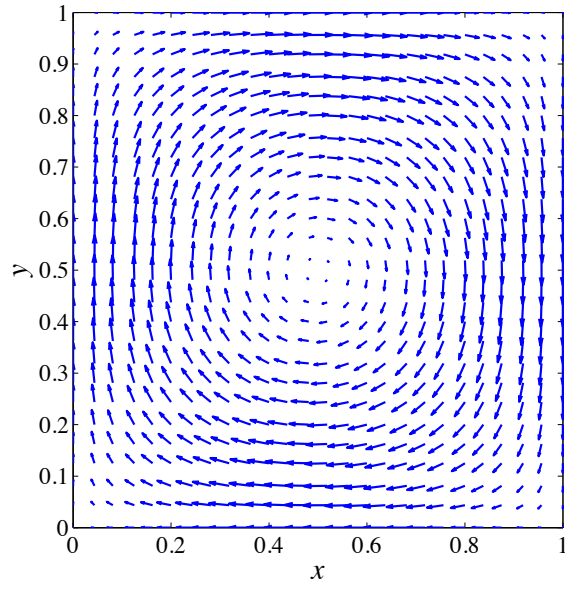
- [3] I Babuška. Error bounds for finite element method. *Numerische Mathematik*, 16:322–333, 1971.
- [4] I Babuška and H-S Oh. Pollution problem of the p - and $h - p$ versions of the finite element method. *Numerical Methods in Biomedical Engineering*, 3:553–561, 1987.
- [5] Y Bazilevs, V M Calo, J A Cottrell, J A Evans, T J R Hughes, S Lipton, M A Scott, and T W Sederberg. Isogeometric analysis using T-splines. *Computer Methods in Applied Mechanics and Engineering*, 199:229–263, 2010.
- [6] Y Bazilevs and T J R Hughes. Weak imposition of Dirichlet boundary conditions in fluid mechanics. *Computers and Fluids*, 36:12–26, 2007.
- [7] Y Bazilevs, C M Michler, V M Calo, and T J R Hughes. Weak Dirichlet boundary conditions for wall-bounded turbulent flows. *Computer Methods in Applied Mechanics and Engineering*, 196:4853–4862, 2007.
- [8] Y Bazilevs, C M Michler, V M Calo, and T J R Hughes. Isogeometric variational multiscale modeling of wall-bounded turbulent flows with weakly-enforced boundary conditions on unstretched meshes. *Computer Methods in Applied Mechanics and Engineering*, 199:780–790, 2010.
- [9] D Boffi, F Brezzi, and M Fortin. Finite elements for the Stokes problem. *Lecture Notes in Mathematics*, 1939:45–100, 2008.
- [10] O Botella and R Peyret. Benchmark spectral results on the lid-driven cavity flow. *Computers and Fluids*, 27:421–433, 1998.
- [11] S C Brenner. Korn’s inequalities for piecewise H^1 vector fields. *Mathematics of Computation*, 73:1067–1087, 2003.
- [12] F Brezzi. On the existence, uniqueness and approximation of saddle-point problems arising from Lagrange multipliers. *Revue Française d’Automatique Informatique et Recherche Operationnellle. Analyse Numérique*, 8:129–151, 1974.
- [13] H C Brinkman. A calculation of the viscous force exerted by a flowing fluid on a dense swarm of particles. *Applied Scientific Research*, A1:27–34, 1947.
- [14] A Buffa, C de Falco, and R Vázquez. Isogeometric analysis: Stable elements for the 2D Stokes equation. *International Journal for Numerical Methods in Fluids*, 65:1407–1422, 20–30, 2011.
- [15] A Buffa, J Rivas, G Sangalli, and R Vázquez. Isogeometric discrete differential forms in three dimensions. *SIAM Journal on Numerical Analysis*, 49:818–844, 2011.

- [16] A Buffa, G Sangalli, and R Vázquez. Isogeometric analysis in electromagnetics: B-splines approximation. *Computer Methods in Applied Mechanics and Engineering*, 199:1143–1152, 2010.
- [17] B Cockburn and J Gopalakrishnan. Incompressible finite elements via hybridization. Part I: The Stokes system in two space dimensions. *SIAM Journal on Numerical Analysis*, 43:1627–1650, 2005.
- [18] B Cockburn and J Gopalakrishnan. Incompressible finite elements via hybridization. Part II: The Stokes system in three space dimensions. *SIAM Journal on Numerical Analysis*, 43:1651–1672, 2005.
- [19] B Cockburn, G Kanschat, and D Schötzau. A note on discontinuous Galerkin divergence-free solutions of the Navier-Stokes equations. *SIAM Journal on Scientific Computing*, 31:61–73, 2007.
- [20] J A Cottrell, T J R Hughes, and Y Bazilevs. *Isogeometric Analysis: Toward Integration of CAD and FEA*. Wiley, 2009.
- [21] L Beirão da Veiga, A Buffa, J Rivas, and G Sangalli. Some estimates for $h-p-k$ refinement in isogeometric analysis. *Numerische Mathematik*, 118:271–305, 2011.
- [22] D B Das. Hydrodynamic modelling for groundwater flow through permeable reactive barriers. *Hydrodynamics Processes*, 16:3393–3418, 2002.
- [23] C R de Boor. *A Practical Guide to Splines*. Springer-Verlag, 1978.
- [24] J Douglas and T Dupont. Interior Penalty Procedures for Elliptic and Parabolic Galerkin Methods. *Lecture Notes in Physics*, 58, 1976.
- [25] J A Evans, Y Bazilevs, I Babuška, and T J R Hughes. n -widths, sup-infs, and optimality ratios for the k -version of the isogeometric finite element method. *Computer Methods in Applied Mechanics and Engineering*, 198:1726–1741, 2009.
- [26] J A Evans and T J R Hughes. Explicit trace inequalities for isogeometric analysis and parametric finite elements. Technical report, ICES Report 11-17, 2011.
- [27] L P Franca and T J R Hughes. Two classes of mixed finite element methods. *Computer Methods in Applied Mechanics and Engineering*, 69:89–129, 1988.
- [28] J Gerbeau, C L Bris, and M Bercovier. Spurious velocities in the steady flow of an incompressible fluid subjected to external forces. *International Journal for Numerical Methods in Fluids*, 25:679–695, 1997.
- [29] V Girault and P A Raviart. *Finite Element Methods for Navier-Stokes Equations. Theory and Algorithms*. Springer-Verlag, 1986.

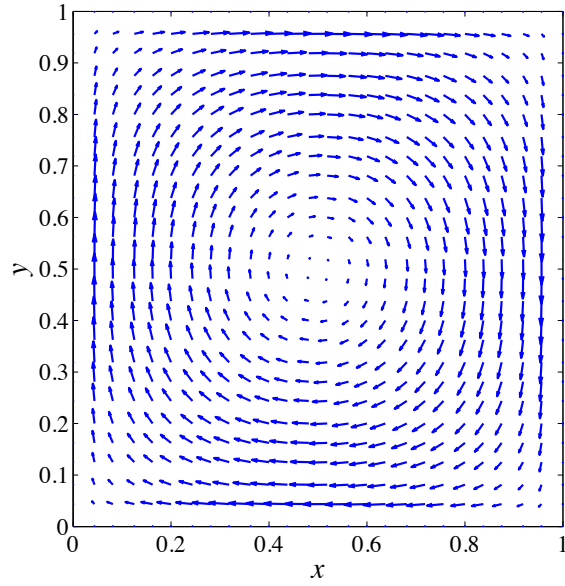
- [30] W Gui and I Babuška. The h , p and hp versions of the finite element method in one dimension. Part 1: The error analysis of the p -version. Part 2: The error analysis of the h - and hp -versions. Part 3: The adaptive hp version. *Numerische Mathematik*, 49:577–683, 1986.
- [31] G Guo and I Babuška. The hp version of the finite element method. Part 1: The basic approximation results. Part 2: General results and applications. *Computational Mechanics*, 1:21–41, 203–220, 1986.
- [32] M M Gupta. A comparison of numerical solutions of convective and divergence forms of the Navier-Stokes equations for the driven cavity problem. *Journal of Computational Physics*, 43:260–267, 1981.
- [33] A Hannukainen, M Juntunen, and R Stenberg. Computations with finite element methods for the Brinkman problem. *Computational Geosciences*, 15:155–166, 2010.
- [34] F H Harlow and J E Welch. Numerical calculation of time-dependent viscous incompressible flow of fluid with free surface. *Physics of Fluids*, 8:2182, 1965.
- [35] K Höllig. *Finite Element Methods with B-splines*. Society for Industrial and Applied Mathematics, 2003.
- [36] P Hood and C Taylor. Navier-Stokes equations using mixed interpolation. In J T Oden, R H Gallagher, O C Zienkiewicz, and C Taylor, editors, *Finite Element Methods in Flow Problems*, pages 121–132. University of Alabama in Huntsville Press, 1974.
- [37] T J R Hughes, L P Franca, and M Balestra. A new finite element formulation for computational fluid dynamics: V. Circumventing the Babuška-Brezzi condition: A stable Petrov-Galerkin formulation of the Stokes problem accomodating equal-order interpolations. *Computer Methods in Applied Mechanics and Engineering*, 59:85–99, 1986.
- [38] G Kanschat. Divergence-free discontinuous Galerkin schemes for the Stokes equations and the MAC scheme. *International Journal for Numerical Methods in Fluids*, 56:941–950, 2008.
- [39] T Kara and J Goldak. Three-dimensional numerical analysis of heat and mass transfer in heat pipes. *Heat Mass Transfer*, 43:775–785, 2007.
- [40] A-R A Khaled and K Vafai. The role of porous media in modeling flow and heat transfer in biological tissues. *International Journal of Heat and Mass Transfer*, 46:4989–5003, 2003.

- [41] B J Kirby. *Micro- and Nanoscale Fluid Mechanics: Transport in Microfluidic Devices*. Cambridge University Press, 2010.
- [42] J Könnö and R Stenberg. Non-conforming finite element method for the Brinkman problem. In G Kreiss, P Lötstedt, A Malqvist, and M Neytcheva, editors, *Numerical Mathematics and Advanced Applications*, 2010.
- [43] P G Lemairé-Rieusset. Analyses multi-résolutions non orthogonales, commutation entre projecteurs et dérivation et ondelettes vecteurs à divergence nulle. *Revista Matemática Iberoamericana*, 8:221–237, 1992.
- [44] A Linke. Collision in a cross-shaped domain - A steady 2d Navier-Stokes example demonstrating the importance of mass conservation in CFD. *Computer Methods in Applied Mechanics and Engineering*, 198:3278–3286, 2009.
- [45] K A Mardal, X-C Tai, and R Winther. A robust finite element method for Darcy-Stokes flow. *SIAM Journal on Numerical Analysis*, 40:1605–1631, 2002.
- [46] G Matthies and L Tobiska. Mass conservation of finite element methods for coupled flow-transport problems. *International Journal for Computing Science and Mathematics*, 1:293–307, 2007.
- [47] H K Moffatt. Viscous and resistive eddies near a sharp corner. *Journal of Fluid Mechanics*, 64:1–18, 1964.
- [48] J A Nitsche. Über ein Variationsprinzip zur Lösung von Dirichlet-Problemen bei Verwendung von Teilräumen, die keinen Randbedingungen unterworfen sind. *Abhandlungen aus dem Mathematischen Seminar der Universität Hamburg*, 36:9–15, 1971.
- [49] P A Raviart and J M Thomas. A mixed finite element method for second order elliptic problems. *Lecture Notes in Mathematics*, 606:292–315, 1977.
- [50] B Rivière and M F Wheeler. A discontinuous Galerkin method applied to non-linear parabolic equations. *Lecture Notes in Computational Science and Engineering*, 11:231–244, 2000.
- [51] W W Schultz, N T Lee, and J P Boyd. Chebyshev pseudospectral method of viscous flows with corner singularities. *Journal of Scientific Computing*, 4:1–24, 1989.
- [52] L L Schumaker. *Spline functions: Basic theory*. Cambridge Mathematical Library, Cambridge University Press, 2007.
- [53] L R Scott and M Vogelius. Norm estimates for a maximal right inverse of the divergence operator in spaces of piecewise polynomials. *Mathematical Modelling and Numerical Analysis*, 19:111–143, 1985.

- [54] G Stadler, M Gurnis, C Burstedde, L C Wilcox, L Alisic, and O Ghattas. The dynamics of plate tectonics and mantle flow: From local to global scales. *Science*, 329:1033–1038, 2010.
- [55] R Stevenson. Divergence-free wavelet bases on the hypercube: Free-slip boundary conditions, and applications for solving the instationary Stokes equations. *Mathematics of Computation*, 80:1499–1523, 2011.
- [56] X-C Tai and R Winther. A discrete de Rham complex with enhanced smoothness. *CALCOLO*, 43:287–306, 2006.
- [57] H Triebel. *Interpolation Theory, Function Spaces, Differential Operators, Second Edition*. Johann Ambrosius Barth, 1995.
- [58] K Urban. Wavelet bases in $\mathbf{H}(\text{div})$ and $\mathbf{H}(\text{curl})$. *Mathematics of Computation*, 70:739–766, 2001.
- [59] K Urban. *Wavelets in Numerical Simulation: Problem Adapted Construction and Applications*. Springer-Verlag, 2002.
- [60] R Verürth. *A Review of a Posteriori Error Estimation and Adaptive Mesh-Refinement Techniques*. B.G. Teubner, 1996.
- [61] J Wang and X Ye. New finite element methods in computational fluid dynamics by $\mathbf{H}(\text{div})$ elements. *SIAM Journal on Numerical Analysis*, 45:1269–1286, 2007.
- [62] M F Wheeler. An elliptic collocation-finite element method with interior penalties. *SIAM Journal on Numerical Analysis*, 15:152–161, 1978.
- [63] S Zhang. A new family of stable mixed finite elements for 3D Stokes equations. *Mathematics of Computation*, 250:543–554, 2005.

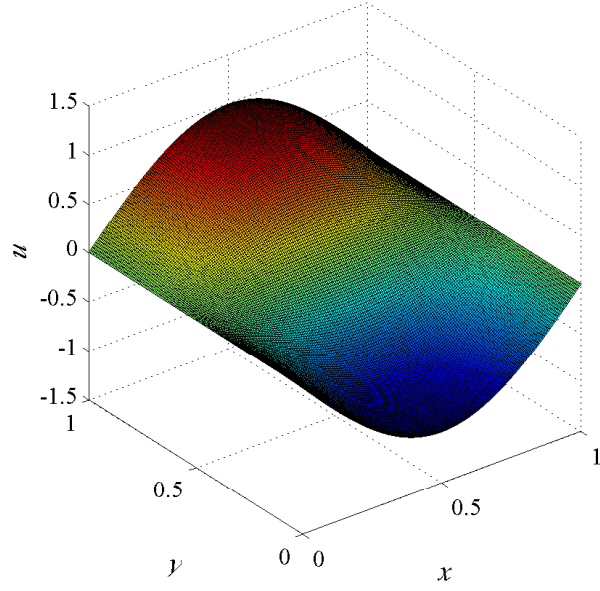


(a)

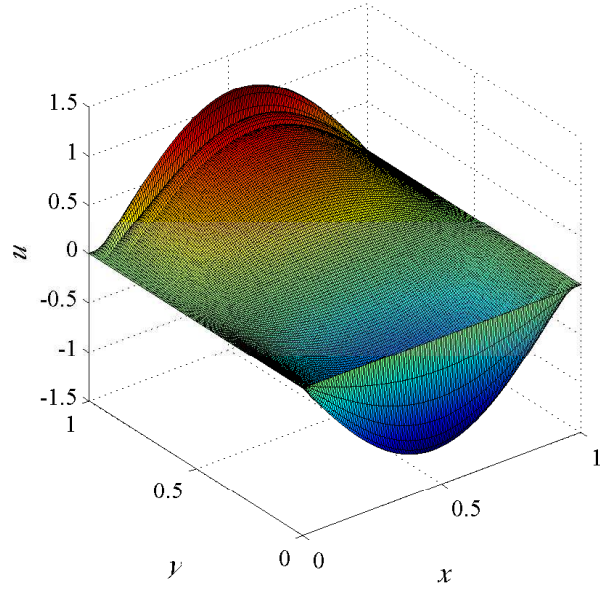


(b)

Figure 26: Darcy-dominated flow with boundary layers: Computed velocity fields: (a) Divergence-free B-splines of degree $k' = 1$, (b) \mathbf{Q}_2/Q_1 Taylor-Hood velocity/pressure pair.

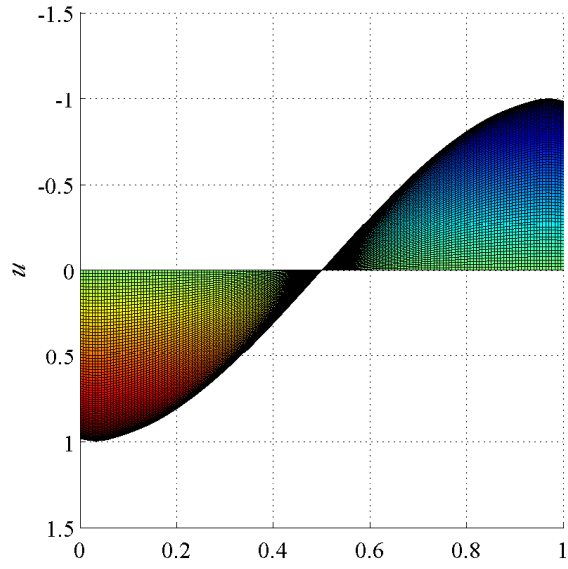


(a)

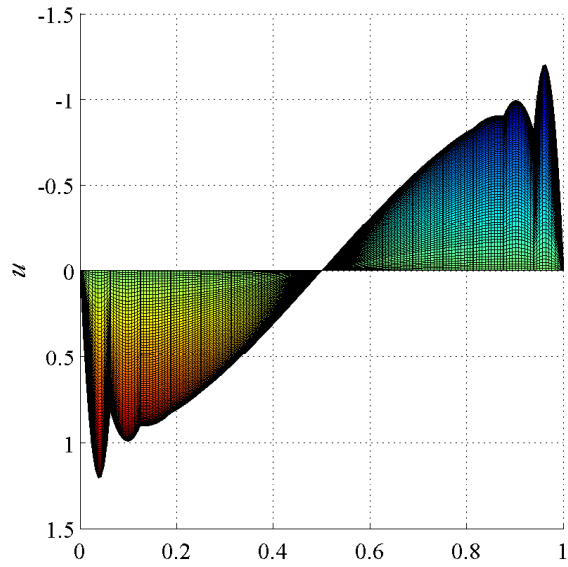


(b)

Figure 27: Darcy-dominated flow with boundary layers: First-component of the velocity field: (a) Divergence-free B-splines of degree $k' = 1$, (b) \mathbf{Q}_2/Q_1 Taylor-Hood velocity/pressure pair.



(a)



(b)

Figure 28: Darcy-dominated flow with boundary layers: Cross-section view of the first velocity component from the $y = 1$ line: (a) Divergence-free B-splines of degree $k' = 1$, (b) \mathbf{Q}_2/Q_1 Taylor-Hood velocity/pressure pair.

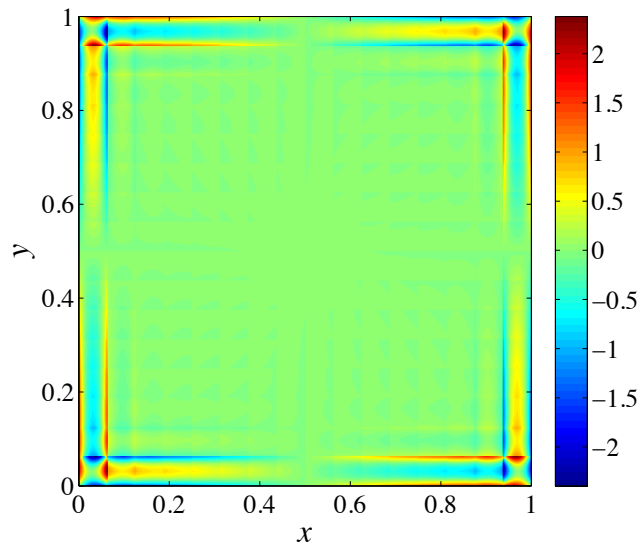


Figure 29: Darcy-dominated flow with boundary layers: Divergence of the discrete flow field corresponding to the \mathbf{Q}_2/Q_1 Taylor-Hood velocity/pressure pair.